REAL-TIME SIMULATION AND EVALUATION OF DATA FROM WEARABLE SMART-DEVICES TO PREVENT MUSCULOSKELETAL SIGNS OF AGING

Dissertation
to obtain the doctoral degree
of Human Sciences
(Dr. sc. hum.)

of the
Faculty of Medicine
of the University of Regensburg

submitted by
Lukas Reinker

2024

Dean:	Prof. Dr. med. Dirk Hellwig
Mentors:	Prof. Dr. med. Markus Weber Prof. Dr. rer. nat. Rudolf Bierl
Supervisor:	Prof. Dr.-Ing. Sebastian Dendorfer
Day of defense:	18.11.2024

Table of contents

List of Figures

List of Tables

Abbreviations

AMMR AnyBody Managed Model Repository
AMS AnyBody Modeling System
BMD bone mineral density
CMJ counter movement jump
DJ drop jump
DXA X-ray absorptiometry
GRF ground reaction forces
GRFP ground reaction force prediction
IMU inertial measurement unit
SJ squat jump
SPM statistical parametric mapping
WHO World Health Organisation

Abstract

The risk of suffering from musculoskeletal disorders increases considerably with age. One of the causes is the decrease in physical activity. Osteoporosis is a disease that is favored precisely by this lack of movement. It is mainly characterized by bone fractures, especially of the femur. Previous studies have shown that regular exercise with high strains on the bones of the lower extremities, such as jumping or running, can prevent osteoporosis. Musculoskeletal models can help in the research of these preventive mechanisms. This work aims to determine the kinematic data relevant to the prevention of osteoporosis, correlate it with simulated kinetic data, and finally interpret it. The findings are to be made measurable and tangible for the user in everyday life with the help of smart devices or smartphones. For this reason, typical positions of smart devices were first evaluated for recording high-impact exercises. A motion capture system based on inertial measurement units was used. The study showed that the accelerations acting on the pelvis can be recorded very well at typical positions where smart devices are worn. However, care must be taken to ensure the exercise is performed correctly. In the next step, a markerless motion capture system was used to record various everyday movements and high-impact exercises and to simulate them using musculoskeletal models. The strains on the femoral neck were analyzed using the models. The results indicate that most exercises place a considerable load on the femoral neck, potentially promoting bone formation and modeling. Despite the simplified assumptions regarding femoral geometry and deformation behavior, which are necessary for accommodating a large number of subjects, the results aligned with previous research findings that highlight the positive effects of strenuous activities on bone health. In the final phase of this work, the findings were integrated to incorporate these preventive mechanisms into everyday life. Acceleration data from an inertial measurement unit were initially compared with data from the markerless motion capture system. This comparison did not yield usable results, so only the motion capture system data were used. The comparison with the calculated load data showed low correlations. It was demonstrated that better results could be achieved with additional input parameters and more extensive calculation models. Possible feedback systems based on this data were also discussed. In summary, this work has shown several promising approaches to integrating practical systems for the prevention of musculoskeletal disorders. The final implementation, which requires further work and methodological evaluation, presents an

exciting opportunity for future research and development in this field.

Zusammenfassung

Die Gefahr an muskuloskelettalen Erkrankungen zu leiden, nimmt stark mit dem Alter zu. Eine der Ursachen ist die Abnahme der physischen Aktivität. Osteoporose ist eine Krankheit, die genau durch diese fehlende Bewegung begünstigt wird. Vor allem macht sie sich durch Knochenbrüche im Speziellen des Femurs bemerkbar. In bereits vergangenen Studien konnte gezeigt werden, dass ein regelmäßiger Umfang an Übungen mit hohen Belastungen auf die Knochen der unteren Extremität, wie beispielsweise Springen oder Rennen, vorbeugend gegenüber Osteoporose sein. Muskuloskelettale Modelle können bei der Erforschung dieser präventiven Mechanismen helfen. Ziel dieser Arbeit ist es, die für die Osteoporoseprävention relevanten kinematischen Daten zu ermitteln und mit simulierten kinetischen Daten zu korrelieren und schließlich zu interpretieren. Mit Hilfe von Smart Devices oder Smartphones sollen die gewonnen Erkenntnisse im Alltag für den Nutzer messbar und greifbar gemacht werden. Deswegen wurden zunächst typische Positionen von Smart Devices in Bezug auf das Aufzeichnen von hochbelastenden Übungen evaluiert. Dabei wurde ein Motion Capture System basierend auf inertiale Messeinheiten verwendet. Die Studie hat gezeigt, dass die Beschleunigungen, die auf den Pelvis wirken, sehr gut an typischen Positionen, an denen Smart Devices getragen werden, aufgezeichnet werden können. Jedoch ist dabei auf die korrekte Ausführung der Übung zu achten. Im nächsten Schritt wurden mittels einem markerlosen Motion Capture System verschiedene Alltagsbewegungen und Übungen mit hohen Belastungen aufgenommen und mit muskuloskelettalen Modellen simuliert. Dabei wurden die Belastungen auf den Femurhals betrachtet, welche sich aus den Modellen ableiten ließen. Die Ergebnisse deuten darauf hin, dass die meisten Übungen den Oberschenkelhals erheblich belasten, was möglicherweise den Knochenaufbau/-modellierung fördert. Trotz starker Vereinfachung der Annahmen für Femurgeometrie und Verformungsverhalten, um eine hohe Anzahl an Probanden zu ermöglichen, waren die Ergebnisse stehen im Einklang mit früheren Forschungsergebnissen, die die positiven Auswirkungen von anstrengenden Aktivitäten auf die Knochengesundheit hervorheben. Im letzten Schritt dieser Arbeit sollten die gewonnen Erkenntnisse zusammengeführt werden, um diese präventiven Mechanismen in den Alltag zu integrieren. Dafür wurden zunächst Beschleunigungsdaten einer intertialen Messeinheit mit denen des markerlosen Motion Capture Systems verglichen. Dies lieferte jedoch keine verwertbaren Ergebnisse, weshalb nur die Daten des Motion Cap-

ture Systems verwendet wurden. Der Vergleich mit den berechneten Belastungsdaten führte nur zu geringen Korrelationen. Jedoch zeigte sich das Potenzial bessere Ergebnisse mit weiteren Eingangsparametern neben den Beschleunigungsdaten und umfangreicheren Berechnungsmodellen zu erzielen. Ansätze für mögliche Feedbacksysteme basierend auf diesen Daten wurde diskutiert. Zusammenfassend konnten in dieser Arbeit einige Ansätze zur Integration von handlichen Systemen hinsichtlich der Prävention von muskuloskelettalen Erkrankungen gezeigt werden. Die finale Umsetzung bedarf jedoch weiterer Arbeit und Methodikevaluierung.

Chapter 1

Introduction

The risk of musculoskeletal disorders considerably rises with age (Bonewald 2019; Hirschfeld et al. 2017). Osteoporosis is one of the most common diseases of the human musculoskeletal system, and its prevalence and the fractures associated with it have increased in recent years. They are expected to continue to rise (Kanis et al. 2021). Osteoporosis comes with many risk factors that need to be considered. In addition to demographic factors such as age and gender, poor nutrition, alcohol consumption, various illnesses, and smoking favor the risk of developing osteoporosis (Bartl 2023a). Physical inactivity is the most relevant biomechanical risk factor. Social events like the COVID-19 pandemic promoted physical inactivity (Woods et al. 2020; Ainsworth and Li 2020). On top of that, physical activity decreases with age (Hirschfeld et al. 2017; Gomes et al. 2017). However, it is easy to address this issue. Several studies have shown the positive effects of exercises with the right stimuli on bone growth and preservation. Jumping and fast movements with a high impact on bones have proven to be particularly preventative (Vainionpää 2007; Vlachopoulos et al. 2018). Even though these positive effects have been observed, it has yet to be determined which exact mechanisms of the musculoskeletal system achieve this result. Musculoskeletal simulations, which can calculate the loads and forces acting on muscles and bones from input movement data, can provide a deeper insight. The results of these simulations will be used to evaluate the implementation and strength of the preventive effect of high-impact exercises. In order to make the intended data more tangible for the user or the patient at risk, data from everyday life must be recorded, and the effect of exercises must be visualized. Digitalization is a great approach to intervene here. Smart devices like wearables are selling incredibly fast and offer more and more features to monitor daily movements and interactions (IDC 2020; Rossi and Veltink 2010; TrendForce 2019; Statista 2023). This massive amount of data includes acceleration data. Most of the data is not reviewed or cannot be interpreted by the user because there is often no context of what this data means to personal health. Therefore, the aim is to extract data relevant to the prevention of osteoporosis, evaluate it, correlate it with the calculated kinetic data, and finally interpret it. These results could then be made avail-

able to the user through apps or feedback systems, thus achieving a preventive effect on osteoporosis.

1.1 Osteoporosis

Anatomy of femur

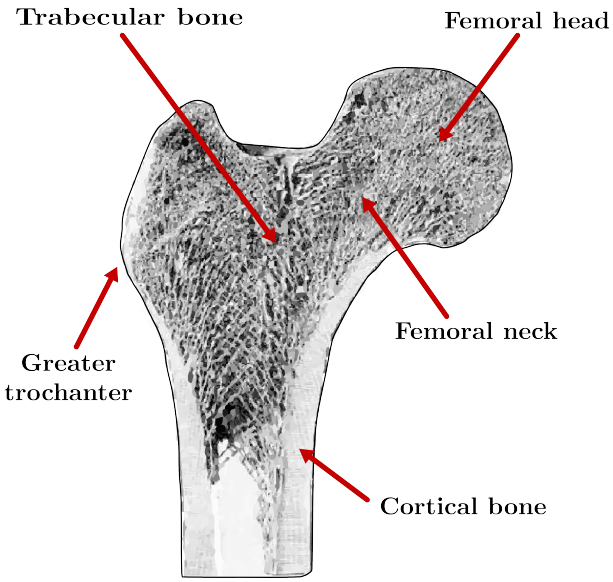

Figure 1.1: Anatomy of the human proximal femur (upper third of the human femur bone), which includes the femoral head, femoral neck, greater trochanter, and upper portion of the femoral stem. Adapted from Voo et al. (2004)

Osteoporosis is mainly manifested by fragility fractures of the femur with 17 %, the forearm with 16 % and the vertebral bodies with 15 % of all fragility fractures (Veronese et al. 2021). 51 % of all fractures in women and 24 % in men can be attributed to osteoporosis (Lippuner et al. 2005). To understand why the femoral head is particularly affected, it is important to look at the anatomy of the femur. The human femur, the largest and strongest bone in the body, is vital in supporting body weight and facilitating movement. The proximal part of the femur, known as the femoral head, articulates with the pelvic acetabulum to form the hip joint. This ball-and-socket joint allows a wide range of motion, essential for activities such as walking and running. The femoral neck connects the head to the stem, and its angle significantly influences biomechanics. The greater and lesser trochanter serve as attachment points for muscles, contributing to hip stability and motion. The trabecular bone in the proximal femur provides structural support and allows for weight distribution (Bartl 2023b; Metcalfe 2008). The femoral neck is the narrowed region directly below the femoral head. Cortical bone is a bone's outer (hard) shell with higher material density. The trabecular bone is the soft, sponge-like bone inside the hard cortical shell. Connectivity density is crucial in the maintenance

of bone strength. It decreases significantly in the femoral neck and vertebra with aging, as the trabecular bone volume decreases (Chen et al. 2013). This relatively thin structure is more prone to fracture than the joint to a dislocation (Metcalfe 2008). Figure 1.1 shows the anatomy of the human proximal femur. The following chapter will explain in more detail the effects of osteoporosis on the anatomy of the femoral head, what causes it, and how it can be prevented.

Prevelance of osteoporosis

Osteoporosis is a pervasive and potentially debilitating bone disorder that affects a significant portion of the global population. While it predominantly impacts postmenopausal women due to hormonal changes and estrogen depletion, men can also be affected (Alswat 2017). The aging process itself contributes to the development of osteoporosis, as bone density naturally diminishes over time. According to the World Health Organisation (WHO) definition of osteoporosis, approximately 21 % of women between the ages of 50-84 suffer from osteoporosis. In the same age range, the prevalence in men is 6 %, making it the most common bone disease worldwide (Kanis, Johnell, Oden, Jonsson, et al. 2000). These global values from 2000 are also reflected in the European population in 2019 (Kanis et al. 2021). For this age group, one in three women and one in five men suffer from an osteoporotic fracture in their remaining lifetime (Kanis, Johnell, Oden, Sernbo, et al. 2000). Osteoporosis is characterized by compromised bone strength and increased susceptibility to fractures. Bones, in individuals with osteoporosis, become porous and brittle, leading to heightened risks of fractures, especially in areas like the spine, hip, and wrist ("Consensus development conference: diagnosis, prophylaxis, and treatment of osteoporosis" 1993). Figure 1.2 shows an example of the effects of osteoporosis on the cortical and trabecular structures of a proximal femur. The left image (a) shows a normal femoral neck with high bone density. The right-hand image (b) shows the reduced bone mineral density (BMD) of a person suffering from osteoporosis. This reduced BMD increases the risk of fracture.

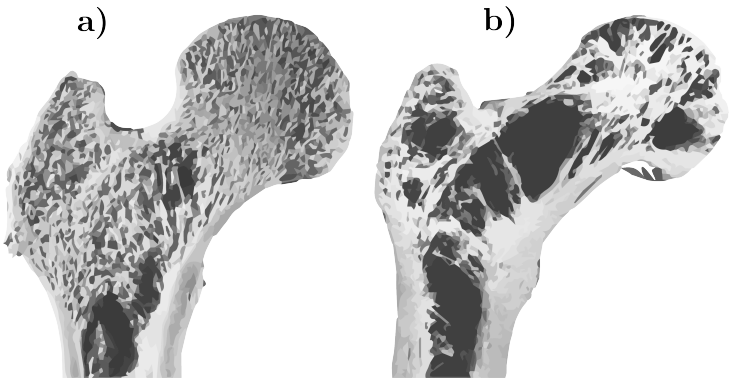

Figure 1.2: (a) Normal cortical and trabecular structure of the proximal femur. (b) Proximal femur of a patient with severe osteoporosis. Note destruction of the trabecular (trajectorial) network indicating a high fracture risk. Adapted from Bartl 2023b, p. 25

Risk factors

Osteoporosis is a commonly overlooked risk factor for fractures that can lead to severe complications, particularly in old age. The focus should be on preventing osteoporosis and reducing the risk factors contributing to its development (Bartl 2023b). However, it is important to note that certain risk factors cannot be prevented, such as genetics, race, gender, and age. To illustrate the change in bone density, it is useful to consider the body's natural aging process. Further details on this change will be provided below. Firstly, modifiable risk factors, which mainly relate to a person's lifestyle, should be listed. Stimulants, such as caffeine and cigarettes, as well as excessive alcohol consumption, have a negative impact on BMD. Nutrition plays an essential role in maintaining bone health, with calcium and vitamin D deficiencies linked to osteoporosis. Therefore, it is crucial to have a sufficient intake of minerals, vitamins, and proteins. (Bartl 2023b; Pouresmaeili et al. 2018). From a biomechanical point of view, physical inactivity is the most critical risk factor that can be influenced. Bone mass and density peak in men and women between 25 and 30. After this peak, bone density decreases steadily. While men experience a relatively even decline, women experience a sharp drop after the menopause. This puts women at a higher risk of fractures in old age compared to men. Due to physical inactivity or an unfavorable genotype score, bones may not reach the same density as individuals who exercise regularly or are genetically predisposed, resulting in lower bone density in old age (Herbert et al. 2019). Figure 1.3 displays the correlation between age and BMD and the impact of genotype and physical activity level.

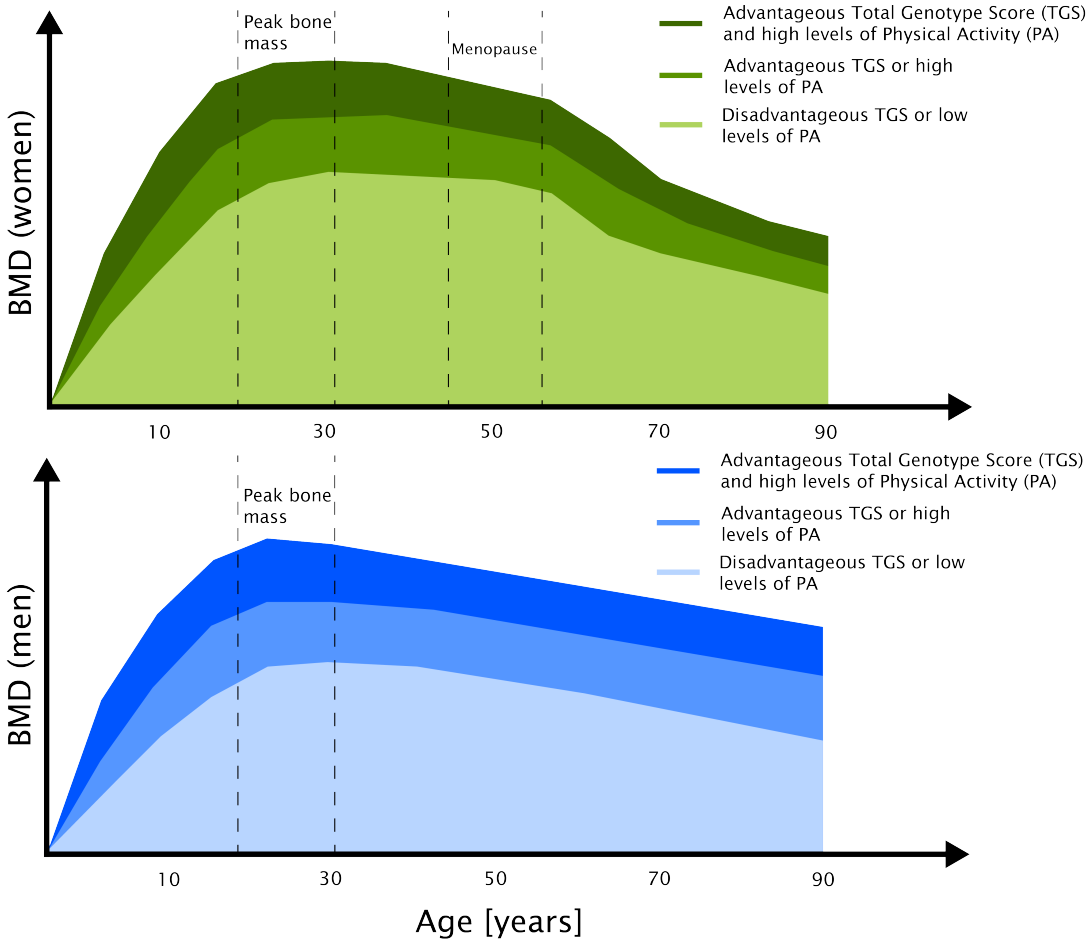

Figure 1.3: Schematic representation of typical age- and sex-related loss of BMD in women (first graph) and men (second graph) and the effect of physical activity and genetics. Adapted from Herbert et al. (2019).

Previous research has demonstrated that exercises with certain stimuli can prevent osteoporosis. The following section will provide a detailed explanation of how these stimuli can be implemented.

Biomechanical approaches of preventing osteoporosis

In 1892, Julius Wolff's book "Das Gesetz der Transformation der Knochen" described how the shape and structure of bones adapt to mechanical stress and the load on the body. Wolff observed that the bone trabeculae in femoral heads align with the mechanical forces, suggesting that mechanical forces determine the architecture of bone structures (Wolff 1892). H. Frost developed the concept of the Mechanostat a few decades later based on these assumptions. The Mechanostat aims to define specific parameters and their threshold values to differentiate how the bone reacts to different loads. The core parameter that describes the deformation of the bone is measured in µStrain, where 1000 µStrain equals a 0.1 % change in length (Frost and Schönau 2000; Frost 2000). Table 1.1 provides an overview of the areas defined for bone loss, preservation, and gain.

Table 1.1: Thresholds of bone remodeling

<800 µStrain	800 – 1500 µStrain	>1500 µStrain	>15 000 µStrain
Disuse	**Adapted State**	**Overload**	**Fracture**
Bone loss/remodeling	Bone perservation	Bone gain/modeling	Bone fracture

High-impact exercises, such as running, jumping, and resistance training, exert dynamic forces on the skeletal system. These mechanical stresses stimulate bone cells, fostering bone remodeling (Koshy et al. 2022). Regular engagement in high-impact exercises has been associated with increased BMD, particularly in weight-bearing bones such as the spine, hips, and legs (Allison et al. 2018). The effects of exercise vary depending on the number, intensity, and type of impact, with running and jumping primarily affecting the lower body (Zhang et al. 2022). In the early 2000s, Vainiopää conducted a study investigating the effect of high-impact exercises (e.g., running, jumping, drop jumps) on the BMD in premenopausal (age 35-40 years) women. Therefore, a body monitor recorded all accelerations the body underwent over 12 months, which were then evaluated. The results indicate that bone stimulation is significantly impacted by accelerations exceeding 4g. To achieve bone stimulation, a minimum of 60 daily impacts is required (Vainionpää 2007). Another study showed that jumping intervention can improve bone mass, bone stiffness, and parameters in adolescent athletes participating in non-osteogenic sports such as swimming and cycling. The jumping intervention resulted in significantly greater bone mineral content and bone stiffness in the legs compared to the control groups (Vlachopoulos et al. 2018). These findings suggest that high-impact jumping interventions in non-osteogenic sports may effectively promote bone health and, thus, prevent osteoporosis. However, only the analyses of the acceleration data and the altered tissue are available. It is unclear which exact mechanisms lead to the changes in bone density and which forces and loads occur in the regions analyzed. The forces and loads can be triggered by muscles and their attachment points or by joint reaction forces. Muscle contractions, joint position, body weight, movement patterns, speed of movement, and the type of load cause these. Unfortunately, they are difficult to measure in vitro or cannot be measured at all. Musculoskeletal modeling and simulations can provide a deeper insight into these parameters, which will be discussed in the following paragraph.

1.2 Musculoskeletal Modeling

General

Musculoskeletal modeling involves using computational techniques to create models of the human musculoskeletal system, allowing for a better understanding of its biomechanics and function. They facilitate a better understanding of complex relationships and are widely used in various fields. Musculoskeletal simulations provide a variety of parameters which are depending on the complexity and purpose of the simulation. These parameters include joint kinematics, muscle forces and activities, joint forces and moments, or ground reaction forcess (GRFs). The models must be constantly adapted and developed to reflect the current state of science and technology. This requires extensive validation work. Engelhardt et al. (2020) developed a detailed hand model using the AnyBody Modeling System (AMS), which includes all extrinsic and intrinsic muscles of the hand. Aurbach et al. (2020) aimed to modify a shoulder model and assess its effects. These models can be used for studies in orthopedics (Weber et al. 2016; Renkawitz et al. 2016; Benditz et al. 2018; Asadi and Arjmand 2020), ergonomics (Hosseini and Arjmand 2024; Melzner et al. 2021) or sports (Simonsen et al. 2023; Auer et al. 2021; Rasmussen et al. 2023). Finally, the general public can benefit from the results in many ways.

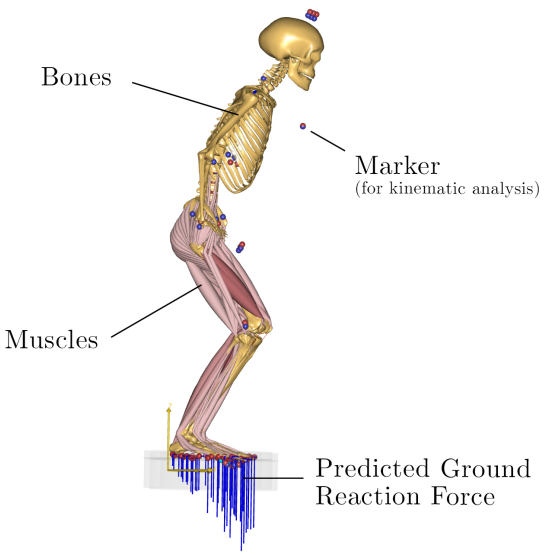

Figure 1.4: Basic elements of a musculoskeletal simulation in the AMS. Bones are depicted in beige, muscles in salmon. The blue lines at the bottom represent the vectors of the predicted GRF.

The requirements and computational possibilities are explained using the AMS (AnyBodyTechnology A/S, Aalborg, Denmark) with its open-code model library, the AnyBody Managed Model Repository (AMMR), which is used in this work. These models repre-

sent the human musculoskeletal system using various elements with adjustable, simplified parameters based on the latest biological knowledge. Solid bodies approximate the bones, while muscles are represented by actuators. Connecting elements serve as tendons and ligaments for the interfaces between bone and bone, as well as muscle and bone. The model's joints are determined by defining degrees of freedom between its bones. Figure 1.4 shows the basic elements of a musculoskeletal simulation in the AMS. Individual factors such as body weight, body height, and other anthropometrics can be adjusted by modifying the parameters of the elements. The musculoskeletal models in the AMS are based on the inverse dynamics approach. This means that the forces and moments within the models are calculated from defined or recorded movements (Damsgaard et al. 2006). The process involves several steps. Firstly, the movements are recorded using motion capture technology. This technology can be categorized as either inertial or optical and can be sensor-based, marker-based, or markerless. The recorded movements are then used as input data in the AMS. Before performing any additional calculations, transferring the captured movement to the model while adhering to the specified boundary conditions is necessary. The accelerations can then be calculated from the position data using the double-time derivative. The resulting forces can be determined by considering the mass distribution of the segments. The force boundary conditions to the environment can be included via force plates or predicted through calculation.

Model anatomy

The hip and femur are surrounded by several muscles responsible for a wide range of motion. These muscles attach to the respective bones at different origin and insertion points, supporting upright posture and mobility. For instance, the gluteus maximus, or the gluteal muscle, helps maintain balance and enables standing and walking as an extensor, external rotator, abductor, and adductor (Hofmann 2021). Additionally, the gluteus maximus stabilizes the pelvis and spine during various movements. In general, the surrounding muscles are essential for performing flexion and extension movements in the hip and knee joints and supporting the rotational movements of the thigh. They are, therefore, crucial for activities such as climbing stairs or turning the body. The hip joint enables a broad spectrum of motion, such as flexion, extension, abduction, adduction, internal rotation, and external rotation. These movements facilitate forward and backward leg bending, sideways leg movement away from and towards the body, and leg rotation inward or outward. These movements are controlled by various muscles. For instance, the hip flexor (iliopsoas muscle), the rectus femoris (part of the quadriceps), and the sartorius are responsible for flexion. The extension is mainly made possible by the gluteus maximus and the hamstrings (leg flexors). Abduction is supported by the gluteus medius and gluteus minimus, while adduction is performed by the adductor

groups, such as the adductor longus, adductor brevis, and adductor magnus. The gluteus medius, adductor magnus, and tensor fasciae latae are the primary muscles responsible for internal rotation, while the gluteus maximus, piriformis, and gemellus superior support external rotation (Tillmann 2016).

To better understand the forces exerted on the femur, particularly during low- and high-impact exercises, it is necessary to analyze the muscles surrounding the hip joint, whose points of origin and insertion are close to the femoral head. Figure 1.5 illustrates these muscles, their origins, insertions, and paths. The muscle forces of these femur-surrounding muscles, the calculated joint reaction forces, and moments of the hip joint are used to determine stress resultants and strains in the femoral neck.

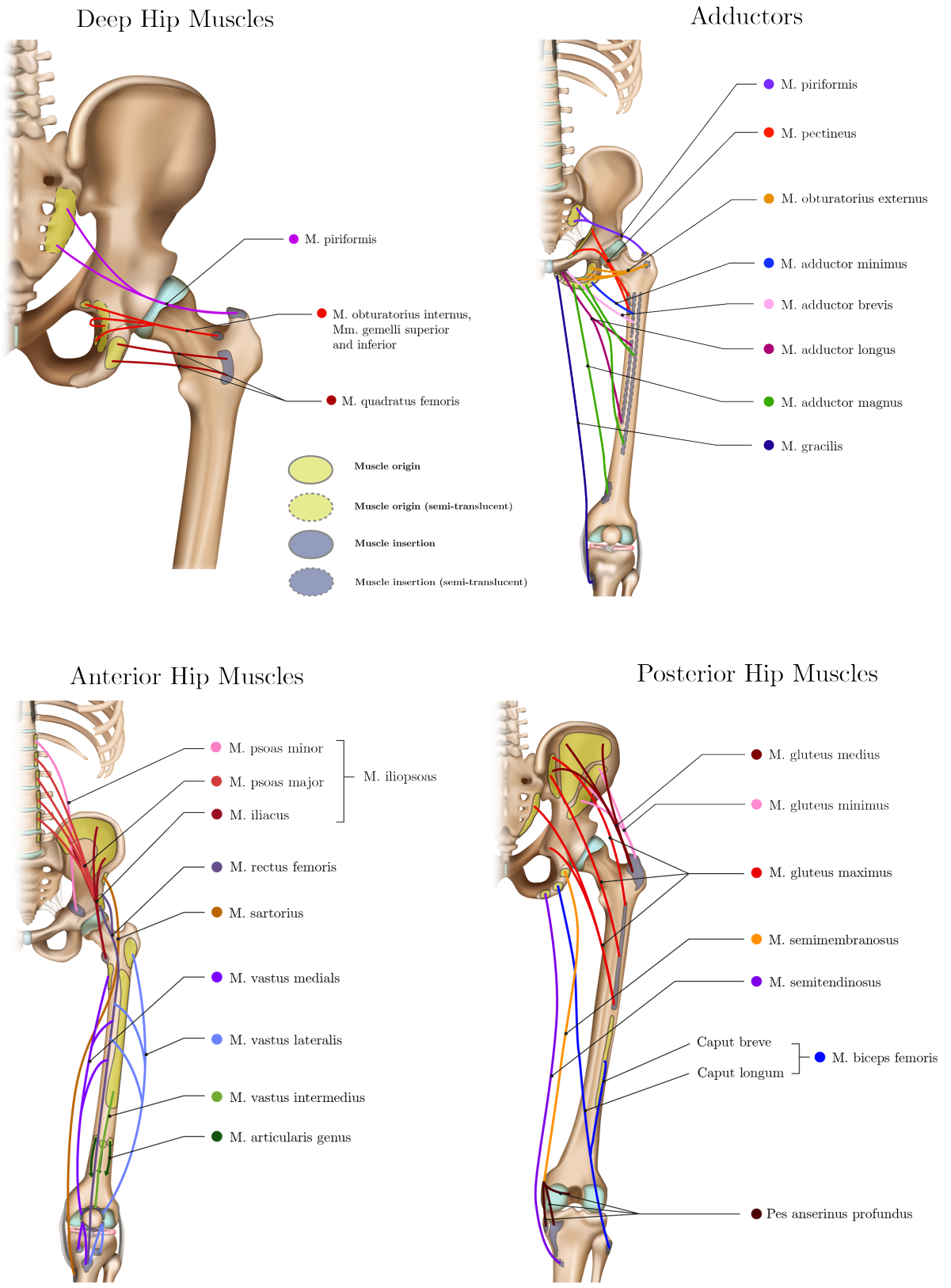

Figure 1.5: Hip muscles divided into deep, anterior and posterior muscles and adductors. The content is based on and adapted from the illustrations in Tillmann (2016, pp. 625, 629).

Calculation principle

The human body comprises numerous muscles, bones, and other structures that work together in complex combinations to facilitate movement. The degrees of freedom of a joint are determined by its type. Muscles are activated to allow or prevent movement around the joint centers. They are arranged around the joints to enable every possible movement, as muscles can only shorten or pull between their origin and insertion. Furthermore, the human body is kinetically overdetermined, meaning that various muscles can be addressed in many different ways for a particular movement. This results in the required force being distributed among different muscles, reducing the maximum force required per muscle, but mathematically results in an infinite number of solutions. However, this creates an optimization problem when calculating individual muscle forces. As stated, the AMS utilizes the inverse dynamic approach. This method enables the determination of muscle and joint forces from the kinematics recorded by motion capture and the given boundary conditions based on an equilibrium. The equations of equilibrium can be expressed as

$$C * f = r \tag{1.1}$$

where f is a vector of muscle and joint forces, r is a vector of external and inertia forces, and C is the matrix of equation coefficients. For vector $f^{(M)}$, the conditions $f^{(M)} \geq 0$ and $f^{(M)} \leq f^{(M)}_{i,max}$ that apply are limited to the fact that muscles can only pull and cannot exceed the maximum defined force. These maximum defined forces, which are standard values in the AMS, are based on previous studies. The optimization problem can be described in the following way on the basis of the sequence of conditions mentioned above:

$$\begin{aligned} \text{minimize} \quad & G(f^{(M)}) \\ \text{subject to} \quad & C * f = r \\ & f^{(M)}_i \geq 0, i = 1...n^{(M)} \end{aligned} \tag{1.2}$$

$G(f^{(M)})$ describes the objective function of the optimization problem, which defines the criterion of muscle recruitment. This function is to be minimized with respect to all unknown forces in the vector f. Various approximations are used to account for the numerical characteristics of the AMS, as it is impossible to reproduce reality exactly. The target function has multiple variations. One commonly used option to describe how the nervous system recruits muscles is through the following polynomial criterion:

$$G = \sum_i \left(\frac{f_i}{N_i} \right)^p \tag{1.3}$$

The power of the polynomial that represents the muscle synergy is denoted by p. A

higher value of p indicates greater muscle synergy, resulting in a more even distribution of forces across all muscles. The normalization factor Ni for a muscle is usually calculated based on its maximum strength f_max. Powerful muscles are required to exert more effort than weaker ones. If $p = 1$, this indicates that the AMS recruits only the minimum number of muscles required to stabilize the system, which is not physiological. Setting the p-value higher can result in a physiological state, but as the strength of the polynomial increases, the model's numerical stability decreases. For motion capture models that use ground reaction force prediction (GRFP), the default value of $p = 2$. Since no force plates were used in this study, the equation in this study is assumed to be as follows:

$$G = \sum_i \left(\frac{f_i}{N_i} \right)^2 \tag{1.4}$$

In addition to the type of muscle recruitment, there are also different muscle models in the AMS. Auer (2023) demonstrated in a study that the simple muscle model is a reliable muscle model for sprinting simulations and, therefore, for high-dynamic movements. The basic muscle model determines the muscle's strength, which uses a scaling factor known as the strength index and the muscle's physiological cross-sectional area.

The AMS is a powerful tool with a possible preventive role. Therefore, making the individual simulation results available and tangible to patients or high-risk groups is reasonable. However, motion capture recordings in gait laboratories and the complex analysis and calculation with musculoskeletal models are costly, time-consuming, and provide only a snapshot. To ensure objectivity, using only simple measurement methods to determine simplified parameters is recommended. Manufacturers of sports watches already offer initial approaches in terms of kinematics. These approaches allow measuring parameters such as stride distance, speed, and cadence. The following section will examine the advantages of this technology and describe the approaches used in this work.

1.3 Wearables and acceleration data

Wearables, encompassing various devices like smartwatches, fitness trackers, and augmented reality glasses, have become integral to modern lifestyles. Acceleration sensors, a fundamental component in many wearables, are crucial in detecting motion and orientation. These sensors, often based on microelectromechanical systems technology, measure acceleration forces in three axes, enabling precise movement tracking (Krishnan et al. 2007). In fitness trackers, acceleration sensors monitor activities like walking, running, and cycling, providing accurate data for step counting and distance traveled (Montes et al. 2020). The integration of accelerometers in wearables has also revolutionized healthcare, enabling the monitoring of body posture, sleep patterns, and fall detection for the elderly (Lin et al. 2023). As technology advances, wearables will likely incorporate more sophisti-

cated acceleration sensors, contributing to a broader range of applications and improved user experiences. The analysis of this data can be continuously improved through various forms of artificial intelligence combined with collected sensor and acceleration data. This allows patterns to be identified and targeted feedback to be given to the user. This technology and the analysis of this non-invasive data are also attracting increasing interest in biomechanics. Mundt et al. (2020) aimed to estimate joint angles and moments using inertial measurement unit (IMU) data and reached mean correlation coefficients of 0.85 for joint angles and 0.95 for joint moments. Riddick et al. (2023) focused on estimating human spine orientation using IMU data and developed a model showing that the error of motion reconstruction depends exponentially on the sampling frequency. Liang et al. (2023) figured out that an IMU can measure lower-limb kinematics during sprinting accurately but has a less accurate estimation of pelvic orientation. However, this technology has not yet been used for high-impact exercises in combination with prevention techniques for osteoporosis. For this reason, this thesis will take a closer look at the possibilities for the prevention of osteoporosis. In the following section, the questions of this thesis are presented and analyzed in the following chapters.

1.4 Hypotheses

There is sufficient evidence to suggest that physical activity, especially vigorous exercise, has a preventive effect on the development and progression of osteoporosis (Vainionpää 2007; Wolff 1892). However, there is a lack of knowledge about the exact mechanisms and the influence of different musculoskeletal components. Approaches have already shown how high and to what extent these effects need to be to affect bone health positively. However, how these effects are reflected biomechanically in the body is unclear. Musculoskeletal models are ideally suited to address these issues as they allow joint and muscle forces analysis. In addition, accelerometers are well suited to recording these impacts, providing information about the impacts experienced by the body without the need for complex measurement setups and computationally intensive simulations. Chapter 2 aims to clarify where on the body these high-impact exercises can be well measured using accelerometers and whether these positions correspond to typical wearable positions. Chapter 3 deals with the musculoskeletal and biomechanical mechanisms during these exercises. Chapter 4 aims to clarify whether linking the results of these elaborate and complex calculations to measured acceleration data alone is possible. The following hypotheses can be derived from these approaches:

1. The accelerations measured at the hip can also be measured at typical wearables positions.
2. A single sensor suitable for everyday use is sufficient to record high-impact exercises and interpret them in terms of the loads on the body.
3. It is possible to conclude possible strains on the bones purely from the acceleration data.

Chapter 2

Evaluation of acceleration data measured on the human body

This chapter deals with the hypothesis "The accelerations measured at the hip can also be measured at typical wearables positions." A part of the following chapter has been published in a similar form in the MDPI Journal sensors under Reinker et al. (2023).

2.1 Introduction

The prevalence of osteoporosis has increased significantly in recent years. World-wide, about 33 % of women and 20 % of men over age 50 will experience osteoporosis fractures (Melton et al. 1998; Kanis, Johnell, Oden, Sernbo, et al. 2000). The first projections for the year 2040 show a doubling of acute cases (Odén et al. 2015; Castrogiovanni et al. 2016). Exercise is one key preventive strategy recommended to reduce the risk of osteoporosis, falls, and fractures (Multanen et al. 2014). But physical activity decreases with age (Gomes et al. 2017; Bonewald 2019). Exit barriers and other restrictions, which can be seen during the Corona pandemic, also promote physical inactivity, even among younger people (Woods et al. 2020; Ainsworth and Li 2020). Additionally, health care services such as doctor's appointments or physical therapy were not allowed or skipped (Litke et al. 2021). To ensure lasting success, timely and comprehensive follow-up of osteoporosis patients it is necessary to monitor success or potential problems of treatment and to offer individualized rehabilitation programs to the patient (Hourigan et al. 2008; Swanenburg et al. 2003). However, regular outpatient and medical visits are very time consuming and costly. So, these current social events show that more independent ways of diagnosis and especially prevention of diseases are essential. Digitalization is a great approach to intervene here. Smart devices like wearables are selling incredibly fast and offer more and more features to monitor daily movements and interactions (IDC 2020; Rossi and Veltink 2010; TrendForce 2019), giving patients the chance to follow their

progress on demand. IMUs are a popular kind of sensor to use in such wearable smart devices. IMUs enable recording of body movements and acceleration to which the body is subjected. In the early 2000s for example, scientists tried to figure out how high-impact exercises (e.g., running, jumping, drop jumps) affect BMD especially of the femur in premenopausal (age 35-40 years) women. For that reason, all accelerations the body underwent over the day were recorded by a IMU placed at the hip for 12 months. Results showed a positive correlation between a minimum number of movements with specific high accelerations and an increased BMD in examined regions which leads to prevention of osteoporosis (Vainionpää et al. 2009; Vainionpää 2007; Vainionpää et al. 2005; Vainionpää et al. 2006; Vainionpää et al. 2007). Another study shows positive effects of a 9-month jumping intervention on BMD and content in non-osteogenic sports, such as swimming and cycling (Vlachopoulos et al. 2018). Based on these findings, this study aims to evaluate acceleration patterns of different body segments during high-impact exercises (jumps), to offer more possibilities of tracking prevention and rehabilitation programs of osteoporosis patients. The intention is to clarify at which segments or body regions impacts on the lower extremities can best be recorded during these exercises compared to findings measured at the hips. Can these loads be tracked at the locations where smart devices are typically worn, such as the wrist (smart watch), upper leg (smartphone), or sternum (chest strap)? In the long term this would allow exercises to be performed not only without supervision but also in any location and without any extra sensors. Physicians or therapists would get an overview of the patient's activity status, can evaluate the collected data and adjust the program based on progress.

2.2 Materials and Methods

2.2.1 Participants

49 participants were recruited for this study. All of them granted informed consent. Bone density peaks at around age 30. Women lose bone density faster than men. After menopause, the risk of developing osteoporosis increases in women. Therefore, the age ranges were chosen to include subjects in whom bone density tends to begin to decline, but women have not yet reached menopause. The upper age limit was standardized for all genders. Therefore, the criterions for taking part in this study were set to an age of 30 to 45 years, two hours of physical activity per week and no musculoskeletal condition and injury for the last 12 months. The idea was to limit the risk of injuries during different jumping tasks. The main kind of sports the subjects usually did were running, cycling and weight training (multiple answers were possible). Data was collected over two weeks, one week at the Laboratory for Biomechanics at the OTH Regensburg and one week at the Greifswald University Medicine. A list of subject characteristics is given in Table 2.1.

Table 2.1: Subject demographic and anthropometric characteristics. Most performed sports were queried (multiple responses were possible).

Variable	**Value**
Sex	
Female	22
Male	27
Age (years)	33.7 ± 4.2
Height (cm)	174.0 ± 7.5
Weight (kg)	74.1 ± 13.4
BMI ($\mathrm{kg\,m^{-2}}$)	24.3 ± 3.3
Sports	
Running	25
Cycling	18
Weight Training	11
Dominant Leg	
Left	3
Right	46

2.2.2 Experimental Setup

The jump exercises were recorded at 60 Hz using 17 IMUs (MVN Awinda, Xsens Technologies B.V., NL) for full-body setup, comprising a 3-axial accelerometer, gyroscope and magnetometer. The sensors were placed on the head, shoulders, upper sternum, pelvis, upper and lower legs, and feet with velcro straps. Beside the motion capture data generated via sensor fusion algorithms, specific parameters like acceleration or orientation can be analyzed separately to imitate smart devices worn on the body. A 30 cm-high wooden box served as a raise to perform the drop jumps. The procedure of the experiment was explained to the participants and their consent was obtained before recording. Demographic and anthropometric data of the subjects, such as age, gender, weight, height, were collected, additionally physically active time and previous musculoskeletal injuries in the last two years. The subjects performed different jumping tasks five times each, containing squat jumps (SJs), counter movement jumps (CMJs) and drop jumps (DJs). The exact execution of the exercises is shown in Figure 2.1. Attention should be paid to not cushion the landing by strong knee flexion for all exercises, but to keep the legs as extended as possible in order to keep the impact on the bones as high as possible (Kanis, Johnell, Oden, Sernbo, et al. 2000). The first landing/ground contact when executing the DJ is followed by a bounce hop. The second landing follows the instruction of the SJ and CMJ. In contrast to the SJ and CMJ, the jump height for the DJ is mainly achieved by reflex plantar flexion of the ankle joint with the knee angle as extended as possible. Before every exercise the right execution was demonstrated, and the subjects were allowed to do a test run first to get used to the task and the system. The subjects had to keep their

hands on their hips during the exercises. If the execution was not done right, the subjects were asked to repeat the trial.

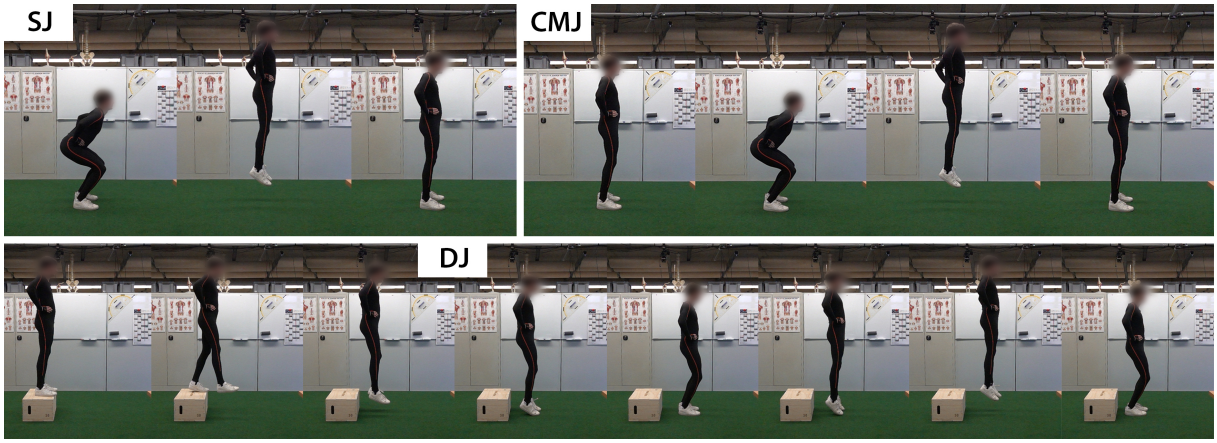

Figure 2.1: Step by step execution of the different high-impact exercises SJ, CMJ and DJ. The hands must remain on the hips during the entire execution. When landing, ensure as little cushioning as possible through knee flexion. The height of the box at the DJ is 30 cm.

2.2.3 Data Processing

Motion capture data from Xsens was reprocessed by MVN Analyze software (version 2021.2; Xsens, Enschede, The Netherlands) (MVNA). Further data processing and analysis was performed using Python (Python Software Foundation; Python Language Reference; version 3.8.3) with the packages numpy (v. 1.18.5), pandas (v. 1.0.5), seaborn (v. 0.10.1) and scipy (v. 1.7.2). Acceleration values in gravitational direction for all 17 IMUs, were extracted from the MVNA post-processed files for all subjects (49), exercises (3), and trials (5). Only accelerations in gravitational direction were considered, as the impacts of the jumping exercises are introduced into the body in the gravitational direction. The exercise of the jumps takes place without significant movements in the transverse plane. In the first step, the measurement data was cut down to the period of the actual exercise. Subsequently, trajectories of the acceleration graphs between the different sensors and the three jumping exercises were compared according to highest accelerations, as these maxima can be equated with a high impact on the body or bone. Maximum jump height for each trial was evaluated using MVNA software. In the further course, the jumping exercises were considered and evaluated separately. The Pearson correlation coefficients ρ were calculated for each possible combination of the time series of the pelvis sensor and the 16 other sensors for each subject and trial. As correlation coefficients are not unbiased, the average of several correlations will not converge to the true correlation. Therefore, the correlation coefficients are transformed with the Fisher z-transformation, then averaged and finally calculated back into the Pearson correlation coefficient. The Pearson correlation coefficients were interpreted according to Cohen (1988), where $\rho \leq 0.29$ should be

considered as low correlation, $0.30 \leq \rho \leq 0.49$ as moderate correlation and $0.50 \leq \rho$ as strong correlation (Cohen 1988).

2.3 Results

The graphs of the acceleration in gravitational direction show very similar curves for all sensors. Positive accelerations in the graphs spatially mean a movement upwards (jump) or the deceleration of the movement at the landing. Clear outliers can only be observed for the accelerations of the foot sensors. The peak accelerations here are partly 2 times that of the remaining sensors. For the DJ, however, the differences are smaller. In order to illustrate what has been described, the graphs of the accelerations for one randomly selected person are shown in Figure 2.2.

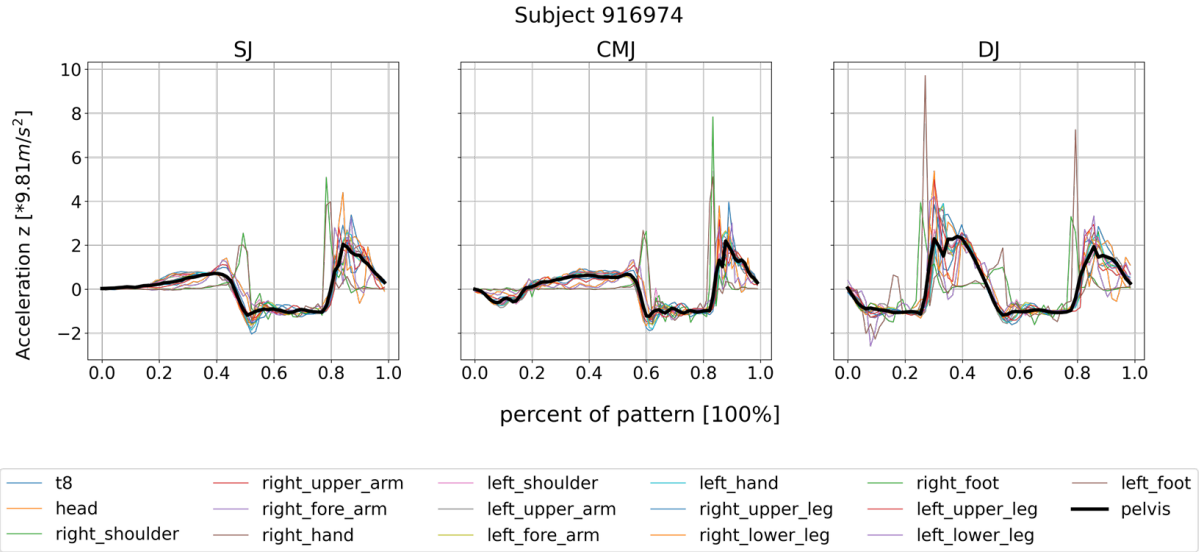

Figure 2.2: Acceleration curves of all 17 sensors during the jumping exercises, illustrated on a single subject for the third trial each. The acceleration is given as a multiple of the acceleration due to gravity.

Comparing the maximum accelerations of the sensors for each exercise, the medians for DJ are higher than for SJ and CMJ. The second highest accelerations occurred for CMJ. The comparison of the sensors for the exercises is shown in Figure 2.3. For the sensor on the left forearm (imitating a smart watch), a median of 3.23 for SJ, 3.62 for CMJ, and 4.9 times the acceleration due to gravity for DJ was obtained.

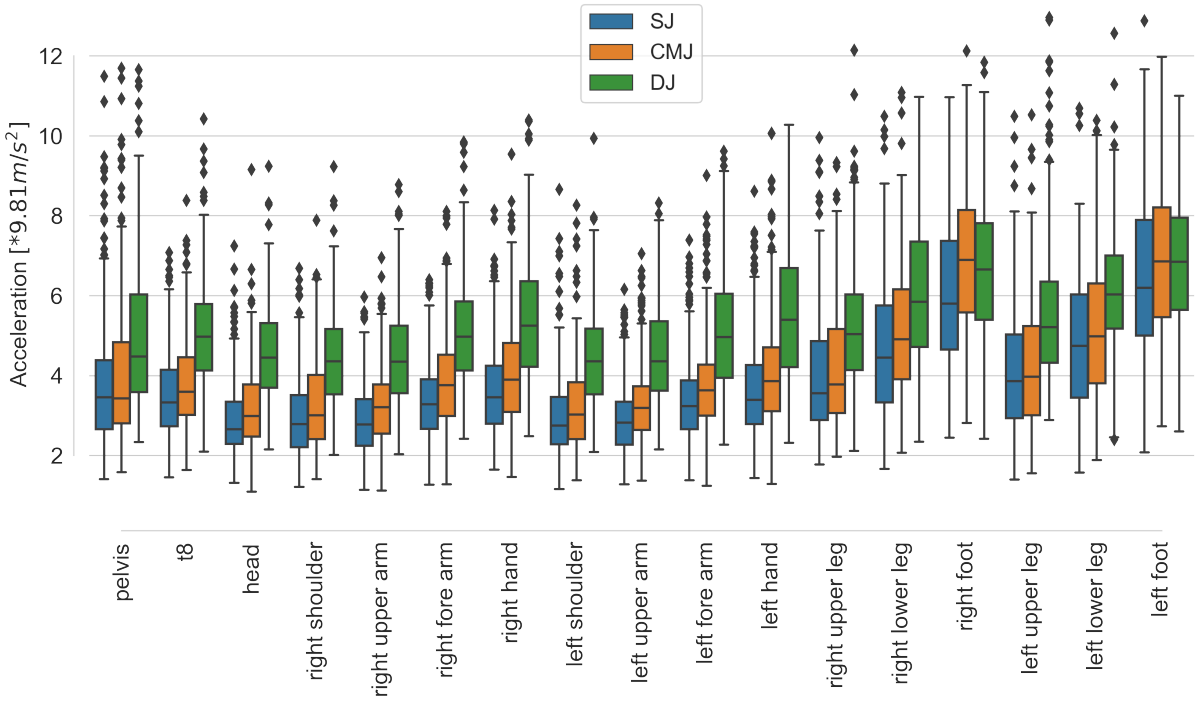

Figure 2.3: Boxplots of maximum accelerations in gravitational direction over all subjects and trials for each sensor and exercise.

The evaluation of the jump height shows that the jump height for the SJ is on average 0.37±0.06 m (min: 0.23 m, max: 0.54 m), for the CMJ 0.41±0.07 m (min: 0.3 m, max: 0.59 m) and for the DJ 0.47±0.02 m (min: 0.42 m, max: 0.55 m). In addition, it must be said that for DJ the height of fall is measured after jumping from the 30 cm high wooden box and not after the bouncing hop. The height was chosen to give the subjects a safe feeling when performing the exercise. Due to the different physical activities performed in their free time, some subjects were less familiar with jumping exercises. The aim was to keep the risk of injury low and still maintain a high impact on the bones. Pearson's correlation matrix over the whole time series shows that the measured accelerations in the direction of gravity correlate very well for all exercises between pelvis sensor and sensors at the upper body. Here, all correlation coefficients are above 0.87 (min: 0.87, max: 0.94). For the thighs, the correlation with the pelvis sensor is still above 0.83 (min: 0.83, max: 0.88). Accelerations in the lower leg correlate less well with the pelvis. The coefficients here take values between 0.66 and 0.74. The foot sensors do not correlate with the upper body with values below 0.27 (min: 0.20, max: 0.27). A heat map, pointing out the correlation strengths is shown in Figure 2.4.

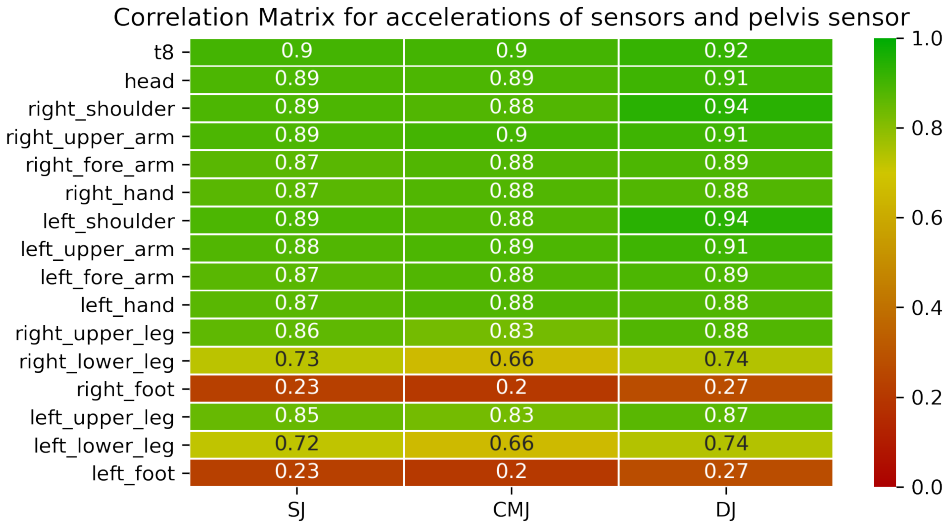

Figure 2.4: Correlation matrix for the acceleration of the pelvis sensor and one other sensor in gravitational direction for SJ, CMJ and DJ. The values correspond to the correlation of the respective sensor combinations concerning the acceleration curves for each exercise. The color scale underlines the strength of the correlation.

2.4 Discussion

The maximum acceleration at the different sensor positions shows, that the impact of the jumping exercises can be measured on all parts of the body. These results can be used as a basis for osteoporosis prevention programs and, in general, for continuous monitoring of movement using IMUs. It still leaves the possibility for the appropriate placement of sensors depending on the application and individual well-being. The DJ exerts the highest loads on the body. The lowest impacts are achieved by the SJ. This gradation can be attributed to the different drop heights, which is highest for the DJ. Another reason for the increased accelerations over the entire body is the bounce hop, in which the deceleration acceleration is mainly absorbed by the ankle joint. The knee does not flex as much here as it does in the other two exercises. There was a tendency for the mean values in this study to be lower, which can be attributed to the lower sampling rate. Vainionpää et al. (2006) used an accelerometer with a sampling rate of 400 Hz. The acceleration data in this study was acquired at a frequency of 60 Hz. This sampling rate was chosen to compare with typical values of wearables. However, when comparing the obtained values with accelerations at the pelvis from previous studies conducted for these exercises, they are in similar ranges (Vainionpää et al. 2006). The high accelerations in the foot sensors can be explained by the kinematic chain. The feet are the first segments of the body to be decelerated when landing. All other segments are cushioned distally via the intermediate joints (ankle, knee, hip) and the muscles running above them. They are also very unstable until they finally come to rest flat on the ground. The strong deviations

in the curve to the other sensors can be attributed to this. These deviations can also be seen in the correlation coefficient matrices. Sensor combinations with a foot sensor have the lowest correlations for all exercises. However, a very good correlation can be read for all combinations between pelvis and sternum, shoulders, upper arms, forearms and hands starting at values of 0.87. To reach these correlation coefficients the hands must remain on the hips throughout the exercise. None of these segments and their connecting joint angles are actively involved in cushioning the movement. Therefore, they all experience very similar accelerations on landing. Slight differences can be explained by the damping effect of the vertebral bodies or compensating movements to maintain balance. This study compares different jumping exercises whose execution is predetermined. Therefore, the results cannot be generalized. Other movements or movement patterns must be evaluated separately, as the extremities experience different accelerations during other movements. In addition, the Xsens sensors cannot be accurately compared to smart devices, even if the placement can be assumed to be the same. In this study, the sensors were fixed to the skin with velcro straps. A consistent position of the sensor is important, as can be assumed with a smartwatch, for example. Smartphones, on the other hand, are not so well suited, as they have leeway in the trouser pocket, which can lead to wrong results. Specifications of wearables must be observed before use. They must be able to record the same parameters and these parameters should also be retrievable to evaluate the performed exercises. The characteristics of the test persons were very different in this study. Especially the different physical conditions and training levels should be emphasized, which made a controlled execution of the exercises difficult due to a lack of coordination and jumping power. Having this wide range of subjects, reinforces the high correlations that can be seen in the correlation matrix.

2.5 Conclusions

The study shows that the accelerations measured at the pelvis during jumping exercises can be tracked very well on the upper body and upper extremities. This includes the locations where smart devices are typically worn, such as the wrist (smart watch) or sternum (chest strap). Sensors positioned at the thighs do not offer as good correlations as the upper body and extremities but are still strong. When performed correctly, it does not matter which segment the sensor is placed on. As shown in past studies, these jumping exercises are sufficient to have a positive effect on bone density and thus a preventive effect on osteoporosis. The impact and effects of these exercises on the legs is difficult to deduce from the accelerations on the upper body. Here, a more farreaching consideration is necessary considering the acting joint and muscle forces for a validation, in order to analyze further statements around the preventive mechanisms and impacts on the femur. This is done in the following chapter.

Chapter 3

Comparison of musculoskeletal loads in proximal femur during low-impact and high-impact exercises

This chapter deals with the musculoskeletal and biomechanical mechanisms caused by high-impact exercises to clarify the hypothesis that "A single sensor suitable for everyday use is sufficient to record high-impact exercises and interpret them in terms of the loads on the body" in Chapter 4.

3.1 Introduction

The study about the "Evaluation of acceleration data measured on the human body" presented in Chapter 2 showed that the accelerations on the upper body and upper extremities might be used for tracking high-impact exercises for prevention programs for osteoporosis. This chapter deals with the preventive mechanisms and impacts on the femur. To better understand these mechanisms, it is important to evaluate the forces and loads the femur experiences during high-impact exercises. Numerical methods, such as the finite element method, allow the calculation of stresses and deformations of the femur under various loads. This has been analyzed in numerous studies. Faisal and Luo (2015) used image-based finite element (FE) analysis to investigate stress variations in the proximal femur during single-stance and sideways falls and drew conclusions about the higher risk of hip fracture from sideways falls in older people. Levadnyi et al. (2021) compared femur strain under a wide range of loading conditions to cover the directional range of the hip joint forces. The study showed that surface strain magnitude and stiffness vary significantly under different loading conditions. To my knowledge, no studies have been conducted on calculating and evaluating stress in the femur using finite element methods during high-impact exercises, such as jumping or running. However, numerous

publications have been published on the effects of these exercises and plyometrics on bone density. Dual X-ray absorptiometry (DXA) is frequently used to analyze this. Rodricks et al. (2024) and Florence et al. (2024) summarise the effects of high-impact exercises on BMD in their meta-analyses. The most common sites of increased BMD were the femoral neck with a significant small-moderate effect and the total hip and trochanter with a significant effect of jump training only in younger adults. The studies analyzed and compared exercise groups with control groups. The exercise groups performed high-impact exercises at regular intervals over defined periods of time. Bone density was measured before, partly during, and after the exercise period and then analyzed. Therefore, effects could be recorded. A small to moderate effect on BMD of the femoral neck was observed with moderate certainty when the average jump load of 50 jumps was performed four times per week. The exact mechanisms following the impacts and responsible for the changes are not specified and appear to be site-specific. Musculoskeletal simulation approaches can be used to model bone geometries, joint structures, and muscle attachment points based on anatomical data. This enables a more precise understanding of force and moment distributions between bones and muscles. Since these effects of force distribution presumably have a significant influence on BMD, the aim of the study is to analyze and evaluate the musculoskeletal loads in the proximal femur during low-impact exercises (walking, stair climbing) and high-impact exercises (running, counter movement jump, box jump). The focus will be on the areas where differences occur and how these can be anatomically attributed to preventative effects and changes in relation to osteoporosis.

3.2 Materials and Methods

3.2.1 Participants

This study involved 211 subjects who gave their informed consent. Inclusion criteria for this study were an age range of 18-45 years to be within the range of the highest BMD and to exclude the possible time of menopause. In addition, subjects should have no previous musculoskeletal conditions and should have been free of lower extremity injury for the previous 12 months to minimize the risk of injury. Recruitment took place at a university, so most participants were students. The measurements were performed at the OTH Regensburg. The study was conducted following the Declaration of Helsinki and approved by the Ethics Committee of the University of Regensburg. A list of the anthropometric and demographic data collected can be found in Table 3.1.

3.2.2 Experimental Setup

The exercises were recorded using an optical markerless motion capture system (CapturyLive v255, The Captury, DE). A total of 8 machine vision cameras (FLIR Blackfly

Table 3.1: Subject demographic and anthropometric characteristics.

Variable	**Value**
Sex	
Female	90
Male	121
Age (years)	24.5 ± 5.3
Height (cm)	177.8 ± 9.8
Weight (kg)	74.3 ± 13.9
BMI ($\mathrm{kg\,m^{-2}}$)	23.3 ± 3.1
Dominant Leg	
Left	32
Right	179

S16S2C, Teledyne FLIR LLC, USA) at a recording rate of 60 Hz and 1440 p * 1080 p were used to cover a measurement volume of approximately 6 m * 4 m with an approximate relative resolution of 2 px/cm. Three cameras were mounted on the short sides and one in the middle of the long side at a height of 2.50 m. The cameras were calibrated using a grid board to determine the distortion of the optics and the alignment of the cameras to each other. The origin is defined using the grid board located at the center of the measuring volume and is kept consistent for all exercises. In addition, each subject was fitted with an IMU (Xsens, Xsens Dot) on the hip to record vertical accelerations/impacts—the acceleration sensor measured at a frequency of 120 Hz. A walking/running track of 6 m length was marked in the center of the measurement volume. Outside of the measuring volume, 2 m were made possible as inlet and outlet sections in front of and behind the track. The length was chosen to allow at least two complete gait cycles to be recorded within the measurement volume. The box and stairs required for the box jump and stair climbing were marked on the side of the track to ensure the same output every time. The measurement setup is shown in the following Figure 3.1.

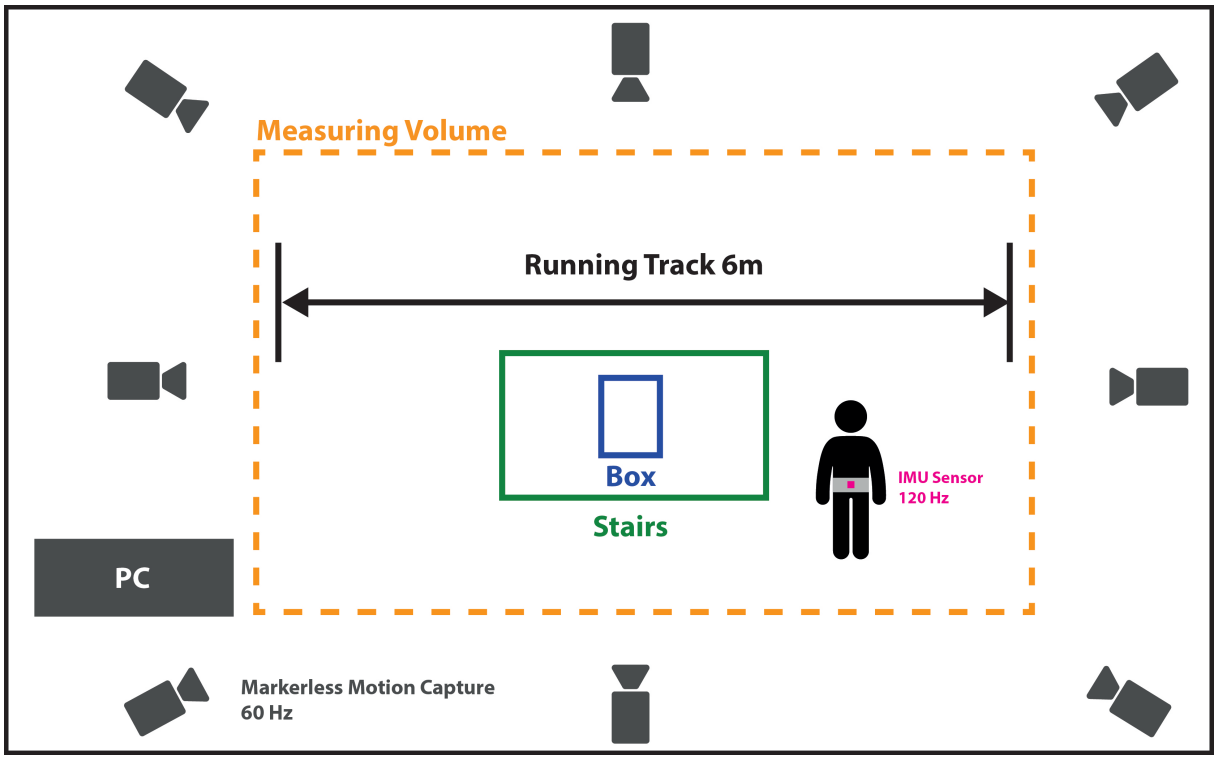

Figure 3.1: The measurement volume enclosed by the cameras of the markerless motion capture system is marked in orange and measures approximately 6 m * 4 m. The track runs the full length of the measurement volume. The stairs and the box are slightly offset from the track. The subject wears an IMU sensor, attached above the pelvis with a Velcro strap.

First, all significant anthropometric and demographic data was recorded. Then, the subjects were asked to complete the track four times at a self-selected speed adapted to their everyday walking speed. The measurement was not stopped at the turning points. The test subjects were asked to turn around independently and continue walking until they had covered four times the distance. The same exercise was then carried out at a self-selected running speed. The subjects performed two jumping exercises. They were instructed to place their hands on their hips for the counter movement jump, and the correct execution was demonstrated. Invalid jumps were repeated immediately. Next, the box was placed in the measurement volume, and the subjects started on the box with their hands on their hips. The subjects stood on their dominant leg with the non-dominant leg bent and jumped off the box, landing only on their dominant leg. They were required to maintain balance for an additional two seconds. Each type of jump was repeated three times. The subjects were then asked to walk up and down a staircase with three steps, both up and down. They were then instructed to stop on the plateau and start the descent with the non-dominant leg to maintain consistency. This exercise was repeated three times. Figure 3.2 shows the exact exercise sequences.

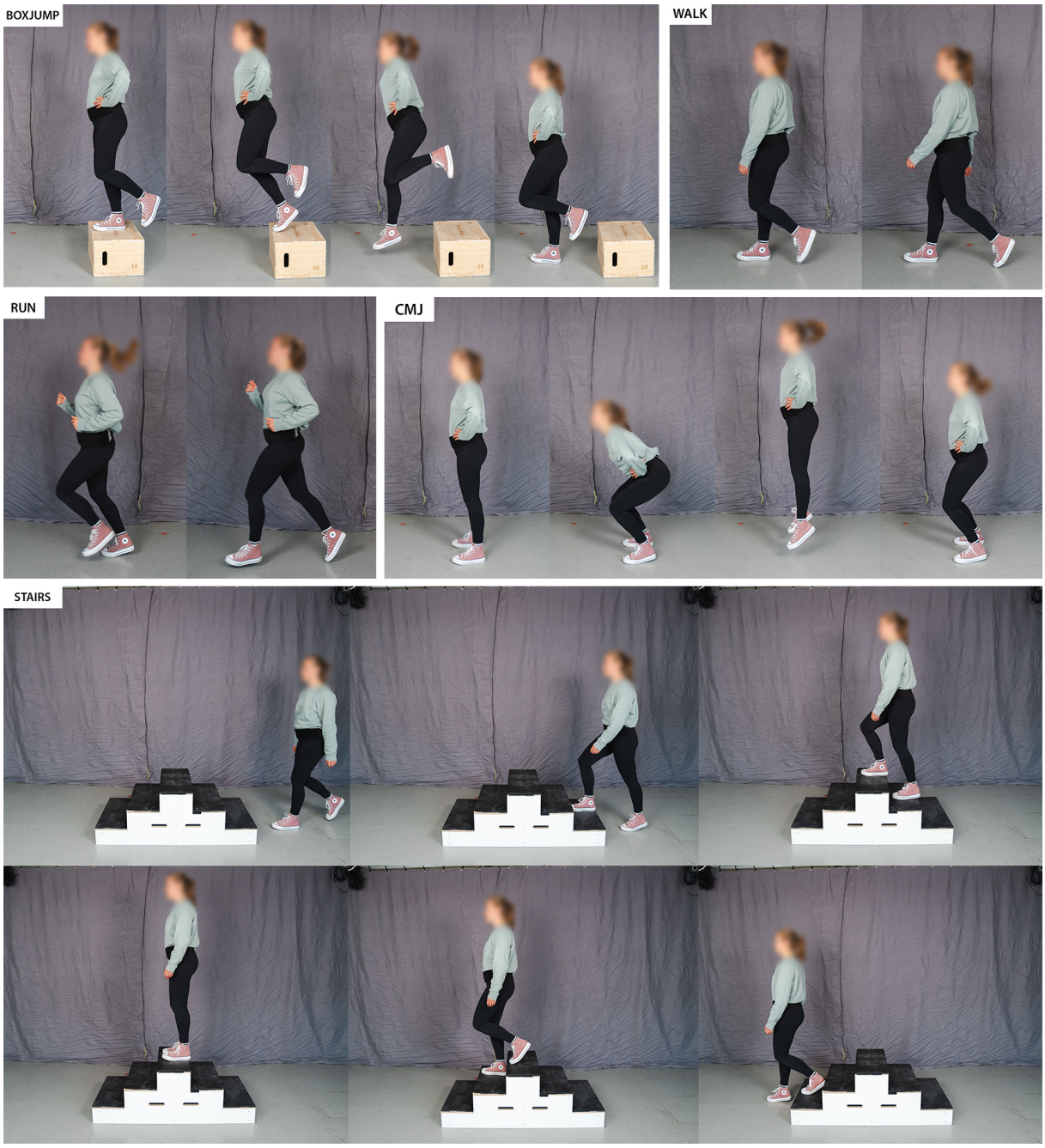

Figure 3.2: The box jump, walk, run, CMJ and stairs exercises are demonstrated step-by-step to illustrate correct execution.

3.2.3 Musculoskeletal Simulation

In the introduction to this work, reference has already been made to the state of the art and the principles of musculoskeletal simulation in general, with the help of inverse dynamics in the AMS. In order to ascertain the strain in the femoral neck, the cutting forces and moments must be determined. The AMS enables the calculation of these values by specifying a reference coordinate system and the decisive forces and moments for these values. Therefore, it is necessary to specify the muscle forces of the aforementioned

muscles and the joint forces in the hip. The reference point for the cutting reactions is specified as the center point between the "Vastus Lateralis Superior" attachment point and the reference coordinate system of the hip joint. This implies that the reference point is consistently adjusted in a uniform manner relative to the scaling of the individual models. The coordinate axes extend from the reference point in the direction of the hip joint reference coordinate system and in the anterior direction, and the third axis is perpendicular to the other two axes in a right-handed coordinate system. The definition of the reference point and the calculation of the internal forces and moments in the AMS can be found in Appendix A - Listing B.1. To determine the strain in the femoral neck, several steps are required, and the following simplifications are assumed: First, a section is made perpendicular to the main axis of the femoral neck. The cross-sectional area shows a composition of the femoral neck consisting of cortical bone as the outer layer and the trabecular bone on the inside. In order to determine the load, a bending load case is assumed, more precisely, the case of an oblique bending. For an initial overview, however, the individual components of the inclined bending are analyzed separately, in each case, regarding the defined coordinate system axes perpendicular to the main axis. The geometry of the cross-section is simplified to a hollowed-out circle. The dimensions for the diameter and the thickness of the edge, which correspond to the thickness of the cortical bone, are taken from Djonic et al. (2011), Nissen et al. (2005) and Kaptoge et al. (2003). Figure 3.3 illustrates the simplified geometry.

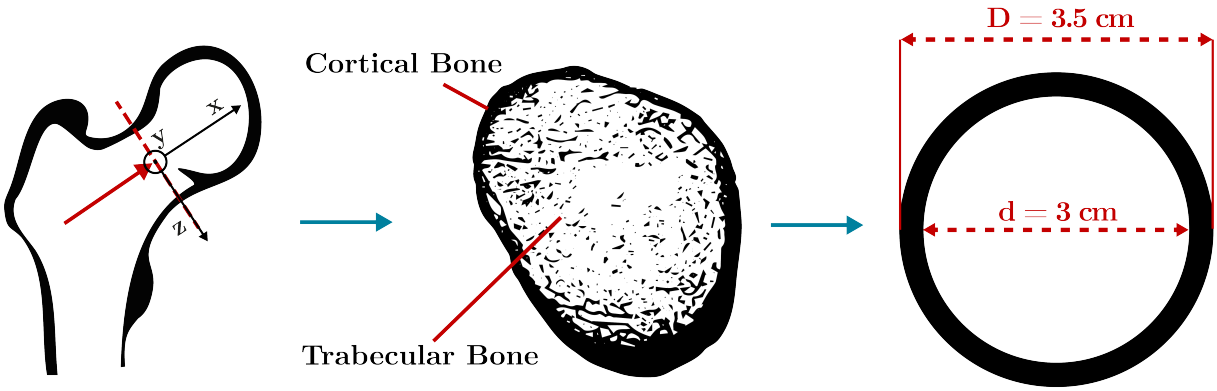

Figure 3.3: Simplified geometry of the cross-section of the femoral neck for calculating stresses and strains

.

The following formulas 3.1 and 3.2 are used to calculate the edge fibre stresses.

$$\sigma_y = \frac{N_x}{A} \pm \frac{M_y}{I_y} * z \tag{3.1}$$

$$\sigma_z = \frac{N_x}{A} \pm \frac{M_z}{I_z} * y \tag{3.2}$$

with I as area moment of inertia

$$I_y/I_z = \frac{\pi * (D^4 - d^4)}{64} \tag{3.3}$$

and N as a normal force in the main axis direction, A as the area on which the normal force acts, M_z as moment around the z-axis, M_y as moment around the y-axis and z or y as the distance from the center of the surface to the edge fiber. In the next step, the oblique bending was considered as a combination of the two isolated bendings (3.4). The tensile and compressive stresses at the edge fibers are considered here.

$$\sigma = \frac{N_x}{A} \pm \frac{M_z}{I_z} * y \pm \frac{M_y}{I_y} * z \tag{3.4}$$

The strains were then calculated (3.5) from the stresses using the Young's modulus of cortical bone E = 19,000 MPa in order to compare it with the values from the literature (Zysset et al. 1999; Turner et al. 1999; Bayraktar et al. 2004). The corresponding code for calculating these parameters in Python can be found in Appendix B - Listing B.2.

$$\epsilon = \frac{\sigma}{E} \tag{3.5}$$

3.2.4 Data Processing

Kinematics of the whole body are tracked automatically by using CapturyLive (v255, The Captury, DE) on the principles of silhouette/color recognition (Bottino and Laurentini 2004; Mündermann et al. 2006) and background subtraction (Piccardi 2004) to gain information about segment lengths, joint positions, and angles of a virtual skeleton (Stoll et al. 2011). The information for each trial is saved in a separate C3D file. The AnyPyTools (v. 1.11.4) tool allows loading motion capture data into the AMS from Python (Python Software Foundation; Python Language Reference; version 3.8.3) and starting simulations, enabling batch processing with the same parameters set in the AMS. The workflow was adapted to the study of (Auer et al. 2024), who compared the kinematics of the markerless motion capture system with a marker-based one. The kinematic input for the model was not filtered to keep the impacts in the data. The results of the simulations were then each saved in an h5 file, a hierarchical data format (HDF) that enables the storage of large amounts of data. Further data processing and analysis were performed using the Python packages NumPy (v. 1.18.5), Pandas (v. 1.0.5), seaborn (v. 0.10.1), and SciPy (v. 1.7.2).

3.2.5 Data Analysis

To use the kinematic data in the AMS, the video recordings of the tests were viewed individually and shortened to the actual exercise. This meant that movements were not analyzed before and after the exercise, at the edge or outside the measurement volume. The stair climbing exercise was divided into ascending and descending. With the input parameters of kinematics - from the motion capture system, anthropometry - collected at the beginning of the measurement, and the defined start and end times, all the exercises could be simulated via batch processing in the AMS. After running the inverse dynamics in the AMS, the ground reaction forces are considered for each exercise. These values can further reduce the data to the time domain. The part of the exercise where the body experiences the impact is selected. In this way, accelerations and muscle forces experienced by the body during jump-off, for example, are ignored in this study in order to give a clear statement. Even though the excluded time ranges were not considered in this part of the work, they were simulated to see if they were relevant to further consideration and merging of the kinematic and kinetic data. The following figures Figure 3.4, Figure 3.5, Figure 3.6, Figure 3.7, Figure 3.8 and Figure 3.9 explain which areas have been considered. The ground reaction forces in these figures are depicted perpendicular to the ground, in the direction of gravity, representing the impact time. The red lines indicate the evaluated area. The CMJ comprises four phases: pre-jump, take-off, flight, and landing. The study focuses on the landing phase of the CMJ, which is where the body experiences the most significant impact. Figure 3.4 displays the ground reaction forces for a CMJ. For all subjects, the evaluated range was set to the first ground contact, regardless of the foot, up to half a second (30 frames) afterward.

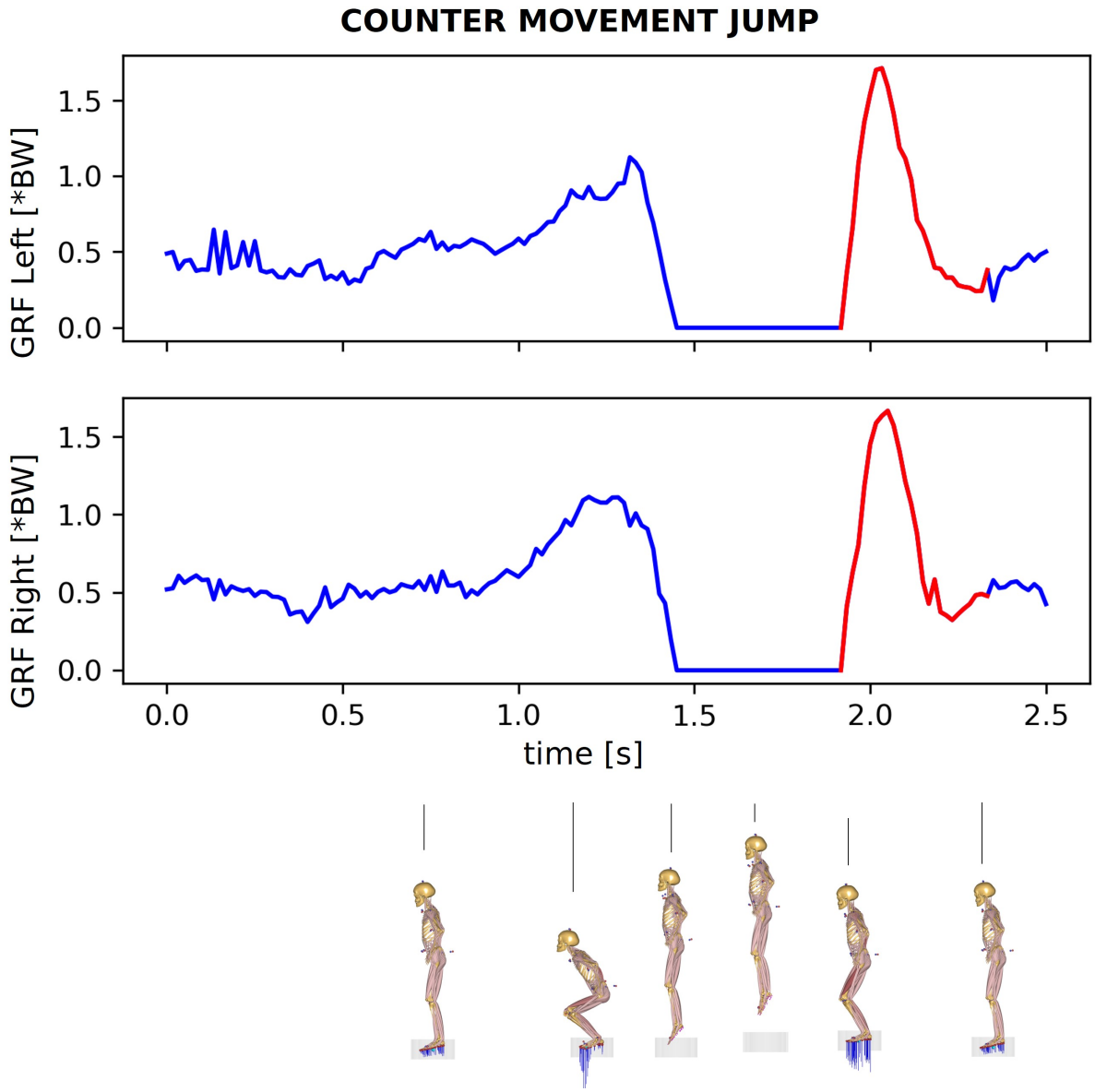

Figure 3.4: Relevant range of the CMJ that is required for analyzing the impacts. The graphs show the course of the ground reaction forces for the left and right foot. The area marked in red is the selected range.

The box jump is a three-phase exercise that includes take-off, flight, and landing. Only the dominant leg is loaded in this exercise, focusing solely on the landing. Figure 3.5 displays the ground reaction forces for a box jump. For all subjects, the evaluated range was set to the first ground contact, regardless of the foot, up to half a second (40 frames) afterward to include the equalizing movement.

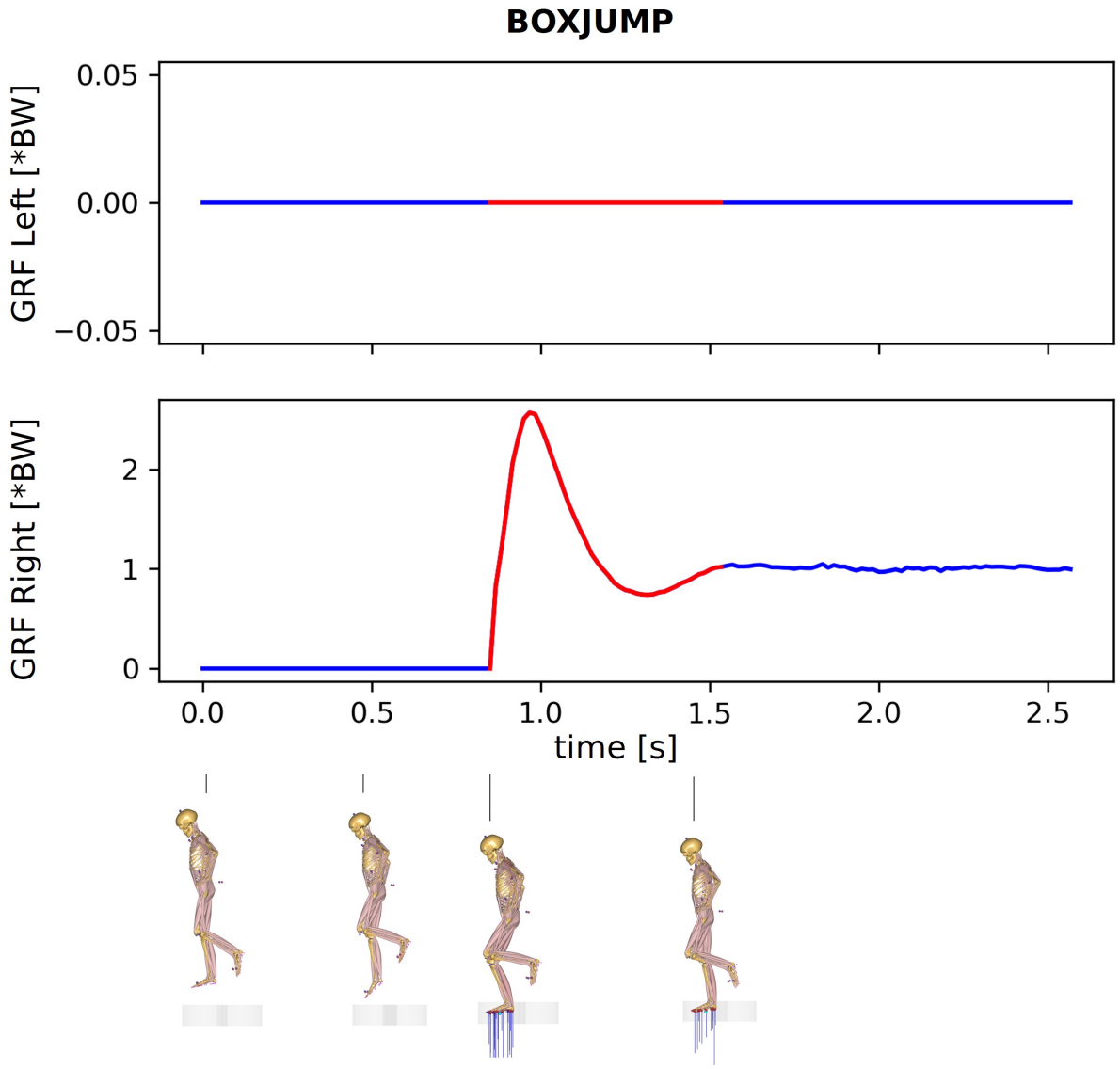

Figure 3.5: Relevant range of the box jump that is required for analyzing the impacts. The graphs show the course of the ground reaction forces for the left and right foot. The area marked in red is the selected range.

The walk/gait is divided into a stance phase, where the foot is in contact with the ground, and a swing phase, where the foot is lifted and moved forwards for each foot. These phases are anticyclical for the left and right foot. Figure 3.6 displays the ground reaction forces for a walk. For all subjects, the evaluated range was set to the first ground contact of the dominant leg, up to right before the first ground contact of the next gait cycle of the dominant leg.

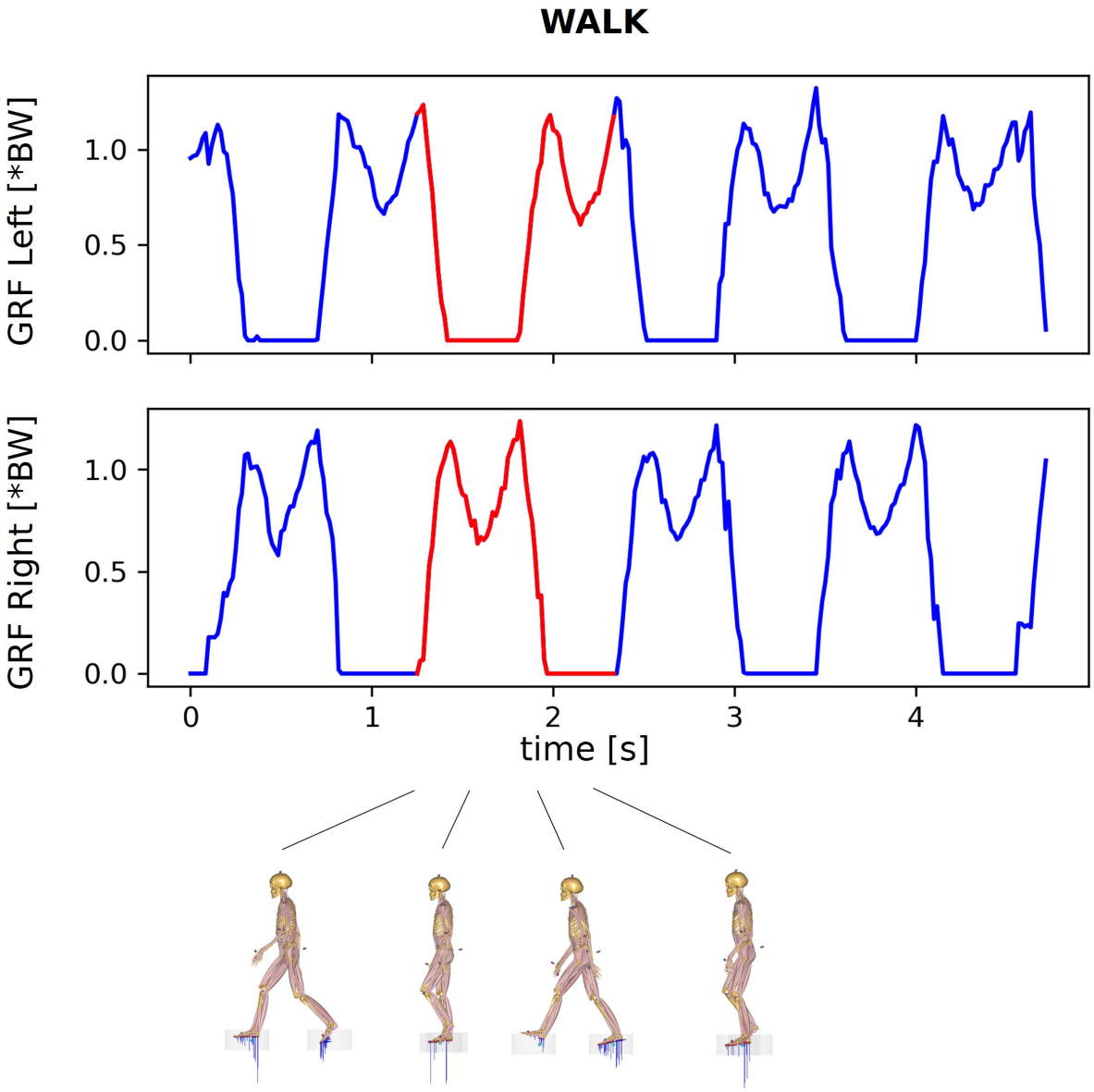

Figure 3.6: Relevant range of the walk that is required for analyzing the impacts. The graphs show the course of the ground reaction forces for the left and right foot. The area marked in red is the selected range.

Like the gait, the run is divided into a stance phase, where the foot is in contact with the ground, and a swing phase, where the foot is lifted and moved forward for each foot. These phases are anticyclical for the left and right foot. However, the curve of the GRF differs here from that of the gaits. The phases are significantly shorter, and the rolling motion mainly occurs via the midfoot and forefoot. Figure 3.7 displays the ground reaction forces for a run. For all subjects, the evaluated range was set to the first ground contact of the dominant leg up to the right before the first ground contact of the next gait cycle of the dominant leg.

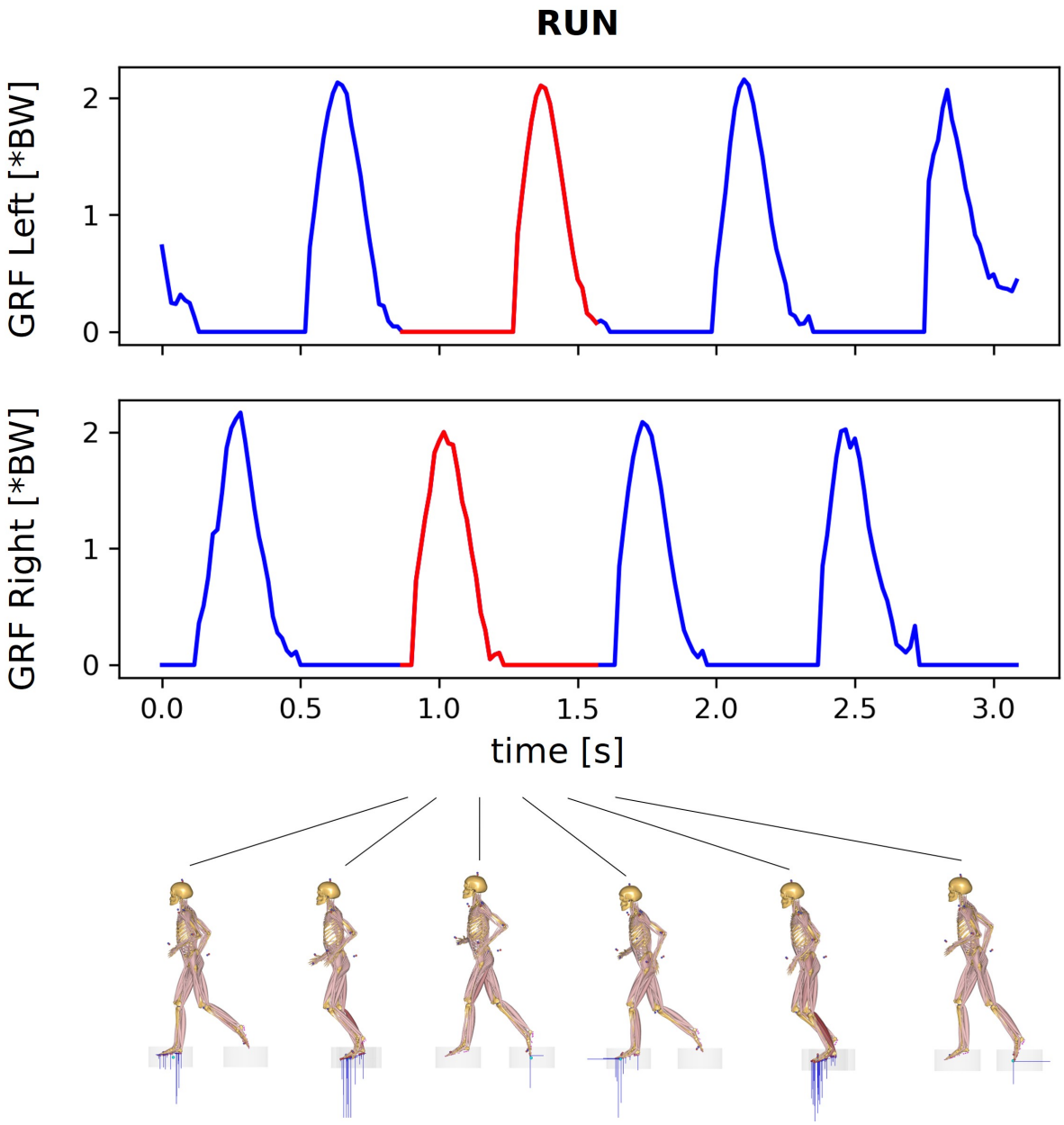

Figure 3.7: Relevant range of the run that is required for analyzing the impacts. The graphs show the course of the ground reaction forces for the left and right foot. The area marked in red is the selected range.

Stair climbing is also divided into stance and swing phases for each foot. These phases are anticyclical for the left and right foot. In this case, only one height difference needs to be overcome. Figure 3.8 displays the ground reaction forces for going up and Figure 3.9 for going down stairs. For all subjects going up the stairs, the evaluated range was set to the first ground contact on the first step, right before the stance phase at the top. For all subjects going down the stairs, the evaluated range was set to the first ground contact on the first step way down, up to the right before the stance phase at the bottom.

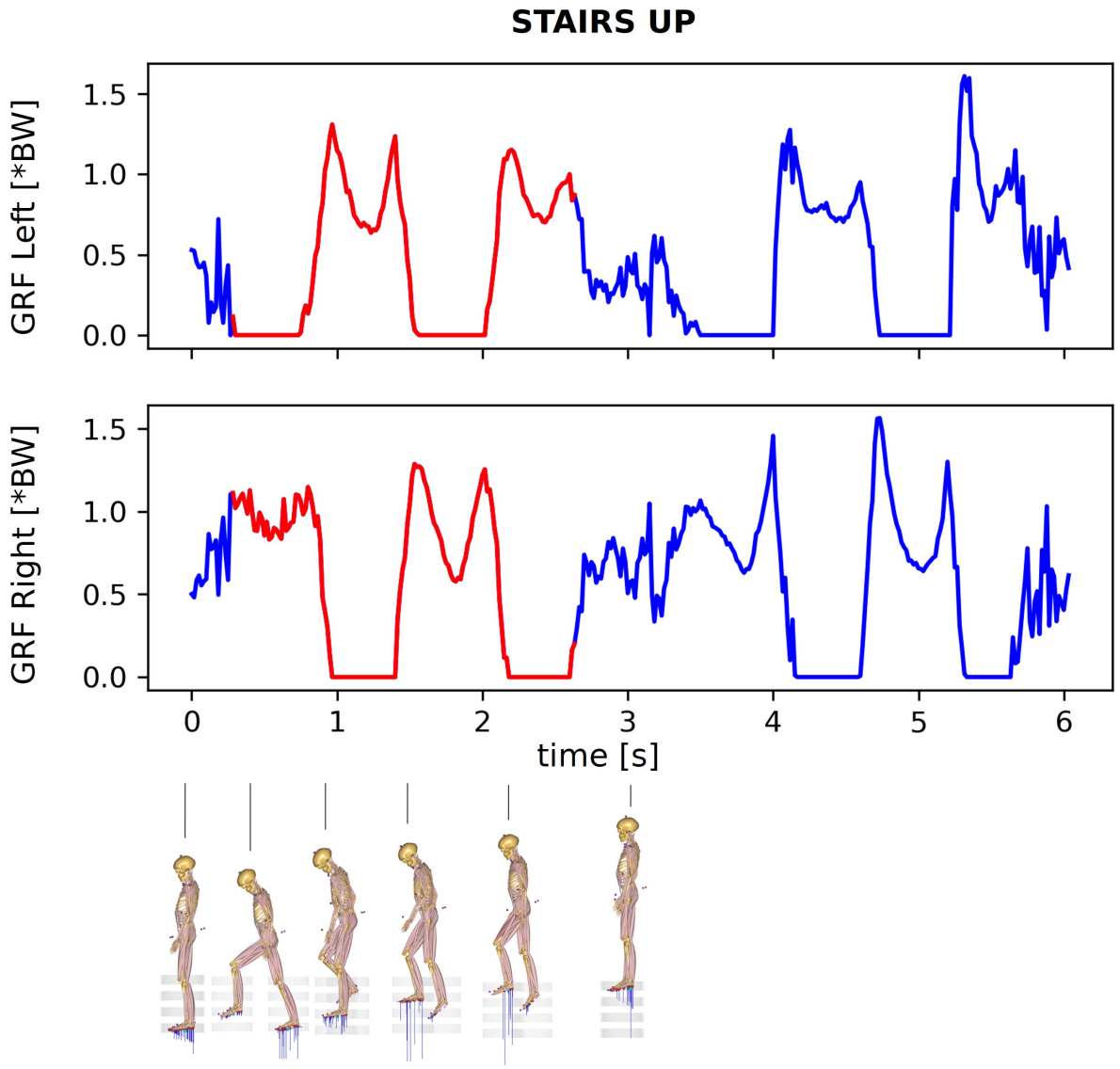

Figure 3.8: Relevant range of the descending stairs that is required for analyzing the impacts. The graphs show the course of the ground reaction forces for the left and right foot. The area marked in red is the selected range.

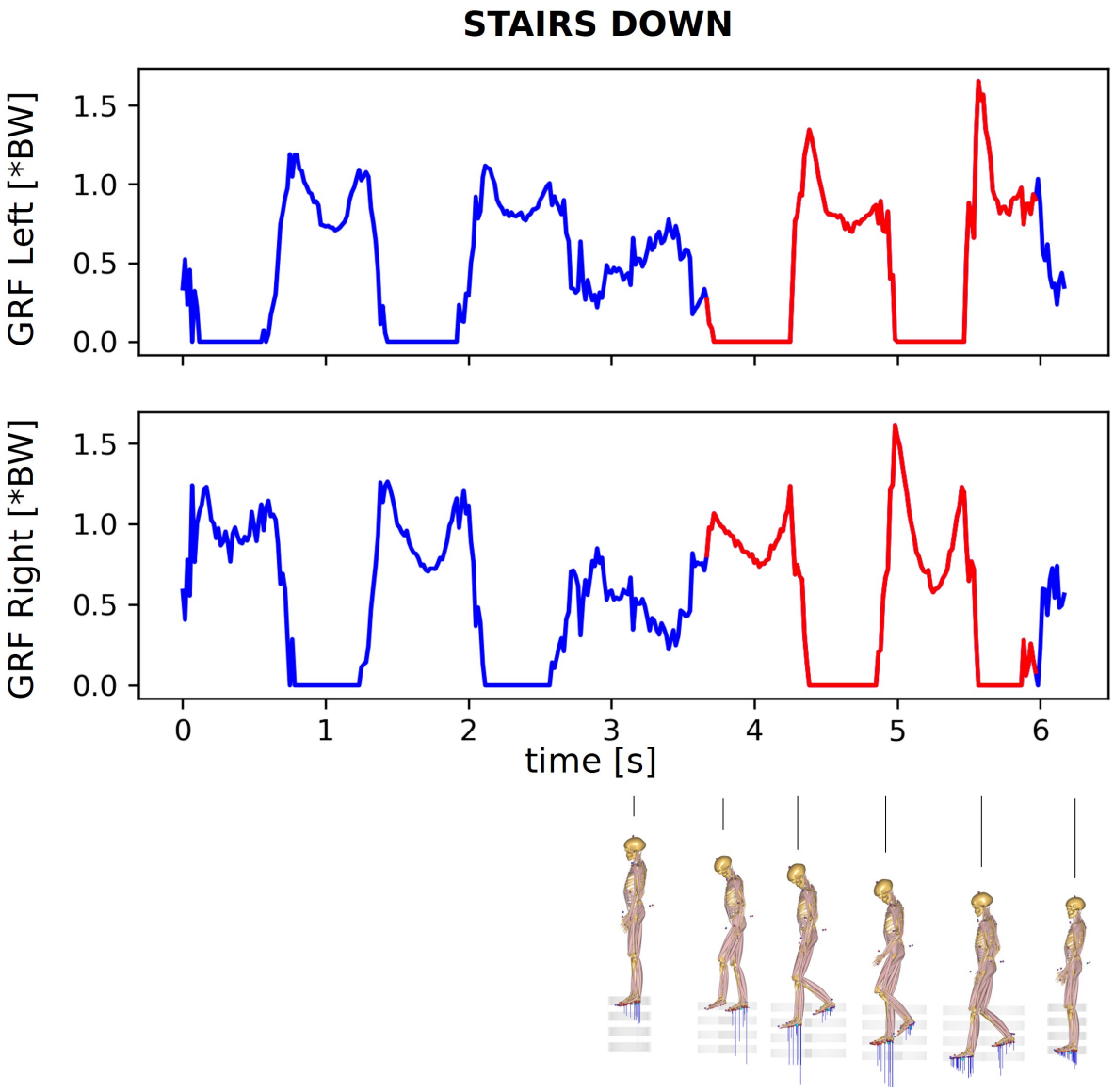

Figure 3.9: Relevant range of the stair climbing that is required for analyzing the impacts. The graphs show the course of the ground reaction forces for the left and right foot. The area marked in red is the selected range.

3.3 Results

The faulty tests were sorted out before the actual evaluation could be carried out. These included incorrect tracking of the subjects by the motion capture system due to clothing that was too loose or a lack of contrast between the clothing and the background, as well as errors in marker tracking or failing inverse dynamics in the AMS. Most of the errors were caused by an incorrect calculation of the ground contacts and, thus, the reaction forces. The following Table 3.2 shows the number of errors excluded from the analysis. The walk achieved the lowest rate of usable trials with 84.4 % of all trials.

Table 3.2: Number of recorded trials per exercise and the number of analysed trials after sorting out incorrect trials.

	Trials per exercise	Total number of trials	Number of trials analyzed	Rate of analyzed trials
cmj	3	633	580	91.6 %
box jump	3	633	562	88.8 %
run	4	844	744	88.1 %
walk	4	844	712	84.4 %
stairs up	3	633	543	85.8 %
stairs down	3	633	543	85.7 %

All further calculations and results refer to the dominant leg indicated by the subjects. Under this definition, a standardized evaluation is only possible because the box jump is performed on the dominant leg.

Ground reaction forces

The GRF were calculated as part of the inverse dynamics in the AMS. They provide an insight into which forces and, therefore, impacts are exerted on the dominant leg by the exercises. They are the basis for all other force calculations in the body (e.g., muscle forces, joint reaction forces), as they define the force boundary conditions of the body in relation to the environment. If you look at the calculated GRF of the individual exercises, you can see that the highest values are achieved in the box jump with a median of the maxima of 2.64 times the body weight. This is followed by the run at 2.18 times, the CMJ at 1.46 times, descending stairs at 1.42 times, climbing stairs at 1.24 times, and the walk at 1.23 times. Table 3.3 shows these median values with the corresponding quartiles.

Table 3.3: Ground reaction forces for the dominant leg in gravitational direction with the corresponding quartiles.

	GRF (grav. dir.) [*BW]	**quartiles**
cmj	1.46	[1.26, 1.72]
box jump	2.64	[2.50, 2.81]
run	2.18	[2.02, 2.29]
walk	1.23	[1.18, 1.28]
stairs up	1.24	[1.19, 1.31]
stairs down	1.42	[1.32, 1.52]

Stresses and strains at the femoral neck

The marginal fibre stresses were first considered separated in the different anatomical directions of impact. All maximum values were calculated in both the positive and negative edge fibre directions for the supero-inferior and antero-posterior directions for each

exercise. The values obtained were then negatively tested for normal distribution. Therefore, the respective median of the maximum values with quartiles were used for further consideration. The results of these calculations are shown in Table 3.4. It can be seen that both tensile and compressive stresses are present in the supero-inferior direction. The compressive stresses in the edge fibre are most pronounced in the box jump with 97.8 MPa, followed by the run with 74.7 MPa. This is followed by the stair climb and the walk with about 49 MPa each. The lowest compressive edge fibre stress was calculated for CMJ with 34.4 MPa. The gradation is the same for the tensile edge fibre stress. Here the highest value is 60.8 MPa for the boxjump and the lowest value is 21.2 MPa for the CMJ. In the antero-posterior direction, the box jump also has the highest value with 36.2 MPa. This is followed by the run with 27.3 MPa, the stair climb with 23.5 MPa, the stair walk with 20.0 MPa, the walk with 15.6 MPa and lastly the cmj with 8.6 MPa. In the positive direction of the edge fibres all values are around 0 MPa, i.e. there is neither tensile nor compressive stress.

Table 3.4: The femoral neck's tensile and compressive edge fiber tensions are divided into supero-inferior and anteroposterior directions for the respective exercises. The values correspond to the median of the maximum values for each exercise and are given in MPa with the corresponding quartiles.

	Supero-Inferior		**Antero-Posterior**	
	Tension [MPa]	Compression [MPa]	Compression/Tension [MPa]	Compression [MPa]
cmj	21.2 [16.6, 27.4]	-34.4 [-43.3, -27.0]	-2.7 [-4.5, -1.4]	-8.6 [-11.2, -6.5]
box jump	60.8 [49.5, 71.8]	-97.8 [-112.5, -81.4]	0.6 [-2.4, 4.5]	-36.2 [-42.8, -30.2]
run	43.1 [34.0, 52.7]	-74.7 [-89.4, -59.9]	-2.0 [-4.6, -0.2]	-27.3 [-33.1, -21.6]
walk	29.0 [22.7, 35.7]	-47.7 [-58.1, -38.5]	-1.1 [-2.7, 0.2]	-15.6 [-18.8, -13.0]
stairs up	30.1 [23.1, 38.2]	-51.3 [-62.8, -41.2]	2.3 [0.6, 3.9]	-23.5 [-27.6, -19.3]
stairs down	28.5 [23.0, 35.1]	-47.4 [-56.7, -38.6]	3.4 [1.4, 5.1]	-20.0 [-24.0, -16.7]

To better visualize the spatial direction and magnitude of the stresses, the following figures show the stresses in the supero-inferior (Figure 3.10) and antero-posterior (Figure 3.11) directions in a bar plot.

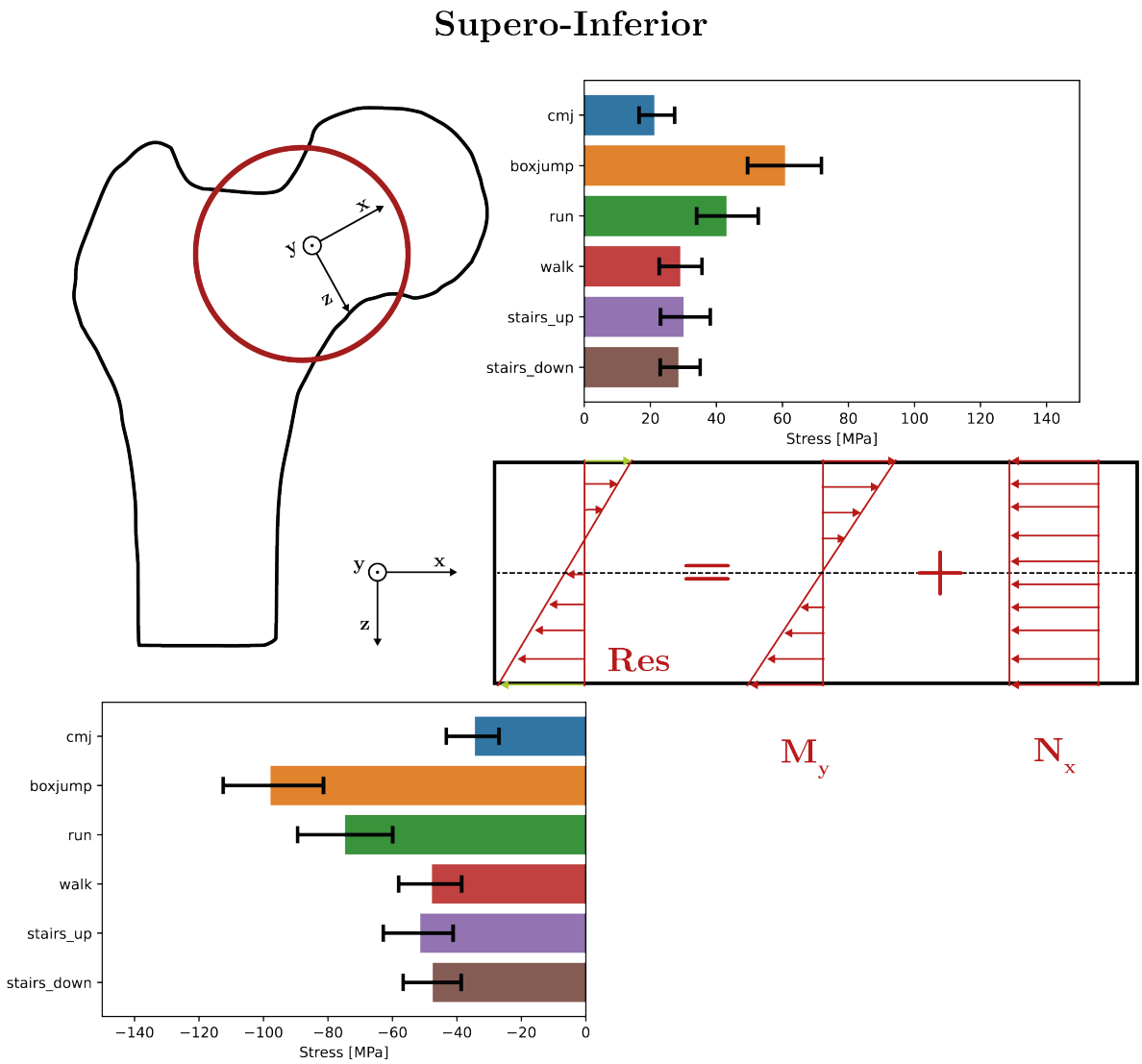

Figure 3.10: Bar plot with the calculated maximum edge fiber stresses in the supero-inferior directions in MPa. The femoral neck is shown as a silhouette. The red circle marks the area that is the subject of further calculations. The coordinate system defines the spatial directions of the calculated stresses. The principle and effect of bending under the influence of a normal force are shown between the bar plots. The green arrows represent the edge fibers for which the stresses are shown in the bar plots above and below.

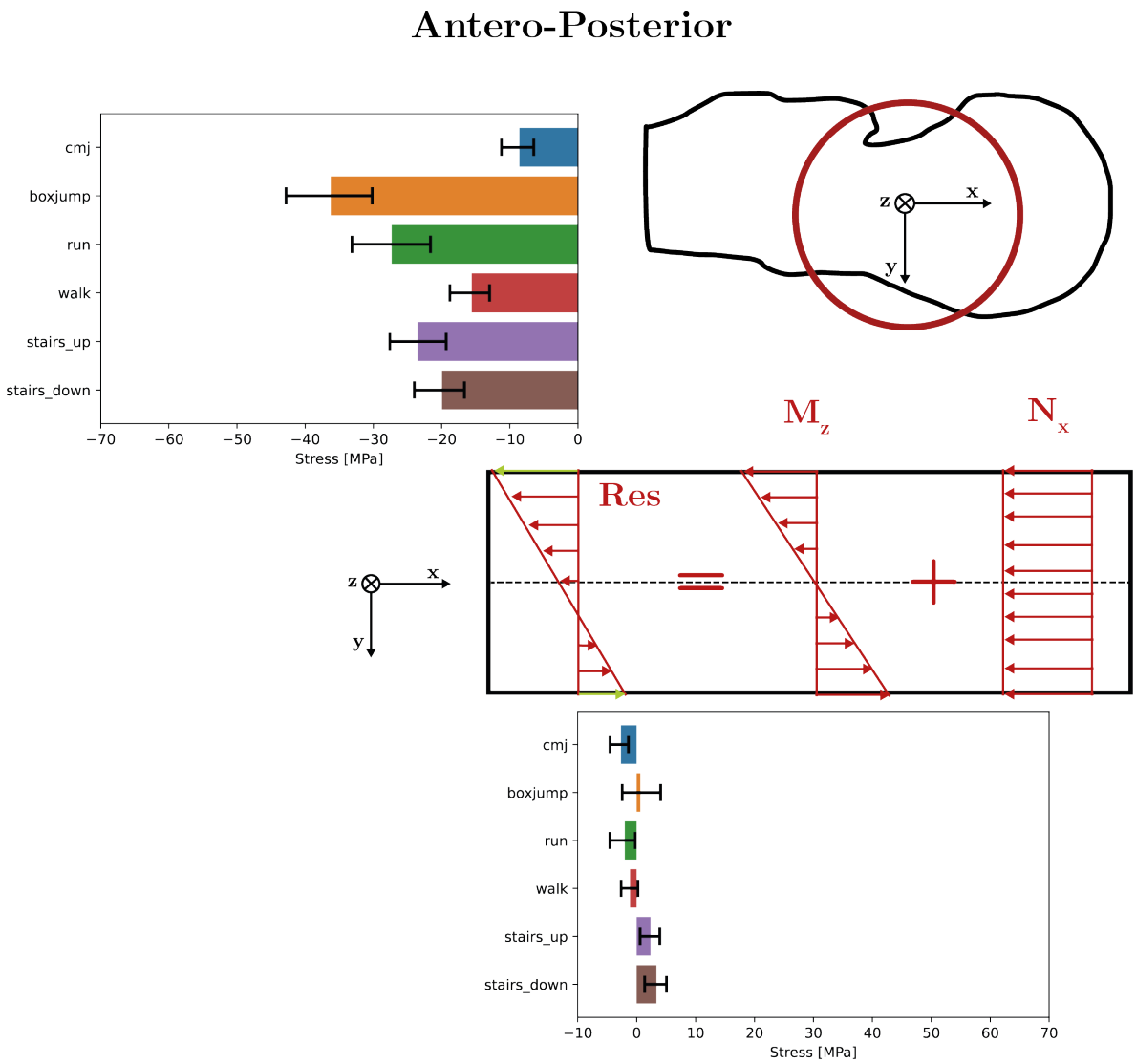

Figure 3.11: Bar plot with the calculated maximum edge fiber stresses in the antero-posterior directions in MPA. The femoral neck is shown as a silhouette. The red circle marks the area that is the subject of further calculations. The coordinate system defines the spatial directions of the calculated stresses. The principle and effect of bending under the influence of a normal force are shown between the bar plots. The green arrows represent the edge fibers for which the stresses are shown in the bar plots above and below.

The combination of the two isolated bending stresses results in the stresses for an oblique bending. The combined axis of rotation rotates in the plane of the cross-sectional area away from the isolated axes of rotation. The greatest stress occurs in the areas perpendicular to the combined axis of rotation. In order to make the stresses more tangible biomechanically and preventively, they are converted into strains with the help of Young's modulus of cortical bone. The results of these calculations are shown in Figure 3.12. A comparison of all polar plots shows that the tensile strains are most pronounced in the supero-anterior direction and the compressive strains in the infero-posterior direction.

For CMJ and walk, the deviation of the total axis of rotation from the axis of rotation around which the moment M_y acts is the smallest. When climbing stairs, the femoral neck experiences the greatest proportion of stress in the antero-posterior direction. The strains tend to act in superior and inferior directions with a small proportion of antero-posterior components. The highest compression (3946 µStrain) and tensile strains (2045 µStrain) can be detected during the box jump. The run follows with values of 2963 µStrain in compression and 1338 µStrain in tension. The femoral neck experiences the lowest loads in the CMJ with 1177 µStrain in compression and 508 µStrain in tension. In between are walking, climbing, and descending stairs. For a better comparison of all calculated values with the corresponding quartiles, see Table 3.5.

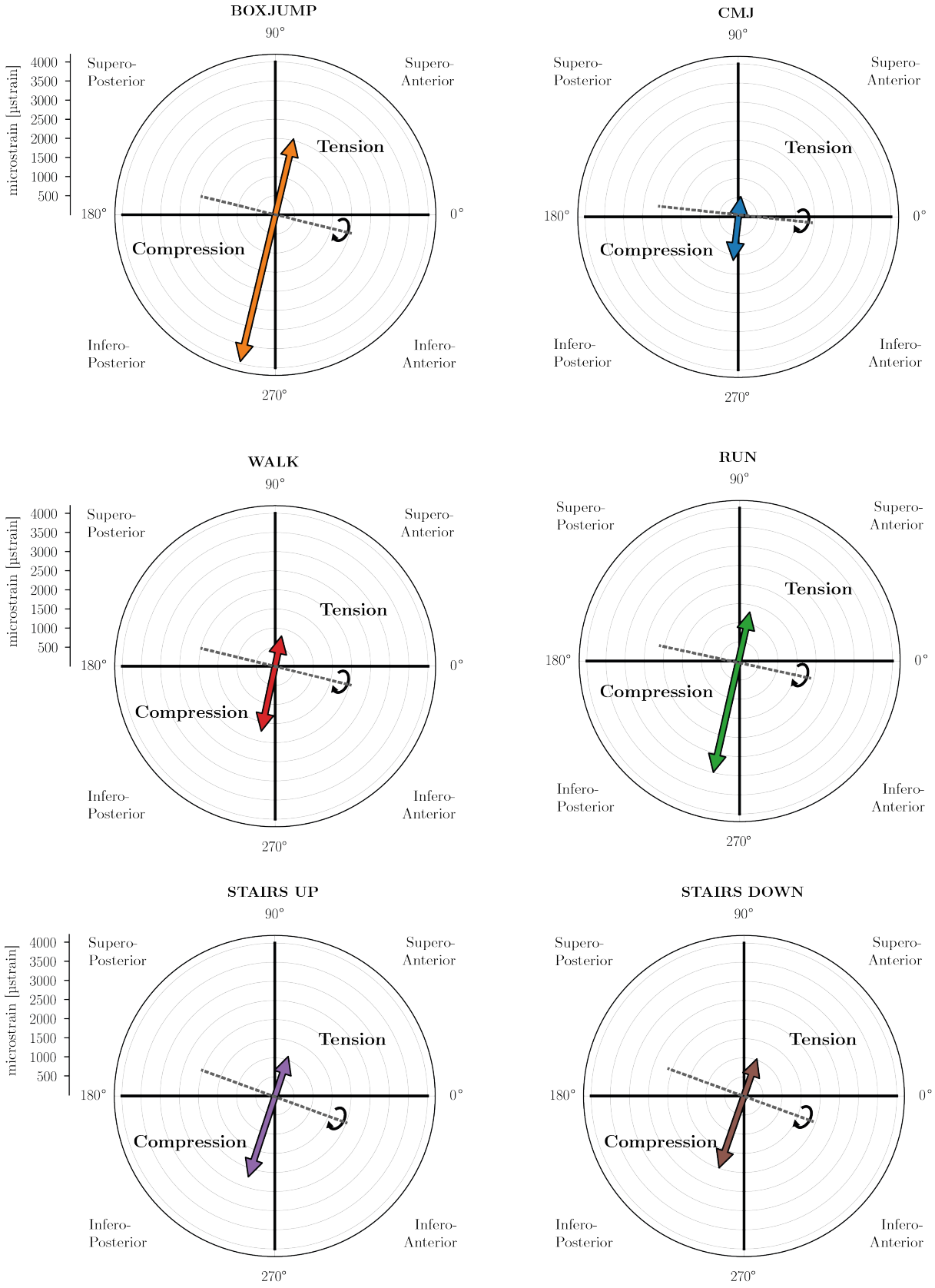

Figure 3.12: Polar plots of tensile and compressive strains in the femoral neck due to oblique bending. The arrows point in the direction of the strongest strains. The length of the arrows indicates how high these strains are. It is also noted whether the loads are tensile or compressive. The rotation of the rotation axis or the angle of the arrows is calculated from the arctangent of the values for the moments around the y- and z-axis.

Table 3.5: Tensile and compressive strains in the femoral neck due to oblique bending for every exercise with the corresponding quartiles.

	Tension strains [µStrain]	Compression strains [µStrain]	Angle between My and Mz axis [°]
cmj	508 [372, 704]	1177 [902, 1503]	84 [81,87]
box jump	2045 [1649, 2496]	3946 [3241, 4638]	77 [75,79]
run	1338 [1040, 1666]	2963 [2373, 3537]	78 [76, 81]
walk	813 [648, 1011]	1736 [1421, 2082]	80 [77, 83]
stairs up	1094 [898, 1349]	2229 [1841, 2656]	72 [68, 74]
stairs down	1033 [841, 1274]	1991 [1616, 2370]	74 [70,77]

3.4 Discussion

This study aimed to analyze various high-impact exercises and everyday movements on the proximal femur. These results should provide conclusions on possible preventive measures for osteoporosis. Motion capture recordings were taken of 211 subjects for these various exercises, from which the loads were subsequently calculated using musculoskeletal simulation in the AMS. The conditions for calculating stresses and strains in the femoral neck based on this were determined using a highly simplified geometry of the cross-section. This enables good comparability of the loads. Decisive for the correct calculation is the determined ground reaction forces, which represent the force boundary conditions of the human body to the environment. For the GRF, the highest values were determined for the box jump and the run. The CMJ follows in third place. Consequently, the highest GRFs are not achieved for the two jumping exercises. This study focuses on the effects of the exercises on the loads in the femoral neck and, therefore, one leg. In contrast to the box jump and the other exercises, the CMJ is performed on both legs. The impact of the jump is, therefore, distributed over both legs. This suggests that single-leg or side alternating high-impact exercises have a greater positive effect on the femoral neck.

If the results of the strain calculations are compared with the values defined by Frost and Schönau (2000) and Frost (2000) all exercises except CMJ are exceeding 1500 µStrain and thus promote bone gain/modeling. Here, too, the low value for the CMJ can be attributed to the bipedal execution of the jump. In the supero-anterior region of the femoral neck, i.e., where the tensile loads act, only the box jump, and the run can exceed this limit. This result is consistent with the positive effect of high-impact exercises identified by Vainionpää (2007) and Vlachopoulos et al. (2018) in their long-term studies. Poole et al. (2010) investigated the effects of aging on femoral neck bone in women. They found out that older women had relative preservation of inferior femoral neck bone over seven years because of the loads of daily activities such as walking or standing. These region is experiencing higher strain in stance and heel strike. Voo et al. (2004) were also able to show the positive effect of jumps and races in their FE approaches. Nikander et al. (2009) reveal that femoral necks of older women are rarely subjected to high impact loads that are associated with physically active young women with thickened femoral neck cortices.

They also recommend so-called odd-impact exercises in old age, i.e., walking forward, backward, and sideward, as these are mechanically less demanding to the body.

However, it is important to consider several points when analyzing and evaluating this study and the results. It was not possible to simulate or analyze all tests for each test subject and exercise due to various influencing factors. The movement recordings in The Captury rely on silhouette/color recognition and background subtraction. The manufacturer warns that loose clothing may cause tracking issues observed during the tests. Test subjects wearing very wide trousers or dresses/skirts were excluded from the analysis and evaluation as the kinematics, visually represented as a skeleton, were not displayed correctly.

In some cases, the measured kinematics could not be transferred to the kinematics of the models in the AMR because there were problems in the calculation of the GRF. Since the forces occurring in the body are calculated via inertia and externally applied forces in inverse dynamics, the determined ground reaction is a decisive part of the kinetics. This could be due to a lack of contrast between the test subjects' footwear and the laboratory floor/environment. This led to an unstable recognition of the foot kinematics, which resulted in a trembling of the feet and, thus, an unstable and incorrect calculation of the ground reaction forces. This can be clearly seen in the data via a difference in the curves or a curve that resembles measurement noise. These tests were also excluded from the analysis. Nevertheless, at least 84.4 % of the trials per exercise could be analyzed with a minimum number of 543 trials or data points per parameter to be analyzed.

Furthermore, the strong simplifications and the assumptions made must be discussed. The material composition of the femoral neck was approximated with a hollow circle, in which only the edge with the material properties of cortical bone was assumed as the cross-sectional area. Of course, the trabecular bone also counteracts the loads on the femoral neck. Due to the large number of test subjects and the lack of means to determine the exact bone structures, this simplification was accepted as sufficient. This study is not concerned with individual results but with a general assessment of the loads. These structures cannot be determined without CT images. Although finite element methods provide individual results, they were omitted since this study focussed on a general assessment. On the other hand, the focus was on a large number of test subjects in order to support the results statistically. Scaling of cortical thickness and cross-sectional area according to height, weight, and gender was also avoided, as this could only be estimated.

It should be noted that the performance of this exercise varies among individuals. Cyclical exercises, such as walking and running, can be compared effectively as the phases of the movement can be clearly categorized, allowing for the standardization of a gait cycle. In this study, a cycle was always selected from the center of the measurement volume. This approach reduces the risk of analyzing a step that is in the initial or

deceleration phase, which differs kinematically from the typical gait pattern. In contrast, individual isolated exercises, such as jumping exercises, make it difficult to distinguish between exact temporal phases. Some test subjects take longer to jump and find their balance less quickly upon landing. They may also jump with different forces, resulting in a different jump height, or have difficulty imitating the exercise in terms of motor skills. A detailed analysis of these factors is provided in the next chapter. It is important to consider kinematics on an individual basis. Therefore, multiple trials were recorded from each subject to analyze and identify patterns or outliers that could go undetected with fewer repetitions. This strengthens the study's validity, leading to more robust and generalizable conclusions.

Even taking into account the aspects above and limitations, this study provides a relatively simple but effective approach to assessing the loads on the femoral neck during various exercises. Although the data do not correspond to in-vivo data and do not allow an individual assessment, they do open up the possibility of comparing different exercises for preventing osteoporosis in the femoral neck. In this way, even small differences in muscle recruitment due to different kinematics are made tangible and less susceptible in this approach. For a generally valid statement, complex FE simulations, for which significantly more input parameters are required, can thus be dispensed with.

3.5 Conclusion

This study aimed to analyze the impact of various high-impact exercises and everyday movements on the proximal femur to draw conclusions about preventive measures for osteoporosis. Results indicated that most exercises placed the femoral neck under considerable strain, potentially promoting bone gain/modeling, except for CMJ, which distributed impact across both legs. These findings were consistent with previous research highlighting the positive effects of high-impact activities on bone health, particularly among physically active individuals. While the study provided valuable insights into femoral neck strains during exercises, further research is needed to address limitations and validate findings. Nonetheless, the study contributes to understanding how different exercises impact bone health and may inform preventive measures for osteoporosis. In the following chapter, approaches will be discussed as to how the results of this study can be combined with the results of the first study in order to make the loads more tangible and measurable and integrate osteoporosis prevention strategies more into everyday life.

Chapter 4

Merging sensor data and kinetic parameters - approaches for preventive feedback systems

This chapter will correlate the accelerations and strains occurring during high-impact exercises. In addition, prominent parameters that are relevant for feedback systems in everyday life are clarified. The chapter follows the verification of the hypotheses "A single sensor suitable for everyday use is sufficient to record high-impact exercises and interpret them in terms of the loads on the body" and "It is possible to draw conclusions about possible strains on the bones purely from the acceleration data".

4.1 Introduction

In chapters 2 and 3 of this thesis, the accelerations and the strains resulting from various high-impact exercises and everyday movements were considered separately. This work aims to combine these two steps and integrate the knowledge generated into everyday life. After the first of the three hypotheses was answered in Chapter 2, the measured acceleration data during the high-impact exercises must be analyzed regarding the calculated strains to answer the remaining two questions. That is why the exercises in the following are limited to the CMJ, box jump, and run. Wearables enable the recording of acceleration data considered in this work. Acceleration sensors are efficient due to their size and are now built into almost all mobile phones and smartphones. Strongman et al. (2023) have conducted a scoping review on the validity and reliability of smartphone accelerometers of gait analyses versus motion capture systems, pressure walkways, and IMUs. The study's result shows these accelerometers' high accuracy and reliability. Only a closer look at the sampling rate is recommended. As a result, smartphones and smartwatches offer a simple, cheap, and handy solution for recording and evaluating

kinematic data. They expand the possible parameters that can be collected to include health parameters. Masoumian Hosseini et al. (2023) describe in their publication how effective the recording and monitoring of health parameters can be for the diagnosis and reporting of symptoms, the early detection of potential health risks and the monitoring of patients with chronic diseases. However, safety considerations must be considered as most smartwatches are designed for lifestyle rather than medical diagnosis. Since, according to an American study, 45 % of smartwatch users use them for activity tracking (Richter 2017), it is necessary to process the data in a well-founded manner and present it to users in order to address these security concerns and generate added value for the user. The term feedback system is often used if the purpose is medical, for example, preventive or rehabilitative. The classic way to improve or adapt exercises, whether in sports, medicine, or physiotherapy, always requires an observer. This means that a therapist or trainer evaluates the exercise performance and usually gives verbal feedback to the person performing the exercise. The circle is closed as soon as the person adapts their performance based on the feedback. Replacing the person giving feedback with a digital system that records and evaluates the movement and provides feedback creates new possibilities for continuous, time-independent, and location-independent monitoring (Pustišek et al. 2021). Feedback systems already offer the possibility of supporting patients in carrying out targeted exercises during rehabilitation at home (Brennan et al. 2019). In sports, too, professional and recreational athletes are constantly trying to improve their skills and performance through a wide range of technology, especially wearable technology (Hribernik et al. 2022). According to Brennan et al. (2019) feedback can be given in different ways. Brennan et al. (2019) present the different approaches in their review. These can be found in Figure 4.1.

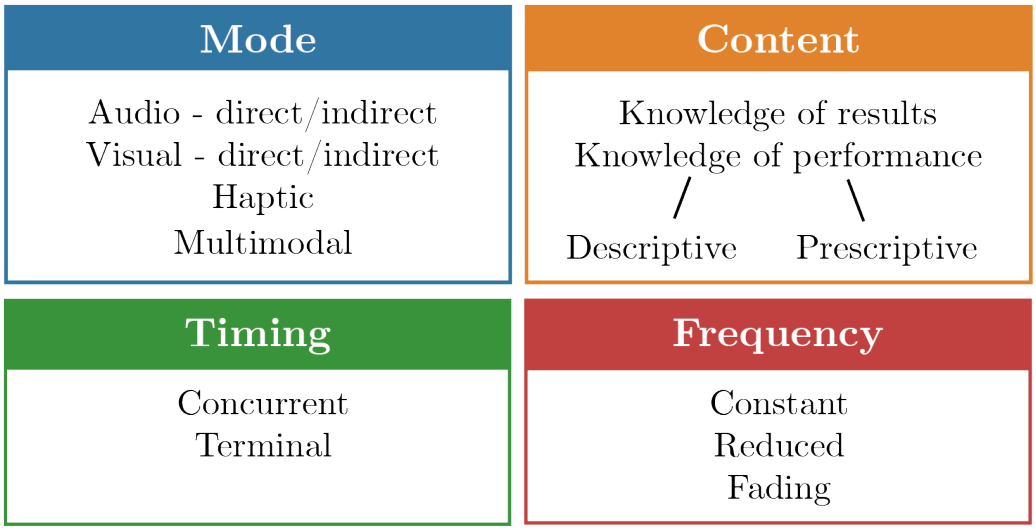

Figure 4.1: Components of feedback adapted from Brennan et al. (2019)

In medicine, feedback systems are mainly used downstream of surgeries or diagnoses.

In this work, however, the focus is on preventing osteoporosis, which should already be used at a young age. A daily impact feedback system can help prevent osteoporosis by continuously collecting and analyzing movement data to ensure that bones are regularly experiencing sufficient stress. The system may encourage optimal physical activity through real-time notifications and suggested adjustments, which maintains bone strength and reduces the risk of bone loss. In addition, such a system raises users' awareness of the importance of weight-bearing exercise, which reinforces preventive behaviors in the long term. In this chapter, the results and findings of the previous two chapters are utilized to serve as a basis for discussing data quality and implications for further use. It will also describe how a feedback system for preventing osteoporosis could look. First approaches will be discussed and evaluated.

4.2 Materials and Methods

In addition to the motion recordings with the markerless optical motion capture system, acceleration data were recorded in the second study with an IMU sensor (Xsens Dot, Xsens Technologies B.V., NL) attached to the hip. This positioning was chosen in the measurement setup and procedure because the sensor could be attached with a Velcro strap to any subject regardless of clothing (see Figure 4.2). The IMU sensor was continuously measured at a frequency of 120 Hz across all exercises. The sensor coordinate system is a right-handed coordinate Cartesian system that is body-fixed to the sensor. However, it is laborious to record the impacts uniformly with this body-fixed coordinate system, as the orientation of the sensor in space would also be necessary. This is why there is an orientation coordinate system in which the accelerations are stored. The local earth-fixed reference coordinate system is a right-handed Cartesian coordinate system with X positive to the East, Y positive to the North, and Z positive when pointing up (Movella Inc. 2022). The accelerations in the Z direction were considered in this study and are called free accelerations. The data set was divided into the time series of the individual measurements based on the recording times of the motion capture system The Captury (CapturyLive v255, The Captury, DE) afterward. There are two ways to analyze the time series. A time series or single values such as minima/maxima can be analyzed. In this study, both options will be considered and finally evaluated in terms of feasibility. All recorded data was extracted with Python (Python Software Foundation; Python Language Reference; version 3.8.3). Further data processing and analysis were performed using the Python packages NumPy (v. 1.18.5), Pandas (v. 1.0.5), seaborn (v. 0.10.1), SciPy (v. 1.7.2) and spm1d (v. 0.4.0).

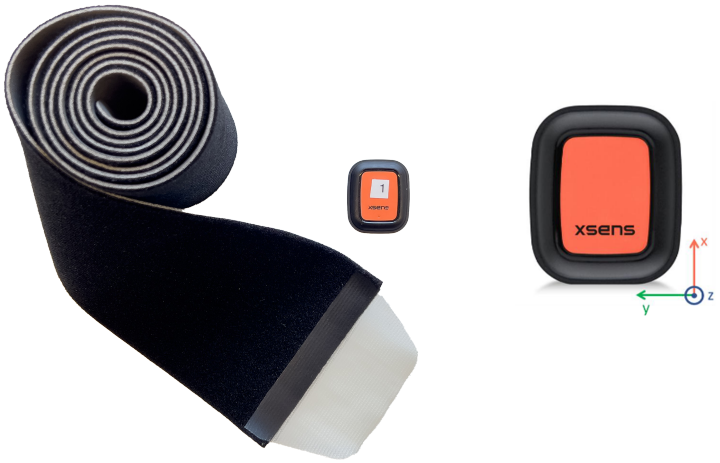

Figure 4.2: IMU sensor with velcro strap and the orientation of the sensor coordinate system (Movella Inc. 2022).

4.3 Comparison of acceleration data

To assess the quality and comparability of the acceleration data over the time series measured with the IMU sensor, the statistical parametric mapping (SPM) was used (Pataky 2012). SPM offers several advantages to biomechanics and movement scientists. The main advantage is that no abstraction of the initially sampled time series is required for the statistical analysis of the data. Here, the recorded time series were tested for statistically significant differences over their course using random field theory (Pataky 2012; Pataky 2016). In order to compare the acceleration data of the acceleration sensor with the load data resulting from the simulation data of the AMS, the kinematic input data for the AMS from the motion capture system must be considered. The data from the sensor is compared with the acceleration of the skeleton's root joint, defined in the BVH file, which, in this case, is the pelvis.

4.3.1 Approaches for comparing the acceleration data

Analysis of time-series

The first step in evaluating the data about a time series is to assess the various exercises' comparability and identify any patterns. The kinematic input data for the AMS from the motion capture system was resampled to a frequency of 120 Hz to enable better comparability of the time series. Afterwards, the data was filtered using a fourth-order Butterworth filter with a 15 Hz cut-off frequency. The individual time series of the various test subjects were then analyzed with the aid of dynamic time warping (DTW) (Müller 2007) and equated to the extreme points that occurred. Mean value curves and their standard deviation could now be formed. These mean value curves were correlated for

each time series and then analyzed for significant differences over time using SPM (Two-sampled, two-tailed T-Test). The complete methodological procedure is shown in the following diagram applied to the box jump data (Figure 4.3).

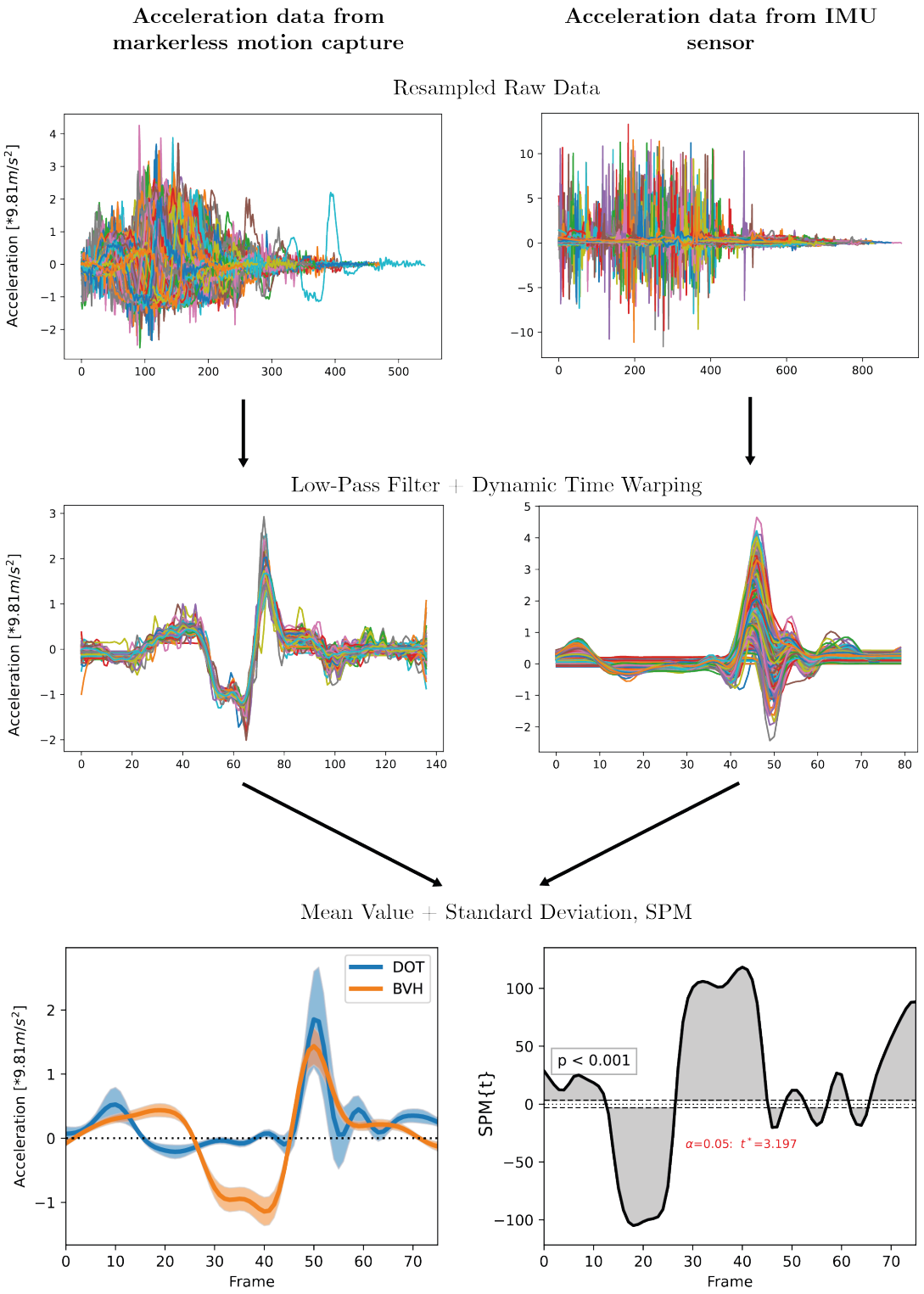

Figure 4.3: Methodological procedure for the comparison of acceleration data. The acceleration data of the markerless motion capture system is shown on the left, and that of the IMU sensor on the right. The data is first smoothed using a Butterworth filter and then analyzed with dynamic time warping and equated to the extreme points that occurred. The last row shows the mean curves with the standard deviation on the left-hand side and the SPM (two-sampled two-tailed T-test) on the right-hand side.

Analysis of single values

As the impacts are relevant to the prevention of osteoporosis, the isolated maximum acceleration values of both systems are considered in the next step. For this purpose, the raw data from the time series observation was used. Now, all maximum values of the acceleration data of both measurement conditions are compared individually for each subject and test and separated by exercise. The results are visualized and evaluated for each in a Bland-Altman plot, a graphical method for evaluating the agreement between two different measurement conditions or methods.

4.3.2 Results

Analysis of time-series

The time series for the acceleration data of both systems were analyzed separately with SPM for the different exercises. The t-value here shows the strength and direction of the effect at each point. A high positive t-value means that the acceleration data of the IMU sensor has significantly higher values than the acceleration data of the motion capture system. A high negative t-value indicates the opposite. The dashed lines are significance thresholds that indicate the statistical significance threshold (e.g., t-value at p=0.05). If t-values exceed these lines, the effect is statistically significant. The results are visualized in Figure 4.4.

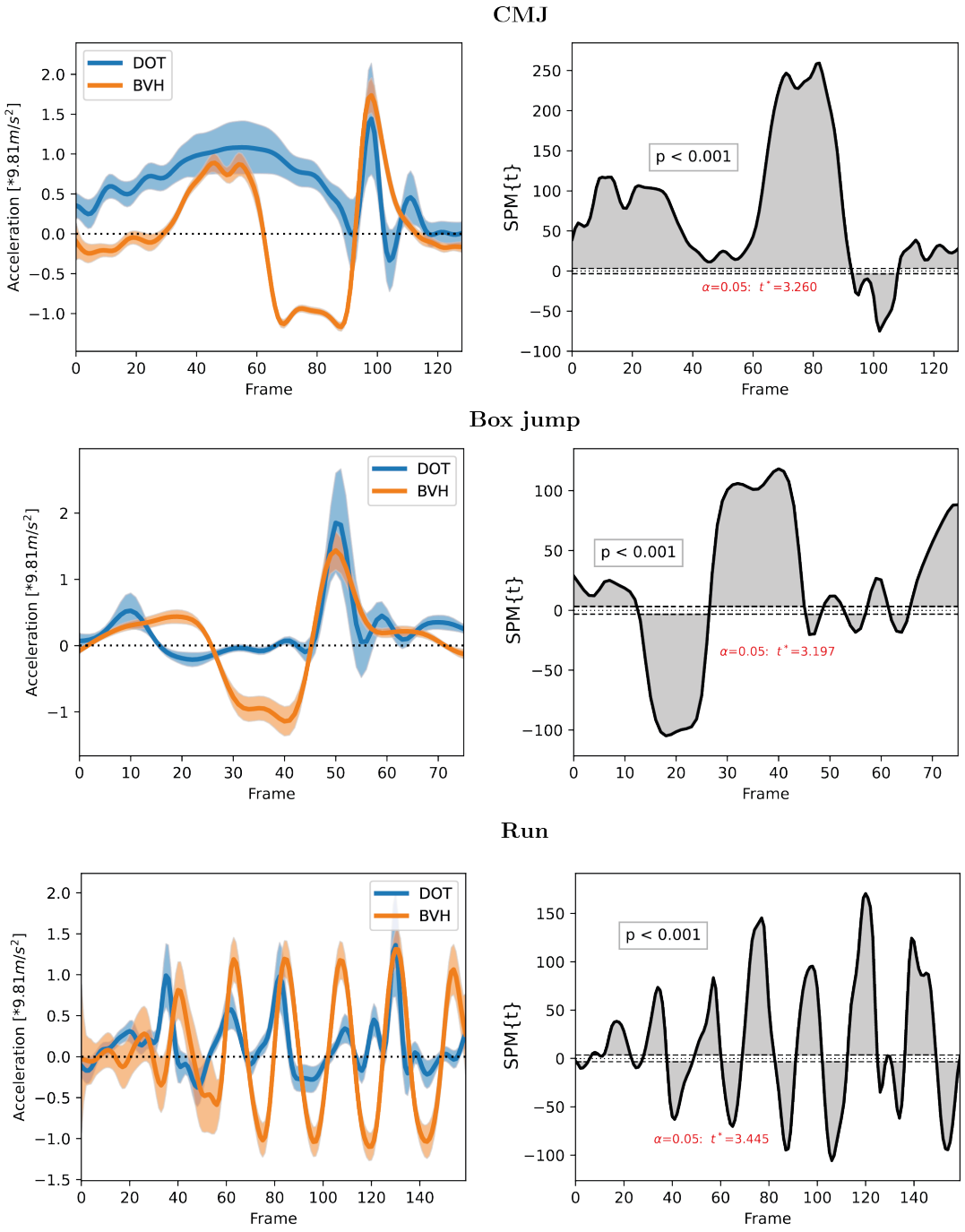

Figure 4.4: SPM results for different exercises. The left side shows the mean curves with the standard deviation for the acceleration data coming from the different systems. The right side shows an SPM (two-sampled two-tailed T-test).

For the CMJ, the t-values are above the statistically significant limit value of t=3.260 over the majority of the time course. Consequently, the acceleration data of the IMU sensor are above those of the motion capture systems. This only changes in the area of impact. For the box jump, the determined t-values also exceed the statistically significant limit value of t=3.197 most of the time. For the take-off and landing, i.e., the impacts, the t-values are in the negative range. The amount of t-values is lowest in the landing

area. For the run, the t-values determined fluctuate between positive and negative. The threshold here is t=3.445.

In a broad comparison, the acceleration data of the IMU sensor consistently registers higher values. However, it's important to note that in the impact areas, the t-value decreases, and the direction changes to negative, indicating a unique characteristic of the IMU sensor in these specific scenarios. The clearly different curves of the two measuring systems can also be recognized in the mean value curves.

Analysis of single values

Bland-Altman plots were used to compare the isolated maximum acceleration values. The bias indicates the average systematic difference between the two measurement conditions. Limits of Agreement (LoA) show the range in which approximately 95 % of the differences should lie. A positively increasing trend line shows that the differences become more significant with increasing mean values, which indicates a proportional bias. Suppose the trend line runs through both positive and negative differences. In that case, this means that the first method provides lower values at low mean values than the second method (negative differences). The first method provides higher values than the second method (positive differences) at high mean values. The Bland-Altman plots for all three exercises are shown in the Figure 4.5. A rising straight line can be seen for the CMJ. The average difference between the methods is 1.33. Isolated outliers can be recognized. In general, the straight line is mainly in the positive range. A rising trend line has also been determined for the box jump. Here, the average difference between the methods is as high as 2.82. A rising trend line was also determined for the run, with an average difference between the methods of 1.34. However, the difference between the methods at higher mean values is partly fan-shaped, which means that the motion capture system delivers higher acceleration data than the IMU sensor in the case of isolated outliers. To summarise, the IMU sensor records significantly higher values for the acceleration data than the markerless motion capture system.

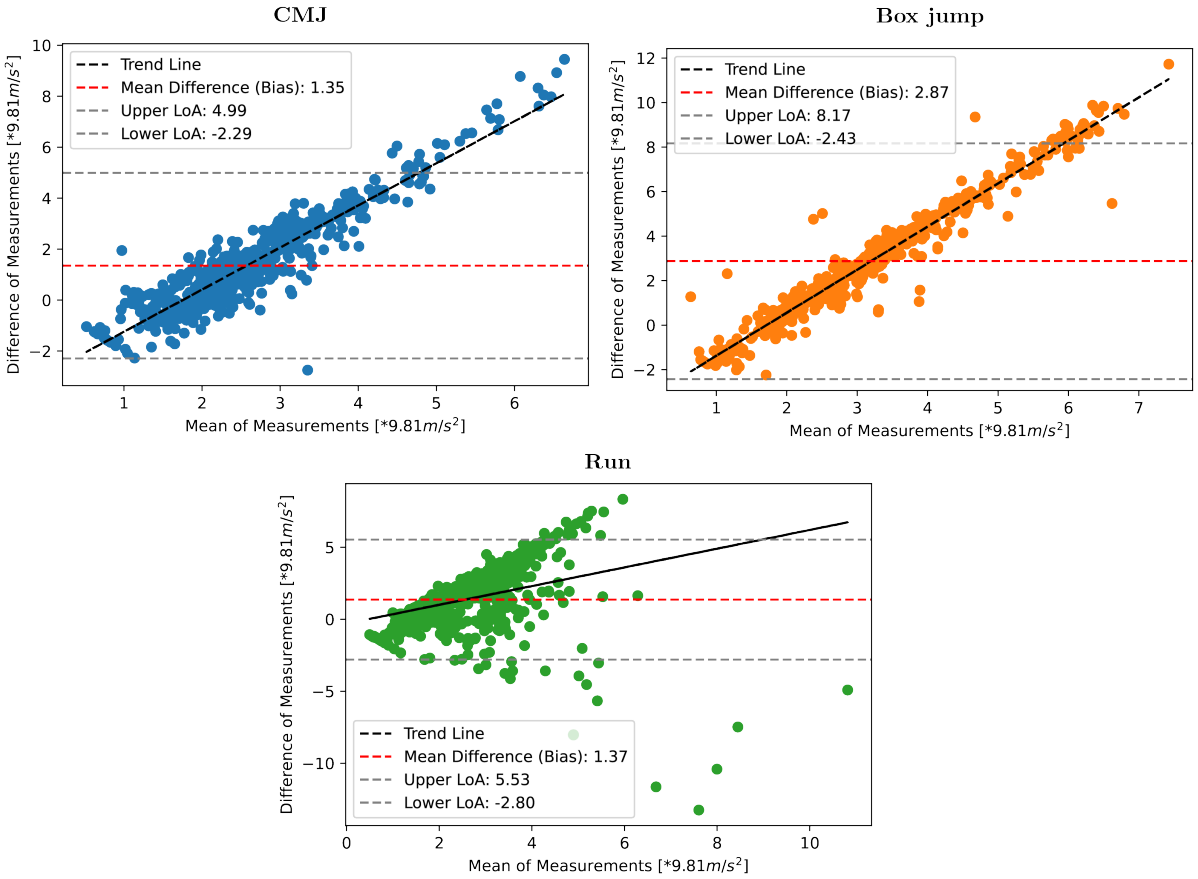

Figure 4.5: Bland-Altman plots for isolated maximum acceleration values for the different exercises.The determined data points might be described with a linear trend line.

4.3.3 Discussion and Conclusion

This section analyzed two methods for comparing the acceleration data of the IMU sensor and the motion capture system. The aim here was to determine whether the measured kinematic data of the two systems match to form a basis for deriving and evaluating the kinetic data. The first approach to comparing the time series provided significant deviations over most sections considered for all exercises. This difference is also visually recognizable when comparing the mean value curves. The standard deviations around the mean value for the motion capture system are lower for all exercises than for the IMU sensor. Despite the visual differences, SPM was used to quantify differences between groups or conditions using statistical tests. It also allows specific regions or time points to be identified where significant differences occur that might be missed in a simple visual inspection, increasing the sensitivity of the observation. The curves for all exercises also correspond more closely to the acceleration curves assumed in theory due to gravity. This may be because the motion capture system's acceleration data for the pelvis is taken from the position of raw data. Another point is processing the raw data using DTW and Butterworth filters to synchronize the salient points of the impacts. Without this

procedure, it would be difficult to compare the time courses since the duration, jump height, speed, or correct execution strongly influence the acceleration curve. However, this causes distortions in the data that influence the course of the mean value curves. However, the mean values of both systems were relatively close to each other in the area of impact. Therefore, the maximum accelerations at the time of impact were analyzed in isolation in the next step. Bland-Altman plots were used for this. This type of diagram is mainly used to compare different measurement conditions. Viecelli et al. (2020) have already compared smartphone acceleration data with that of a video-based motion capture system for a weight stack to extract single repetition, contraction-phase specific, and total time under tension (TUT) during resistance exercise training and found a very good match. The evaluation in this study showed that the IMU sensor records much higher values for the acceleration data than the markerless motion capture system. One explanation could be the higher sampling rate of 120 Hz for the IMU sensor compared to the 60 Hz of the markerless motion capture system. Furthermore, it needs to be made clear which processing steps are taken between the camera-based kinematic recording of the test subject and the export of a 3D model in the form of a motion data file. Another point that could explain the large differences in how the IMU sensor is attached is that it is attached using a Velcro strap that contains a small pocket where the sensor is placed. The sensor could have shifted in this pocket during the measurement or not recorded the actual accelerations caused by the impact, but those caused by the sensor slipping. As Wilhelm and Weidt (2011) report in their article, measurements with acceleration sensors on the human body show exactly these observed problems. Depending on how the sensor is attached to the body, the sensor can be subject to superimposed vibrations. If the sensor is attached to clothing, the measurement data is challenging to reproduce. However, even if the sensor is attached directly to the skin, the skin can vibrate, leading to incorrect curves. This is comparable to the Velcro tape of the IMU sensor.

In summary, the significant measurement discrepancies stem from the potential for the IMU sensor to shift within its Velcro strap pocket, resulting in inaccurate data. This underscores the importance of secure sensor attachment for ensuring reliable and reproducible outcomes. Additionally, caution is advised when handling IMU acceleration data to mitigate inaccuracies. Therefore, the IMU sensor acceleration data will not be considered further in the following section. The focus will be on the acceleration data obtained from the motion capture system for comparison with the simulated strains.

4.4 Merging acceleration and strain data

In order to implement the feedback system, specific input parameters must be calculated, determined or assigned for specific output parameters. In this case, the recorded acceleration data from the motion capture system serves as input for the feedback system.

The strains on the femoral neck will be calculated from this acceleration data and then evaluated.

4.4.1 Methodology

A simple method is to calculate a correlation coefficient. The Pearson coefficient is used in this chapter, as in chapter 2, And measures the strength and direction of a linear relationship between two variables. The reason for using it here is that it is easy to interpret and does not depend on the scaling of the data. When comparing the acceleration and strain data, a linear relationship is assumed, which can be well represented by the coefficient, i.e., at higher accelerations or impacts, the strains on the femoral neck are also higher. The influence of other subject- and test-specific parameters, such as body weight, jump height, and speed, on the result is also analyzed. The speed during a run might influence the strains on the femoral neck, as faster running speeds result in greater ground reaction forces. In a countermovement jump, the jump height may be significant since higher jumps might involve more forceful landings, possibly exerting greater strain on the femoral neck. Generally, body weight is presumed to affect all high-impact activities, as greater mass might lead to higher forces during movement, potentially increasing the mechanical load on the bones and joints. These considerations highlight the importance of evaluating different parameters when assessing the stress on the femoral neck in various physical activities. The parameters are visualized with color scales to make the influence recognizable.

4.4.2 Results

Low values could be achieved for the correlations, according to Pearson (ρ), for all three exercises. For the strains in the femoral neck caused by compression, the values were $\rho = 0.34$ for the CMJ, $\rho = 0.23$ for the box jump, and $\rho = 0.22$ for the run. For the loads in the femoral neck caused by tension, the values were $\rho = 0.27$ for the CMJ, $\rho = 0.22$ for the box jump, and $\rho = 0.29$ for the run. All values were significant (two-sided t-test, $p < 0.05$). Since the scatter around the regression line was very high, various parameters that could be related to the exercises were examined. The parameters of body weight, jump height, and speed normalized in the direction of movement were reviewed in more detail. Figure 4.6 shows the graphs for the loads caused by tension as an example. Higher jump heights in the CMJ are often reached with greater accelerations. For box jumps, the body weight of the individual is a key factor affecting the strains on the femoral neck, with heavier weights leading to higher strains. Additionally, as running speed increases, so do the accelerations in the direction of gravity. All other graphs can be found in Appendix B. The following can be seen from this. In all exercises, both for the strains caused by tension and compression, the body weight has a decisive influence on the strain level. A tendency

can also be seen in the jump height, which is the maximum height the foot raises when running. Higher jump heights lead to higher accelerations. The speed/velocity parameter is mainly an influencing factor when running, leading to higher accelerations.

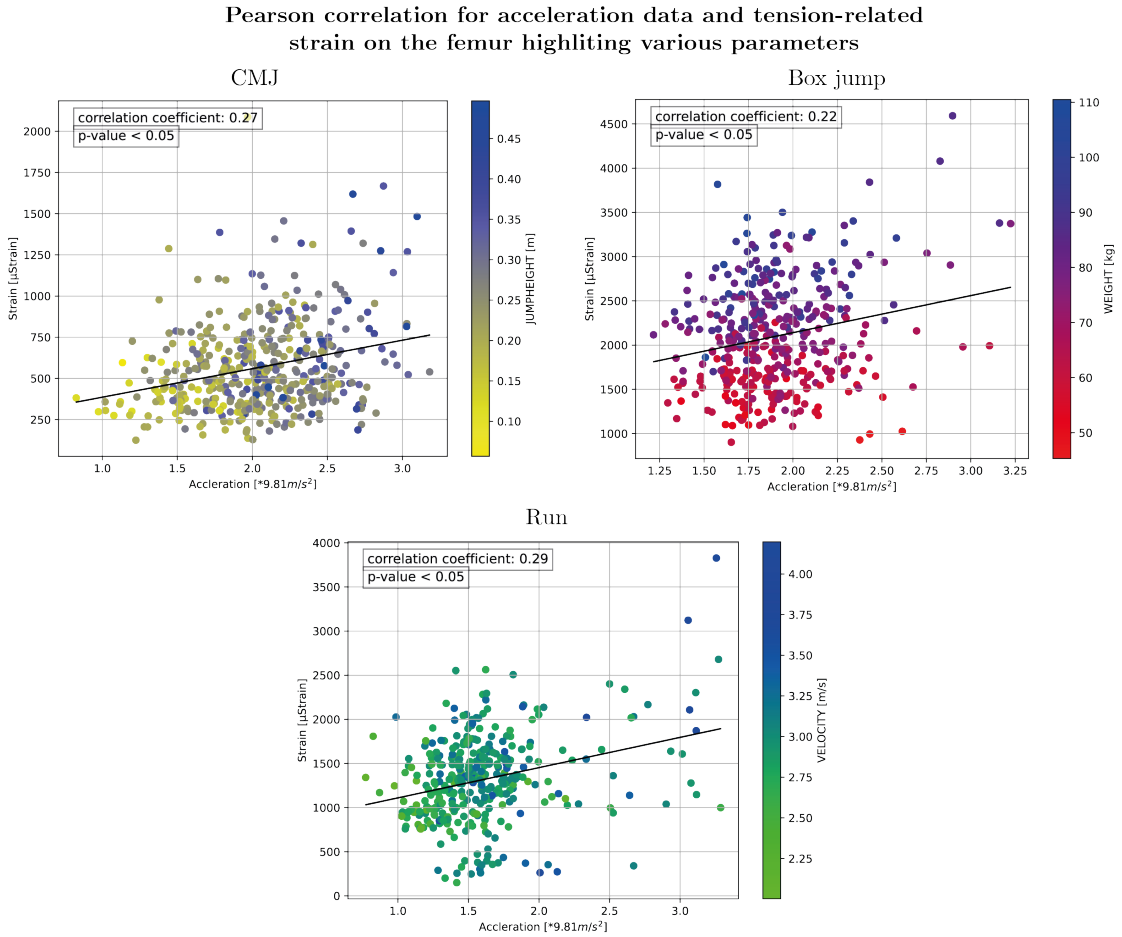

Figure 4.6: Pearson correlation between acceleration data and strains on the femoral neck for all exercises. The line indicates the best-fit linear regression line.

4.4.3 Discussion and Conclusion

The Pearson correlation coefficient did not reveal any clear correlation between the acceleration of the pelvis in the direction of gravity and the strains achieved in the femoral neck. However, the additional consideration of the parameters of body weight, jump height, and speed in the plane provided insight into possible correlations. Also, to enable the calculation of the loads, major simplifications were made in the musculoskeletal models to allow the calculation of 211 test subjects. No anatomical adjustments were made regarding the exact cross-section of the femoral neck. The data available in the literature could be more straightforward. The most accurate method involves adapting the models using anthropometric data from imaging procedures, which is a very time-consuming process. In this study, many test subjects were preferred over individual model adaptations due to

the lack of appropriate measuring equipment. Additionally, this approach allowed for the simulation of more test subjects. In conclusion, it can be said that it is not possible to derive strains purely from acceleration data with the available data, but the approaches described offer potential for further investigation methods.

4.5 Approaches for feedback systems

In the introduction different types of feedack are discussed. Depending on the application, target parameters, or suitability for everyday use, different approaches can be used here. Based on the literature and the results of this work, two different approaches were tested during this project. The feedback systems only deal with the kinematic input parameters and provide feedback on the impacts on the body. Kinetic data or strains on the femoral neck were initially omitted, as no validated implementation was possible at that time.

Visual feedback

Visual feedback systems integrated with gamification offer significant advantages in various contexts, particularly educational and training environments. These systems enhance user engagement and motivation by employing gamified elements such as progress bars and interactive visuals. Research indicates that gamification can effectively promote learning outcomes by providing immediate feedback on performance, which facilitates iterative improvement and goal attainment (Dichev and Dicheva 2017; Mazeas et al. 2022). Moreover, the visual representation of progress and achievements helps users track their development more intuitively and encouraging continued participation. In this approach pelvis accelerations in the direction of gravity were evaluated to compare the kinematic data. The markerless motion capture system used makes it possible to stream this data and all joint angles live via a network interface. Another programme can then access these. In this approach, visual feedback from the user was chosen. With the help of the Unity game engine (Unity Technologies, San Francisco, USA), this data stream was accessed and transferred to an avatar. Figure Figure 4.7 shows an example of what the feedback system for a DJ looks like. Next to the avatar is a green bar that grows larger depending on the acceleration of the pelvis during landing. The maximum value reached is marked with a red line, and the value is on the bar. Next to the bar, various values for maximum acceleration on the pelvis during different exercises are adapted from the literature with a reference value of 1.5 g for walking at v = 4 km/h and 3 g for running at v = 10 km/h. The marked value can be reset to zero using a reset button. This feedback system also offers the potential to display kinetic parameters visually. In the future, corresponding methods could also be used to display the strains on the femoral neck. Until then, it has been possible to arouse interest and awareness of the need for more high-impact exercises

in everyday life at public events. In addition, the system offered the user an assessment of the accelerations experienced by the body during various movements or exercises.

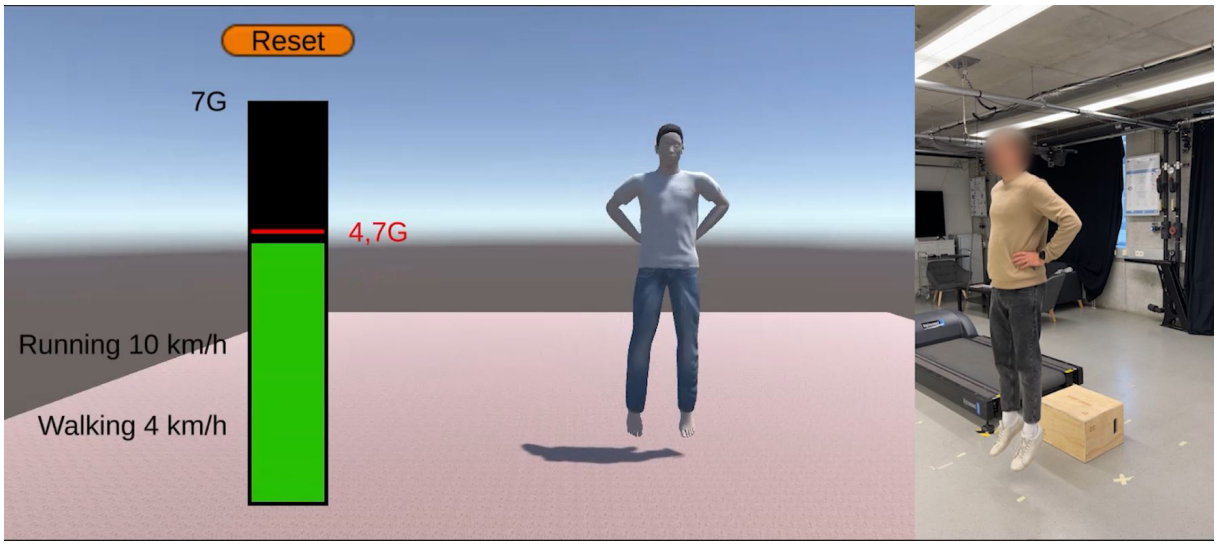

Figure 4.7: User interface of the visual feedback system. The motion data from the motion capture system is streamed into the Unity game engine, where it is analyzed and evaluated. The green bar indicates the maximum acceleration measured on the pelvis.

The visual feedback system brings gamification and a simple, clear user interface. The disadvantage, however, is the handiness and the costs. The system can currently only be used with the markerless motion capture system used. One approach for further applications would be to implement this system in a mobile app that accesses the camera and uses it to capture motion data. Move.ai (Move.ai, London, UK), for example, already allows the collection of motion data using a smartphone. However, this implementation is also not very handy and only records the impacts during use. Therefore, another approach was also pursued during this project.

App-based feedback

As mentioned, the ownership and use of smart devices and smartphones is increasing. The technology built into them makes it possible to record acceleration data. Therefore, the approach was to use an smartphone app to access, permanently record, and evaluate the sensor data. Similar to visual feedback, thresholds for acceleration values are stored here. As soon as these are exceeded, these high values should be stored and available for viewing on demand at any time. This should be able to track the impacts on the body over the day. In summary, you will then receive the values for each day, and you can see which days you were more or less active, similar to a pedometer. This idea was implemented but still requires further adjustments. However, what has become apparent in this doctoral thesis is that the values of these acceleration sensors often need to be revised. In addition, the smartphone is even less fixed in this application than the IMU in the movement

study. Swinging up and sliding around in your pocket are enormous disadvantages of this system, which could, however, be minimized or even avoided by improved analyses and further developed models for evaluating the acceleration data. Another point is the high measurement accuracy and sampling rate required for these impacts, which remains system-dependent. Furthermore, the type of exercise or movement must be recorded or determined based on the loads on the femoral neck. As the results in chapter 3 show, whether an exercise is performed with both legs or with one leg is crucial.

4.6 Discussion

Estimating kinetics from inertial sensor data through musculoskeletal movement simulations is a promising approach for accurate motion analysis. In this work, high-impact exercises were considered. Acceleration data on the pelvis in the direction of gravity were measured and compared using an IMU sensor and a markerless motion capture system. Research has shown that integrating sensor-to-segment calibration methods in musculoskeletal models significantly improves the accuracy of joint kinematics estimation, ensuring consistency with gold standard motion capture systems (Di Raimondo et al. 2022). Sparse sensor setups, particularly those including a pelvis sensor, have been found to enhance the reconstruction quality of spatiotemporal, kinematic, and kinetic variables during walking and running, offering usability with minor reductions in accuracy (Dorschky et al. 2023; Nitschke et al. 2024). Although running movements were also investigated here, in contrast to the literature, no good agreement between the two systems could be found, neither in terms of time course nor individual maximum acceleration values. It should be mentioned, however, that in this work, only the acceleration in the fixed spatial direction was examined, namely in the direction of gravity, to simplify the condition and thus to approach smart devices worn in everyday life. Under this application, laboratory conditions cannot be assumed. Another critical point for the use of IMUs in everyday life is the already discussed fixation of the sensors. Swinging up and slipping are already observed phenomena that make it difficult to interpret the measured values. No clear conclusion could be drawn from the combination of kinematic and kinetic data. However, methods of artificial intelligence and deep learning are promising. Developing a novel deep learning model for predicting joint moments and ground reaction forces using IMU sensors has demonstrated high accuracy across diverse subjects and walking conditions, outperforming existing deep learning models significantly (Hossain et al. 2023). Further studies using the available data should, therefore, be sought. If it is possible to correlate the kinematic and kinetic data, the approaches presented here provide a reasonable basis for developing feedback systems suitable for everyday use. Therefore, the goal of implementing preventive measures against osteoporosis or other musculoskeletal diseases is still possible.

Chapter 5

Discussion

This work aimed to collect, correlate, analyze, and make accessible, relevant data for preventing osteoporosis in everyday life. These individual steps were processed and discussed in different sections. First, recorded accelerations from high-impact exercises at various points on the body, which correspond to typical positions of smart devices, were evaluated in a study with 49 subjects. A further study simulated high-impact exercises on 211 subjects using musculoskeletal models, and the loads on the femoral neck were calculated. Finally, the results of the first and second studies were compared, and similarities were sought. Based on this, initial approaches for feedback systems on the prevention of osteoporosis were developed and discussed. Three hypotheses guided this work.

The first hypothesis to be investigated was "The accelerations measured at the hip can also be measured at typical wearables positions". Previous studies (Vainionpää 2007; Vainionpää et al. 2007) that had already looked into the topic of osteoporosis prevention were able to derive certain limit values for accelerations measured at the hip. This study was used to integrate these findings into everyday life. The first study's results showed that the accelerations measured at the pelvis during jumping exercises can be very well measured at the upper body and the upper extremities. In particular, the positions of typical smart devices such as smartwatches or chest straps provided very good matches. It is essential to ensure that the exercise is performed correctly according to the instructions to ensure comparability.

The second hypothesis, "A single sensor suitable for everyday use is sufficient to record high-impact exercises and interpret them in terms of the loads on the body", was examined in the next step. The acceleration data of an IMU sensor was compared to the acceleration data of a markerless motion capture system - dealing as input for musculoskeletal simulations - during high-impact exercises to determine their kinematic data alignment. The time series comparison showed significant deviations, with the motion capture system providing more accurate data due to lower standard deviations and better theoretical

alignment. Maximum accelerations at impact were closer between systems, but the IMU sensor recorded higher values, likely due to a higher sampling rate and attachment issues. Therefore, the hypothesis cannot be confirmed with the approaches and methods used. It might be possible that a connection can be established with more complex algorithms or other physical or mathematical models. This requires further investigation.

To test the third hypothesis, "It is possible to draw conclusions about possible strains on the bones purely from the acceleration data", the high-impact exercises and the loads on the femoral neck were first simulated using musculoskeletal models. A distinction was made between the strains occurring due to compression and tension. The values were calculated by simplifying the boundary conditions. They could then be compared with the maximum acceleration values at the pelvis. A Pearson correlation did not provide any clear results. However, it was possible to show that the loads of the exercises are dependent on certain parameters. For example, body weight plays a decisive role in the loads that occur in the femoral neck. Therefore, it seems likely that further parameters are needed to derive kinetic parameters from acceleration data. These must first be determined and tested in future work.

Even though many subjects have already taken part in these studies, the number of subjects needs to be increased to conduct a more comprehensive analysis and use artificial intelligence methods. Some of the data collected is lost due to faulty measurements by the IMU sensor, clothing prone to errors when using the markerless optical motion capture system, and problems when transferring the kinematic data to the musculoskeletal models. It can be said that this study already has a high number of subjects in the field of biomechanics. This is facilitated by the uncomplicated movement data collection using the novel markerless motion capture system. Here, it is possible to measure the subjects in their clothes, thus generating a setup that is as natural and close to everyday life as possible despite laboratory conditions. It was clear from the first and second studies that non-cyclical exercises are challenging to normalize. To be more precise, this means that the subjects performed the jumping exercises in the studies in very different ways. Although the exercises were explained and demonstrated before the subjects performed them, there were apparent differences in how they were carried out. For example, the jump exercises were performed at different speeds, the starting positions differed in some cases, and the effort put into the jumps led to different jump heights. The exercise sequences were attempted to be approximated using DTW and Butterworth filters. This can only be done downstream and based on the entire data set, which minimizes the suitability for everyday use and makes it impossible to consider the time series. One possibility for obtaining unambiguous data in future applications would be creating explanatory videos or precise training for the exercises. Recognizing specific exercises similar to a step

counter is almost impossible when recording continuously using an IMU. The observation of individual values provided a more tangible result. However, a difference between the measurement systems can be seen. More literature is also needed regarding the best sampling rate for different measurement systems for high-impact exercises. Riddick et al. (2023) successfully developed an approach for estimating human spine orientation with inertial measurement units (IMU) at a low sampling rate. However, the result cannot be transferred to fast movements, and the measured impacts of the results require further research. The exercises considered in the first study, SJ, CMJ, and DJ, were replaced by a CMJ, box jump, and a run in the second study. The reason for this was the similarity of the SJ and CMJ. In addition, all three exercises were followed by a landing on both legs and were based on the studies by Vainionpää (2007) and Vlachopoulos et al. (2018). The box jump and run were chosen to test one-sided loads and more everyday situations, which proved to be very positive in terms of the results for the prevention of osteoporosis. Several insights can be gained from this work. On the one hand, accelerations acting on the pelvis during high-impact exercises can be tracked very well at typical smart device positions, such as the wrist or chest. In addition, it is possible to determine loads confirmed as preventive against osteoporosis because they stimulate bone maintenance and formation using musculoskeletal models. These simulations make it possible to explain the cause behind the effects determined by in vivo measurements. The calculations have shown that, in addition to the strains caused by compression in the inferior region of the femoral neck, high-impact exercises, unlike everyday movements, also cause high strains in the superior region due to tension. Finally, it should be mentioned that these high-impact exercises are difficult to measure over time using IMUs. Individual value analyses of significant points, such as the maximum accelerations, can be better recorded and determined in this work. A derivation of the kinetic parameters determined in this work purely from the acceleration data could not be confirmed. Nevertheless, relevant points and approaches have emerged on which future research work can be built.

Chapter 6

Conclusion

The risk of developing musculoskeletal diseases decreases with decreasing physical activity and, consequently, with increasing age. However, regular high-impact exercise can help maintain bone density and increase bone formation even at a young age. Often, a lack of information on this topic or even an awareness of what a good amount of exercise is leads to failure. Smart devices such as smartphones and smartwatches, which have seen a massive increase in popularity in recent years, can make a positive contribution here in the form of feedback systems. This work examines the steps necessary to create a preventive feedback system and then evaluates them. Both measurable and previously only calculable variables using musculoskeletal simulations were considered and examined in depth. Two movement studies supported the work. These showed that precisely these smart device positions are well suited to measuring the impacts in the form of accelerations on the body, which can also be measured on the pelvis. In addition, the musculoskeletal simulations offer the opportunity to better understand biological mechanisms. The results of the second study suggest that the preventive effect of high-impact exercises is caused by the pronounced stresses caused by tension in the superior region of the femoral neck, more so than in everyday movements. Even though the combination of kinematic and kinetic data presented some difficulties, it was shown that individual maximum accelerations are better suited as measurement variables than entire time series. This study also demonstrated the strength of the new markerless optical motion capture systems. These enable many subjects to be tested with high accuracy, thus providing a broader cross-section of the population. This work provides a sound basis for further research on the prevention of osteoporosis and other age-related musculoskeletal diseases.

Bibliography

Ainsworth, B. E. and F. Li (2020). "Physical activity during the coronavirus disease-2019 global pandemic". In: *Journal of sport and health science* 9.4, pp. 291–292. DOI: 10.1016/j.jshs.2020.06.004.

Allison, S. J., K. Brooke-Wavell, and J. Folland (2018). "High and odd impact exercise training improved physical function and fall risk factors in community-dwelling older men". In: *Journal of Musculoskelet Neuronal Interact* 18.1, pp. 100–107.

Alswat, K. A. (2017). "Gender Disparities in Osteoporosis". In: *Journal of clinical medicine research* 9.5, pp. 382–387. DOI: 10.14740/jocmr2970w.

Asadi, F. and N. Arjmand (2020). "Marker-less versus marker-based driven musculoskeletal models of the spine during static load-handling activities". In: *Journal of biomechanics* 112, p. 110043. DOI: 10.1016/j.jbiomech.2020.110043.

Auer, S. (2023). "Musculoskeletal models in highly dynamic motion: effects of model parameters and mental stress". PhD thesis. Universität Regensburg. DOI: 10.5283/epub.55106.

Auer, S., S. Kubowitsch, F. Süß, T. Renkawitz, W. Krutsch, and S. Dendorfer (2021). "Mental stress reduces performance and changes musculoskeletal loading in football-related movements". In: *Science & medicine in football* 5.4, pp. 323–329. DOI: 10.1080/24733938.2020.1860253.

Auer, S., F. Süß, and S. Dendorfer (2024). "Using markerless motion capture and musculoskeletal models: An evaluation of joint kinematics". In: *Technology and health care : official journal of the European Society for Engineering and Medicine*. DOI: 10.3233/THC-240202.

Aurbach, M., J. Spicka, F. Süß, and S. Dendorfer (2020). "Evaluation of musculoskeletal modelling parameters of the shoulder complex during humeral abduction above 90°". In: *Journal of biomechanics* 106, p. 109817. DOI: 10.1016/j.jbiomech.2020.109817.

Bartl, R. (2023a). *Osteoporose: Biologie, Prophylaxe, Diagnose und Therapie*. Essentials. Berlin and Heidelberg: Springer. URL: https://link.springer.com/978-3-662-67210-5.

— (2023b). *Osteoporosis in Clinical Practice*. 1st ed. 2023. Cham: Springer International Publishing and Imprint Springer. DOI: 10.1007/978-3-031-14652-7.

Bayraktar, H. H., E. F. Morgan, G. L. Niebur, G. E. Morris, E. K. Wong, and T. M. Keaveny (2004). "Comparison of the elastic and yield properties of human femoral trabecular and cortical bone tissue". In: *Journal of biomechanics* 37.1, pp. 27–35. DOI: 10.1016/S0021-9290(03)00257-4.

Benditz, A., S. Auer, J. F. Spörrer, S. Wolkerstorfer, J. Grifka, F. Suess, and S. Dendorfer (2018). "Regarding loads after spinal fusion, every level should be seen separately: a musculoskeletal analysis". In: *European spine journal : official publication of the European Spine Society, the European Spinal Deformity Society, and the European Section of the Cervical Spine Research Society* 27.8, pp. 1905–1910. DOI: 10.1007/s00586-018-5476-5.

Bonewald, L. (2019). "Use it or lose it to age: A review of bone and muscle communication". In: *Bone* 120, pp. 212–218. DOI: 10.1016/j.bone.2018.11.002.

Bottino, A. and A. Laurentini (2004). "The visual hull of smooth curved objects". In: *IEEE transactions on pattern analysis and machine intelligence* 26.12, pp. 1622–1632. DOI: 10.1109/TPAMI.2004.130.

Brennan, L., E. Dorronzoro Zubiete, and B. Caulfield (2019). "Feedback Design in Targeted Exercise Digital Biofeedback Systems for Home Rehabilitation: A Scoping Review". In: *Sensors (Basel, Switzerland)* 20.1. DOI: 10.3390/s20010181.

Castrogiovanni, P., F. M. Trovato, M. A. Szychlinska, H. Nsir, R. Imbesi, and G. Musumeci (2016). "The importance of physical activity in osteoporosis. From the molecular pathways to the clinical evidence". In: *Histology and histopathology* 31.11, pp. 1183–1194. DOI: 10.14670/HH-11-793.

Chen, H., X. Zhou, H. Fujita, M. Onozuka, and K.-Y. Kubo (2013). "Age-related changes in trabecular and cortical bone microstructure". In: *International journal of endocrinology* 2013, p. 213234. DOI: 10.1155/2013/213234.

Cohen, J. (1988). *Statistical Power Analysis for the Behavioral Sciences*. 2nd ed. Hillsdale, NJ: Erlbaum.

"Consensus development conference: diagnosis, prophylaxis, and treatment of osteoporosis" (1993). In: *The American Journal of Medicine* 94.6, pp. 646–650. DOI: 10.1016/0002-9343(93)90218-e.

Damsgaard, M., J. Rasmussen, S. T. Christensen, E. Surma, and M. de Zee (2006). "Analysis of musculoskeletal systems in the AnyBody Modeling System". In: *Simulation Modelling Practice and Theory* 14.8, pp. 1100–1111. DOI: 10.1016/j.simpat.2006.09.001.

Di Raimondo, G., B. Vanwanseele, A. van der Have, J. Emmerzaal, M. Willems, B. A. Killen, and I. Jonkers (2022). "Inertial Sensor-to-Segment Calibration for Accurate 3D Joint Angle Calculation for Use in OpenSim". In: *Sensors* 22.9, p. 3259. DOI: 10.3390/s22093259.

Dichev, C. and D. Dicheva (2017). "Gamifying education: what is known, what is believed and what remains uncertain: a critical review". In: *International Journal of Educational Technology in Higher Education* 14.1. DOI: 10.1186/s41239-017-0042-5.

Djonic, D., P. Milovanovic, S. Nikolic, M. Ivovic, J. Marinkovic, T. Beck, and M. Djuric (2011). "Inter-sex differences in structural properties of aging femora: implications on differential bone fragility: a cadaver study". In: *Journal of bone and mineral metabolism* 29.4, pp. 449–457. DOI: 10.1007/s00774-010-0240-x.

Dorschky, E., M. Nitschke, M. Mayer, I. Weygers, H. Gassner, T. Seel, B. Eskofier, and A. Koelewijn (2023). *Comparing sparse inertial sensor setups for sagittal-plane walking and running reconstructions*. DOI: 10.1101/2023.05.25.542228.

Engelhardt, L., M. Melzner, L. Havelkova, P. Fiala, P. Christen, S. Dendorfer, and U. Simon (2020). "A new musculoskeletal AnyBody™ detailed hand model". In: *Computer methods in biomechanics and biomedical engineering*, pp. 1–11. DOI: 10.1080/10255842.2020.1851367.

Faisal, T. R. and Y. Luo (2015). "Stress variations owing to single-stance load and sideways fall result in fracture at proximal femur". In: *2015 IEEE 12th International Symposium on Biomedical Imaging (ISBI)*. IEEE, pp. 1–4. DOI: 10.1109/ISBI.2015.7163802.

Florence, G. E., T. Oosthuyse, and A. N. Bosch (2024). "Skeletal site-specific effects of jump training on bone mineral density in adults: a systematic review and meta-analysis". In: *Journal of sports sciences*, pp. 1–14. DOI: 10.1080/02640414.2024.2312052.

Frost, H. M. and E. Schönau (2000). "The "Muscle-Bone Unit" in Children and Adolescents: A 2000 Overview". In: *Journal of Pediatric Endocrinology & Metabolism* 13, pp. 571–590.

Frost, H. M. (2000). "The Utah paradigm of skeletal physiology: an overview of its insights for bone, cartilage and collagenous tissue organs". In: *J Bone Miner Metab* 18, pp. 305–316.

Gomes, M., D. Figueiredo, L. Teixeira, V. Poveda, C. Paúl, A. Santos-Silva, and E. Costa (2017). "Physical inactivity among older adults across Europe based on the SHARE database". In: *Age and ageing* 46.1, pp. 71–77. DOI: 10.1093/ageing/afw165.

Herbert, A. J., A. G. Williams, P. J. Hennis, R. M. Erskine, C. Sale, S. H. Day, and G. K. Stebbings (2019). "The interactions of physical activity, exercise and genetics and their associations with bone mineral density: implications for injury risk in elite athletes". In: *European journal of applied physiology* 119.1, pp. 29–47. DOI: 10.1007/s00421-018-4007-8.

Hirschfeld, H. P., R. Kinsella, and G. Duque (2017). "Osteosarcopenia: where bone, muscle, and fat collide". In: *Osteoporosis international : a journal established as result of cooperation between the European Foundation for Osteoporosis and the National Os-*

teoporosis Foundation of the USA 28.10, pp. 2781–2790. DOI: 10.1007/s00198-017-4151-8.

Hofmann, G. O. (2021). *Medizin für Ingenieure*. München: Carl Hanser Verlag GmbH & Co. KG. DOI: 10.3139/9783446464230.

Hossain, M. S. B., Z. Guo, and H. Choi (2023). "Estimation of Lower Extremity Joint Moments and 3D Ground Reaction Forces Using IMU Sensors in Multiple Walking Conditions: A Deep Learning Approach". In: *IEEE journal of biomedical and health informatics* 27.6, pp. 2829–2840. DOI: 10.1109/JBHI.2023.3262164.

Hosseini, N. and N. Arjmand (2024). "An artificial neural network for full-body posture prediction in dynamic lifting activities and effects of its prediction errors on model-estimated spinal loads". In: *Journal of biomechanics* 162, p. 111896. DOI: 10.1016/j.jbiomech.2023.111896.

Hourigan, S. R., J. C. Nitz, S. G. Brauer, S. O'Neill, J. Wong, and C. A. Richardson (2008). "Positive effects of exercise on falls and fracture risk in osteopenic women". In: *Osteoporosis international : a journal established as result of cooperation between the European Foundation for Osteoporosis and the National Osteoporosis Foundation of the USA* 19.7, pp. 1077–1086. DOI: 10.1007/s00198-007-0541-7.

Hribernik, M., A. Umek, S. Tomažič, and A. Kos (2022). "Review of Real-Time Biomechanical Feedback Systems in Sport and Rehabilitation". In: *Sensors (Basel, Switzerland)* 22.8. DOI: 10.3390/s22083006.

IDC (2020). *Impact of coronavirus (COVID-19) outbreak on global wearables market growth forecast in 2019, 2020 and 2024 [Graph]*. Ed. by IDC. www.idc.com. URL: https://www.statista.com/statistics/1106297/worldwide-wearables-market-growth-impacted-by-covid-19-outbreak/.

Kanis, J. A., O. Johnell, A. Oden, B. Jonsson, C. De Laet, and A. Dawson (2000). "Risk of Hip Fracture According to the World Health Organization Criteria for Osteopenia and Osteoporosis". In: *Bone* 27.5, pp. 585–590.

Kanis, J. A., O. Johnell, A. Oden, I. Sernbo, I. Redlund-Johnell, A. Dawson, C. De Laet, and B. Jonsson (2000). "Long-Term Risk of Osteoporotic Fracture in Malmö". In: *International Osteoporosis Foundation and National Osteoporosis Foundation* 11, pp. 669–674.

Kanis, J. A., N. Norton, N. C. Harvey, T. Jacobson, H. Johansson, M. Lorentzon, E. V. McCloskey, C. Willers, and F. Borgström (2021). "SCOPE 2021: a new scorecard for osteoporosis in Europe". In: *Archives of osteoporosis* 16.1, p. 82. DOI: 10.1007/s11657-020-00871-9.

Kaptoge, S., N. Dalzell, N. Loveridge, T. J. Beck, K.-T. Khaw, and J. Reeve (2003). "Effects of gender, anthropometric variables, and aging on the evolution of hip strength in men and women aged over 65". In: *Bone* 32.5, pp. 561–570. DOI: 10.1016/s8756-3282(03)00055-3.

Koshy, F. S., K. George, P. Poudel, R. Chalasani, M. R. Goonathilake, S. Waqar, S. George, W. Jean-Baptiste, A. Yusuf Ali, B. Inyang, and L. Mohammed (2022). "Exercise Prescription and the Minimum Dose for Bone Remodeling Needed to Prevent Osteoporosis in Postmenopausal Women: A Systematic Review". In: *Cureus* 14.6, e25993. DOI: 10.7759/cureus.25993.

Krishnan, G., C. Kshirsagar, G. Ananthasuresh, and N. Bhat (2007). "MicromachinedHigh-Resolution Accelerometers". In: *Journal of the Indian Institute of Science* 87.3, pp. 333–361.

Levadnyi, I., J. Awrejcewicz, Y. Zhang, and Y. Gu (2021). "Comparison of femur strain under different loading scenarios: Experimental testing". In: *Proceedings of the Institution of Mechanical Engineers. Part H, Journal of engineering in medicine* 235.1, pp. 17–27. DOI: 10.1177/0954411920951033.

Liang, W., F. Wang, A. Fan, W. Zhao, W. Yao, and P. Yang (2023). "Extended Application of Inertial Measurement Units in Biomechanics: From Activity Recognition to Force Estimation". In: *Sensors (Basel, Switzerland)* 23.9. DOI: 10.3390/s23094229.

Lin, H.-C., M.-J. Chen, C.-H. Lee, L.-C. Kung, and J.-T. Huang (2023). "Fall Recognition Based on an IMU Wearable Device and Fall Verification through a Smart Speaker and the IoT". In: *Sensors (Basel, Switzerland)* 23.12. DOI: 10.3390/s23125472.

Lippuner, K., M. Golder, and R. Greiner (2005). "Epidemiology and direct medical costs of osteoporotic fractures in men and women in Switzerland". In: *Osteoporosis international : a journal established as result of cooperation between the European Foundation for Osteoporosis and the National Osteoporosis Foundation of the USA* 16 Suppl 2, S8–S17. DOI: 10.1007/s00198-004-1696-0.

Litke, N., T. Daniel, S. Wallacher, L. Cordes, D. Henning, E. Schmidt, L. Doll, and M. Wensing (2021). "Einfluss der COVID-19 Pandemie auf die ambulante Physiotherapie". In: *Zeitschrift fur Evidenz, Fortbildung und Qualitat im Gesundheitswesen* 165, pp. 58–67. DOI: 10.1016/j.zefq.2021.07.002.

Masoumian Hosseini, M., S. T. Masoumian Hosseini, K. Qayumi, S. Hosseinzadeh, and S. S. Sajadi Tabar (2023). "Smartwatches in healthcare medicine: assistance and monitoring; a scoping review". In: *BMC medical informatics and decision making* 23.1, p. 248. DOI: 10.1186/s12911-023-02350-w.

Mazeas, A., M. Duclos, B. Pereira, and A. Chalabaev (2022). "Evaluating the Effectiveness of Gamification on Physical Activity: Systematic Review and Meta-analysis of Randomized Controlled Trials". In: *Journal of medical Internet research* 24.1, e26779. DOI: 10.2196/26779.

Melton, L. J., E. J. Atkinson, M. K. O'Connor, W. M. O'Fallon, and B. L. Riggs (1998). "Bone Density and Fracture Risk in Men". In: *Journal of bone and mineral research : the official journal of the American Society for Bone and Mineral Research* 12.

Melzner, M., K. M. Ismail, Z. Rušavý, V. Kališ, F. Süß, and S. Dendorfer (2021). "Musculoskeletal lower back load of accoucheurs during childbirth - A pilot and feasibility study". In: *European journal of obstetrics, gynecology, and reproductive biology* 264, pp. 306–313. DOI: 10.1016/j.ejogrb.2021.07.042.

Metcalfe, D. (2008). "The pathophysiology of osteoporotic hip fracture". In: *Mcgill J Med.* 11.1, pp. 51–57.

Montes, J., R. Tandy, J. Young, S. P. Lee, and J. W. Navalta (2020). "Step Count Reliability and Validity of Five Wearable Technology Devices While Walking and Jogging in both a Free Motion Setting and on a Treadmill". In: *Int J Exerc Sci.* 13.7, pp. 410–426.

Movella Inc. (2022). *Xsens DOT User Manual: Document XD0502P, Revision G, 9 June 2022*. URL: https://www.xsens.com/hubfs/Downloads/Manuals/Xsens%20DOT%20User%20Manual.pdf.

Müller, M. (2007). *Information Retrieval for Music and Motion*. SpringerLink Bücher. Berlin, Heidelberg: Springer-Verlag BerlinHeidelberg. DOI: 10.1007/978-3-540-74048-3. URL: https://swbplus.bsz-bw.de/bsz273299425err.htm.

Multanen, J., M. T. Nieminen, A. Häkkinen, U. M. Kujala, T. Jämsä, H. Kautiainen, E. Lammentausta, R. Ahola, H. Selänne, R. Ojala, I. Kiviranta, and A. Heinonen (2014). "Effects of high-impact training on bone and articular cartilage: 12-month randomized controlled quantitative MRI study". In: *Journal of bone and mineral research : the official journal of the American Society for Bone and Mineral Research* 29.1, pp. 192–201. DOI: 10.1002/jbmr.2015.

Mündermann, L., S. Corazza, and T. P. Andriacchi (2006). "The evolution of methods for the capture of human movement leading to markerless motion capture for biomechanical applications". In: *Journal of neuroengineering and rehabilitation* 3, p. 6. DOI: 10.1186/1743-0003-3-6.

Mundt, M., A. Koeppe, S. David, T. Witter, F. Bamer, W. Potthast, and B. Markert (2020). "Estimation of Gait Mechanics Based on Simulated and Measured IMU Data Using an Artificial Neural Network". In: *Frontiers in bioengineering and biotechnology* 8, p. 41. DOI: 10.3389/fbioe.2020.00041.

Nikander, R., P. Kannus, P. Dastidar, M. Hannula, L. Harrison, T. Cervinka, N. G. Narra, R. Aktour, T. Arola, H. Eskola, S. Soimakallio, A. Heinonen, J. Hyttinen, and H. Sievänen (2009). "Targeted exercises against hip fragility". In: *Osteoporosis international : a journal established as result of cooperation between the European Foundation for Osteoporosis and the National Osteoporosis Foundation of the USA* 20.8, pp. 1321–1328. DOI: 10.1007/s00198-008-0785-x.

Nissen, N., E. M. Hauge, B. Abrahamsen, J. E. B. Jensen, L. Mosekilde, and K. Brixen (2005). "Geometry of the proximal femur in relation to age and sex: a cross-sectional

study in healthy adult Danes". In: *Acta radiologica (Stockholm, Sweden : 1987)* 46.5, pp. 514–518. DOI: 10.1080/02841850510021562.

Nitschke, M., E. Dorschky, S. Leyendecker, B. M. Eskofier, and A. D. Koelewijn (2024). "Estimating 3D kinematics and kinetics from virtual inertial sensor data through musculoskeletal movement simulations". In: *Frontiers in bioengineering and biotechnology* 12, p. 1285845. DOI: 10.3389/fbioe.2024.1285845.

Odén, A., E. V. McCloskey, J. A. Kanis, N. C. Harvey, and H. Johansson (2015). "Burden of high fracture probability worldwide: secular increases 2010-2040". In: *Osteoporosis international : a journal established as result of cooperation between the European Foundation for Osteoporosis and the National Osteoporosis Foundation of the USA* 26.9, pp. 2243–2248. DOI: 10.1007/s00198-015-3154-6.

Pataky, T. C. (2012). "One-dimensional statistical parametric mapping in Python". In: *Computer methods in biomechanics and biomedical engineering* 15.3, pp. 295–301. DOI: 10.1080/10255842.2010.527837.

— (2016). "rft1d : Smooth One-Dimensional Random Field Upcrossing Probabilities in Python". In: *Journal of Statistical Software* 71.7. DOI: 10.18637/jss.v071.i07.

Piccardi, M. (2004). "Background subtraction techniques: a review". In: *2004 IEEE International Conference on Systems, Man and Cybernetics (IEEE Cat. No.04CH37583)*. IEEE, pp. 3099–3104. DOI: 10.1109/ICSMC.2004.1400815.

Poole, K. E. S., P. M. Mayhew, C. M. Rose, J. K. Brown, P. J. Bearcroft, N. Loveridge, and J. Reeve (2010). "Changing structure of the femoral neck across the adult female lifespan". In: *Journal of bone and mineral research : the official journal of the American Society for Bone and Mineral Research* 25.3, pp. 482–491. DOI: 10.1359/jbmr.090734.

Pouresmaeili, F., B. Kamalidehghan, M. Kamarehei, and Y. M. Goh (2018). "A comprehensive overview on osteoporosis and its risk factors". In: *Therapeutics and clinical risk management* 14, pp. 2029–2049. DOI: 10.2147/TCRM.S138000.

Pustišek, M., Y. Wei, Y. Sun, A. Umek, and A. Kos (2021). "The role of technology for accelerated motor learning in sport". In: *Personal and Ubiquitous Computing* 25.6, pp. 969–978. DOI: 10.1007/s00779-019-01274-5.

Rasmussen, J., S. Skejø, and R. P. Waagepetersen (2023). "Predicting Tissue Loads in Running from Inertial Measurement Units". In: *Sensors (Basel, Switzerland)* 23.24. DOI: 10.3390/s23249836.

Reinker, L., D. Bläsing, R. Bierl, S. Ulbricht, and S. Dendorfer (2023). "Correlation of Acceleration Curves in Gravitational Direction for Different Body Segments during High-Impact Jumping Exercises". In: *Sensors (Basel, Switzerland)* 23.4. DOI: 10.3390/s23042276.

Renkawitz, T., T. Weber, S. Dullien, M. Woerner, S. Dendorfer, J. Grifka, and M. Weber (2016). "Leg length and offset differences above 5mm after total hip arthroplasty are

associated with altered gait kinematics". In: *Gait & posture* 49, pp. 196–201. DOI: 10.1016/j.gaitpost.2016.07.011.

Richter, F. (2017). *What Smartwatches Are Actually Used For [Digital Image]*. Ed. by NPD Connected Intelligence/WEAR. URL: https://www.statista.com/chart/10783/use-cases-for-smartwatches/.

Riddick, R., E. Smits, G. Faber, C. Shearwin, P. Hodges, and W. van den Hoorn (2023). "Estimation of human spine orientation with inertial measurement units (IMU) at low sampling rate: How low can we go?" In: *Journal of biomechanics* 157, p. 111726. DOI: 10.1016/j.jbiomech.2023.111726.

Rodricks, N., S. Deccy, M. E. Saint Louis, D. Quintero, J. Ramirez, and K. J. Paultre (2024). "Effect of Plyometrics on Bone Mineral Density in Young Adults: A Systematic Review and Meta-Analysis". In: *Translational Journal of the American College of Sports Medicine* 9.1. DOI: 10.1249/TJX.0000000000000242.

Rossi, D. de and P. Veltink (2010). "Wearable technology for biomechanics: e-textile or micromechanical sensors?" In: *IEEE engineering in medicine and biology magazine : the quarterly magazine of the Engineering in Medicine & Biology Society* 29.3, pp. 37–43. DOI: 10.1109/MEMB.2010.936555.

Simonsen, E. B., M. Stensvig, T. B. Andersen, and M. S. Andersen (2023). "Propulsive fractions of joint work during maximal sprint running". In: *Sport Sciences for Health*. DOI: 10.1007/s11332-023-01121-4.

Statista (2023). *Wearable devices usage in selected countries as of September 2023 [Graph]*. Ed. by Statista. https://www.statista.com. URL: https://www.statista.com/forecasts/1101110/wearables-devices-usage-in-selected-countries.

Stoll, C., N. Hasler, J. Gall, H.-P. Seidel, and C. Theobalt (2011). "Fast articulated motion tracking using a sums of Gaussians body model". In: *2011 International Conference on Computer Vision*. IEEE, pp. 951–958. DOI: 10.1109/ICCV.2011.6126338.

Strongman, C., F. Cavallerio, M. A. Timmis, and A. Morrison (2023). "A Scoping Review of the Validity and Reliability of Smartphone Accelerometers When Collecting Kinematic Gait Data". In: *Sensors (Basel, Switzerland)* 23.20. DOI: 10.3390/s23208615.

Swanenburg, J., T. Mulder, E. D. de Bruin, and D. Uebelhart (2003). "Physiotherapeutische Interventionen bei Osteoporose". In: *Zeitschrift fur Rheumatologie* 62.6, pp. 522–526. DOI: 10.1007/s00393-003-0562-3.

Tillmann, B. N. (2016). *Atlas der Anatomie des Menschen*. Berlin, Heidelberg: Springer Berlin Heidelberg. DOI: 10.1007/978-3-662-49288-8.

TrendForce (2019). *Smartwatch unit shipments worldwide from 2016 to 2022 (in millions): Unit shipment of smartwatches worldwide 2016-2022*. Ed. by TrendForce. TrendForce. URL: https://www.statista.com/study/15607/wearables-statista-dossier/.

Turner, C. H., J. Rho, Y. Takano, T. Y. Tsui, and G. M. Pharr (1999). "The elastic properties of trabecular and cortical bone tissues are similar: results from two micro-

scopic measurement techniques". In: *Journal of biomechanics* 32.4, pp. 437–441. DOI: 10.1016/S0021-9290(98)00177-8.

Vainionpää, A., R. Korpelainen, H. K. Väänänen, J. Haapalahti, T. Jämsä, and J. Leppäluoto (2009). "Effect of impact exercise on bone metabolism". In: *Osteoporosis international : a journal established as result of cooperation between the European Foundation for Osteoporosis and the National Osteoporosis Foundation of the USA* 20.10, pp. 1725–1733. DOI: 10.1007/s00198-009-0881-6.

Vainionpää, A., R. Korpelainen, E. Vihriälä, A. Rinta-Paavola, J. Leppäluoto, and T. Jämsä (2006). "Intensity of exercise is associated with bone density change in premenopausal women". In: *Osteoporosis international : a journal established as result of cooperation between the European Foundation for Osteoporosis and the National Osteoporosis Foundation of the USA* 17.3, pp. 455–463. DOI: 10.1007/s00198-005-0005-x.

Vainionpää, A. (2007). *Bone adaptation to impact loading: Significance of loading intensity*. Vol. 935. Acta Universitatis Ouluensis. Series D, Medica. Oulu: Oulun yliopisto.

Vainionpää, A., R. Korpelainen, H. Kaikkonen, M. Knip, J. Leppäluoto, and T. Jämsä (2007). "Effect of impact exercise on physical performance and cardiovascular risk factors". In: *Medicine and science in sports and exercise* 39.5, pp. 756–763. DOI: 10.1249/mss.0b013e318031c039.

Vainionpää, A., R. Korpelainen, J. Leppäluoto, and T. Jämsä (2005). "Effects of high-impact exercise on bone mineral density: a randomized controlled trial in premenopausal women". In: *Osteoporosis international : a journal established as result of cooperation between the European Foundation for Osteoporosis and the National Osteoporosis Foundation of the USA* 16.2, pp. 191–197. DOI: 10.1007/s00198-004-1659-5.

Veronese, N., H. Kolk, and S. Maggi (2021). *Orthogeriatrics: The Management of Older Patients with Fragility Fractures: Epidemiology of Fragility Fractures and Social Impact*. 2nd. Cham (CH). DOI: 10.1007/978-3-030-48126-1{\textunderscore}2.

Viecelli, C., D. Graf, D. Aguayo, E. Hafen, and R. M. Füchslin (2020). "Using smartphone accelerometer data to obtain scientific mechanical-biological descriptors of resistance exercise training". In: *PloS one* 15.7, e0235156. DOI: 10.1371/journal.pone.0235156.

Vlachopoulos, D., A. R. Barker, E. Ubago-Guisado, C. A. Williams, and L. Gracia-Marco (2018). "The effect of a high-impact jumping intervention on bone mass, bone stiffness and fitness parameters in adolescent athletes". In: *Archives of osteoporosis* 13.1, p. 128. DOI: 10.1007/s11657-018-0543-4.

Voo, L., M. Armand, and M. Kleinberger (2004). "Stress fracture risk analysis of the human femur based on computational biomechanics". In: *Johns Hopkins APL Technical Digest (Applied Physics Laboratory)* 25.

Weber, T., S. Dendorfer, S. K. Bulstra, J. Grifka, G. J. Verkerke, and T. Renkawitz (2016). "Gait six month and one-year after computer assisted Femur First THR vs.

conventional THR. Results of a patient- and observer- blinded randomized controlled trial". In: *Gait & posture* 49, pp. 418–425. DOI: 10.1016/j.gaitpost.2016.06.035.

Wilhelm, T. and M. Weidt (2011). "Bewegungen des eigenen Körpers – Möglichkeiten der Messwerterfassung im Vergleich". In: *PhyDid B - Didaktik der Physik - Beiträge zur DPG-Frühjahrstagung*. URL: https://ojs.dpg-physik.de/index.php/phydid-b/article/view/260.

Wolff, J. (1892). *Das Gesetz der Transformation der Knochen*. Berlin: Aug. Hirschwald.

Woods, J. A., N. T. Hutchinson, S. K. Powers, W. O. Roberts, M. C. Gomez-Cabrera, Z. Radak, I. Berkes, A. Boros, I. Boldogh, C. Leeuwenburgh, H. J. Coelho-Júnior, E. Marzetti, Y. Cheng, J. Liu, J. L. Durstine, J. Sun, and L. L. Ji (2020). "The COVID-19 pandemic and physical activity". In: *Sports Medicine and Health Science* 2.2, pp. 55–64. DOI: 10.1016/j.smhs.2020.05.006.

Zhang, S., X. Huang, X. Zhao, B. Li, Y. Cai, X. Liang, and Q. Wan (2022). "Effect of exercise on bone mineral density among patients with osteoporosis and osteopenia: A systematic review and network meta-analysis". In: *Journal of clinical nursing* 31.15-16, pp. 2100–2111. DOI: 10.1111/jocn.16101.

Zysset, P. K., X. E. Guo, C. E. Hoffler, K. E. Moore, and S. A. Goldstein (1999). "Elastic modulus and hardness of cortical and trabecular bone lamellae measured by nanoindentation in the human femur". In: *Journal of biomechanics* 32.10, pp. 1005–1012. DOI: 10.1016/S0021-9290(99)00111-6.

Acknowledgments

Completing this doctoral dissertation has been an extraordinary journey, and it would not have been possible without the support, guidance, and encouragement of many people. I am deeply grateful to everyone who has contributed to this thesis in various ways. I would like to express my sincere thanks to my supervisor Sebastian for making this doctorate possible and for his great support and guidance during this project. Your supervision has been instrumental in shaping this dissertation and my growth as a researcher. I am profoundly thankful to my mentors for their constructive feedback and encouragement, which have significantly enhanced the quality of this work. To my colleagues and friends in the Laboratory for Biomechanics, thank you for the stimulating discussions and the countless moments of shared laughter and support. To my wife, thank you for your endless patience, understanding, and emotional support during the ups and downs of this journey. I would like to thank my family and friends from the bottom of my heart for their support and for always being there for me. Without your support, I would not have been able to do it. I am very happy to have so many great people around me.

Declaration of authorship

I, Lukas Reinker, born on 27.03.1996 in Augsburg declare that this thesis titled, "Real-time simulation and evaluation of data from wearable smart-devices to prevent musculoskeletal signs of aging" and the work presented in it are my own. I confirm that

- this work was done wholly or mainly while in candidature for a research degree at this University.
- where any part of this thesis has previously been submitted for a degree or any other qualification at this University or any other institution, this has been clearly stated.
- where I have consulted the published work of others, this is always clearly attributed.
- where I have quoted from the work of others, the source is always given. With the exception of such quotations, this thesis is entirely my own work. I did not receive paid help from mediation and advisory services e.g. PhD consultants.
- I have acknowledged all main sources of help.
- where the thesis is based on work done by myself jointly with others, I have made clear exactly what was done by others and what I have contributed myself.

Regensburg, 28.06.2024

Lukas Reinker, M.Sc.

Appendix A

Supplementary material to chapter 3

Listing B.1: Excerpts from the AMS code for calculating the cutting forces and moments in the femoral neck

```
AnyRefNode FemurHeadNode =
{
  sRel = 0.5*(.VastusLateralisSuperior2Node.sRel+.HipJointAnatomicalFrame.sRel);
  AnyDrawRefFrame drws = {ScaleXYZ = {1,1,1}*0.3;RGB={1,1,0};};
  ARel = RotMat(-2*.RotAngle+(5*pi/4),x);
};

AnyForceMomentMeasure2 FemurForceMomentHip = {

  RefPoint = &Main.HumanModel.BodyModel.Right.Leg.Seg.Thigh.FemurHeadNode;
  IncludeSegments = {&Main.HumanModel.BodyModel.Right.Leg.Seg.Thigh};


  IncludeForces = {
    &Main.HumanModel.BodyModel.Right.Leg.Mus.SoleusMedialis1,
    &Main.HumanModel.BodyModel.Right.Leg.Mus.SoleusMedialis2,
    &Main.HumanModel.BodyModel.Right.Leg.Mus.SoleusMedialis2,
    &Main.HumanModel.BodyModel.Right.Leg.Mus.SoleusMedialis3,
    &Main.HumanModel.BodyModel.Right.Leg.Mus.SoleusLateralis1,
    &Main.HumanModel.BodyModel.Right.Leg.Mus.SoleusLateralis2,
    &Main.HumanModel.BodyModel.Right.Leg.Mus.SoleusLateralis3,
    &Main.HumanModel.BodyModel.Right.Leg.Mus.GastrocnemiusLateralis1,
    &Main.HumanModel.BodyModel.Right.Leg.Mus.GastrocnemiusMedialis1,
    &Main.HumanModel.BodyModel.Right.Leg.Mus.FlexorDigitorumLongus1,
    &Main.HumanModel.BodyModel.Right.Leg.Mus.FlexorDigitorumLongus2,
    &Main.HumanModel.BodyModel.Right.Leg.Mus.FlexorDigitorumLongus3,
    &Main.HumanModel.BodyModel.Right.Leg.Mus.FlexorHallucisLongus1,
    &Main.HumanModel.BodyModel.Right.Leg.Mus.FlexorHallucisLongus2,
    &Main.HumanModel.BodyModel.Right.Leg.Mus.FlexorHallucisLongus3,
    &Main.HumanModel.BodyModel.Right.Leg.Mus.TibialisPosteriorLateralis1,
    &Main.HumanModel.BodyModel.Right.Leg.Mus.TibialisPosteriorLateralis2,
    &Main.HumanModel.BodyModel.Right.Leg.Mus.TibialisPosteriorLateralis3,
    &Main.HumanModel.BodyModel.Right.Leg.Mus.TibialisPosteriorMedialis1,
    &Main.HumanModel.BodyModel.Right.Leg.Mus.TibialisPosteriorMedialis2,
```

&Main.HumanModel.BodyModel.Right.Leg.Mus.TibialisPosteriorMedialis3,
&Main.HumanModel.BodyModel.Right.Leg.Mus.TibialisAnterior1,
&Main.HumanModel.BodyModel.Right.Leg.Mus.TibialisAnterior2,
&Main.HumanModel.BodyModel.Right.Leg.Mus.TibialisAnterior3,
&Main.HumanModel.BodyModel.Right.Leg.Mus.PeroneusBrevis1,
&Main.HumanModel.BodyModel.Right.Leg.Mus.PeroneusBrevis2,
&Main.HumanModel.BodyModel.Right.Leg.Mus.PeroneusBrevis3,
&Main.HumanModel.BodyModel.Right.Leg.Mus.PeroneusLongus1,
&Main.HumanModel.BodyModel.Right.Leg.Mus.PeroneusLongus2,
&Main.HumanModel.BodyModel.Right.Leg.Mus.PeroneusLongus3,
&Main.HumanModel.BodyModel.Right.Leg.Mus.ExtensorDigitorumLongus1,
&Main.HumanModel.BodyModel.Right.Leg.Mus.ExtensorDigitorumLongus2,
&Main.HumanModel.BodyModel.Right.Leg.Mus.ExtensorDigitorumLongus3,
&Main.HumanModel.BodyModel.Right.Leg.Mus.ExtensorHallucisLongus1,
&Main.HumanModel.BodyModel.Right.Leg.Mus.ExtensorHallucisLongus2,
&Main.HumanModel.BodyModel.Right.Leg.Mus.ExtensorHallucisLongus3,
&Main.HumanModel.BodyModel.Right.Leg.Mus.VastusLateralisInferior1,
&Main.HumanModel.BodyModel.Right.Leg.Mus.VastusLateralisInferior2,
&Main.HumanModel.BodyModel.Right.Leg.Mus.VastusLateralisInferior3,
&Main.HumanModel.BodyModel.Right.Leg.Mus.VastusLateralisInferior4,
&Main.HumanModel.BodyModel.Right.Leg.Mus.VastusLateralisInferior5,
&Main.HumanModel.BodyModel.Right.Leg.Mus.VastusLateralisInferior6,
&Main.HumanModel.BodyModel.Right.Leg.Mus.VastusLateralisSuperior1,
&Main.HumanModel.BodyModel.Right.Leg.Mus.VastusLateralisSuperior2,
&Main.HumanModel.BodyModel.Right.Leg.Mus.VastusMedialisInferior1,
&Main.HumanModel.BodyModel.Right.Leg.Mus.VastusMedialisInferior2,
&Main.HumanModel.BodyModel.Right.Leg.Mus.VastusMedialisMid1,
&Main.HumanModel.BodyModel.Right.Leg.Mus.VastusMedialisMid2,
&Main.HumanModel.BodyModel.Right.Leg.Mus.VastusMedialisSuperior1,
&Main.HumanModel.BodyModel.Right.Leg.Mus.VastusMedialisSuperior2,
&Main.HumanModel.BodyModel.Right.Leg.Mus.VastusMedialisSuperior3,
&Main.HumanModel.BodyModel.Right.Leg.Mus.VastusMedialisSuperior4,
&Main.HumanModel.BodyModel.Right.Leg.Mus.VastusIntermedius1,
&Main.HumanModel.BodyModel.Right.Leg.Mus.VastusIntermedius2,
&Main.HumanModel.BodyModel.Right.Leg.Mus.VastusIntermedius3,
&Main.HumanModel.BodyModel.Right.Leg.Mus.VastusIntermedius4,
&Main.HumanModel.BodyModel.Right.Leg.Mus.VastusIntermedius5,
&Main.HumanModel.BodyModel.Right.Leg.Mus.VastusIntermedius6,
&Main.HumanModel.BodyModel.Right.Leg.Mus.RectusFemoris1,
&Main.HumanModel.BodyModel.Right.Leg.Mus.RectusFemoris2,
&Main.HumanModel.BodyModel.Right.Leg.Mus.Semitendinosus1,
&Main.HumanModel.BodyModel.Right.Leg.Mus.Semimembranosus1,
&Main.HumanModel.BodyModel.Right.Leg.Mus.Semimembranosus2,
&Main.HumanModel.BodyModel.Right.Leg.Mus.Semimembranosus3,
&Main.HumanModel.BodyModel.Right.Leg.Mus.BicepsFemorisCaputLongum1,
&Main.HumanModel.BodyModel.Right.Leg.Mus.BicepsFemorisCaputBreve1,
&Main.HumanModel.BodyModel.Right.Leg.Mus.BicepsFemorisCaputBreve2,

&Main.HumanModel.BodyModel.Right.Leg.Mus.BicepsFemorisCaputBreve3,
&Main.HumanModel.BodyModel.Right.Leg.Mus.Sartorius1,
&Main.HumanModel.BodyModel.Right.Leg.Mus.IliacusLateralis1,
&Main.HumanModel.BodyModel.Right.Leg.Mus.IliacusLateralis2,
&Main.HumanModel.BodyModel.Right.Leg.Mus.IliacusMid1,
&Main.HumanModel.BodyModel.Right.Leg.Mus.IliacusMid2,
&Main.HumanModel.BodyModel.Right.Leg.Mus.IliacusMedialis1,
&Main.HumanModel.BodyModel.Right.Leg.Mus.IliacusMedialis2,
&Main.HumanModel.BodyModel.Right.Leg.Mus.GluteusMinimusAnterior1,
&Main.HumanModel.BodyModel.Right.Leg.Mus.GluteusMinimusMid1,
&Main.HumanModel.BodyModel.Right.Leg.Mus.GluteusMinimusPosterior1,
&Main.HumanModel.BodyModel.Right.Leg.Mus.GluteusMediusAnterior1,
&Main.HumanModel.BodyModel.Right.Leg.Mus.GluteusMediusAnterior2,
&Main.HumanModel.BodyModel.Right.Leg.Mus.GluteusMediusAnterior3,
&Main.HumanModel.BodyModel.Right.Leg.Mus.GluteusMediusAnterior4,
&Main.HumanModel.BodyModel.Right.Leg.Mus.GluteusMediusAnterior5,
&Main.HumanModel.BodyModel.Right.Leg.Mus.GluteusMediusAnterior6,
&Main.HumanModel.BodyModel.Right.Leg.Mus.GluteusMediusPosterior1,
&Main.HumanModel.BodyModel.Right.Leg.Mus.GluteusMediusPosterior2,
&Main.HumanModel.BodyModel.Right.Leg.Mus.GluteusMediusPosterior3,
&Main.HumanModel.BodyModel.Right.Leg.Mus.GluteusMediusPosterior4,
&Main.HumanModel.BodyModel.Right.Leg.Mus.GluteusMediusPosterior5,
&Main.HumanModel.BodyModel.Right.Leg.Mus.GluteusMediusPosterior6,
&Main.HumanModel.BodyModel.Right.Leg.Mus.GluteusMaximusSuperior1,
&Main.HumanModel.BodyModel.Right.Leg.Mus.GluteusMaximusSuperior2,
&Main.HumanModel.BodyModel.Right.Leg.Mus.GluteusMaximusSuperior3,
&Main.HumanModel.BodyModel.Right.Leg.Mus.GluteusMaximusSuperior4,
&Main.HumanModel.BodyModel.Right.Leg.Mus.GluteusMaximusSuperior5,
&Main.HumanModel.BodyModel.Right.Leg.Mus.GluteusMaximusSuperior6,
&Main.HumanModel.BodyModel.Right.Leg.Mus.GluteusMaximusInferior1,
&Main.HumanModel.BodyModel.Right.Leg.Mus.GluteusMaximusInferior2,
&Main.HumanModel.BodyModel.Right.Leg.Mus.GluteusMaximusInferior3,
&Main.HumanModel.BodyModel.Right.Leg.Mus.GluteusMaximusInferior4,
&Main.HumanModel.BodyModel.Right.Leg.Mus.GluteusMaximusInferior5,
&Main.HumanModel.BodyModel.Right.Leg.Mus.GluteusMaximusInferior6,
&Main.HumanModel.BodyModel.Right.Leg.Mus.TensorFasciaeLatae1,
&Main.HumanModel.BodyModel.Right.Leg.Mus.TensorFasciaeLatae2,
&Main.HumanModel.BodyModel.Right.Leg.Mus.Piriformis1,
&Main.HumanModel.BodyModel.Right.Leg.Mus.Gracilis1,
&Main.HumanModel.BodyModel.Right.Leg.Mus.Gracilis2,
&Main.HumanModel.BodyModel.Right.Leg.Mus.AdductorLongus1,
&Main.HumanModel.BodyModel.Right.Leg.Mus.AdductorLongus2,
&Main.HumanModel.BodyModel.Right.Leg.Mus.AdductorLongus3,
&Main.HumanModel.BodyModel.Right.Leg.Mus.AdductorLongus4,
&Main.HumanModel.BodyModel.Right.Leg.Mus.AdductorLongus5,
&Main.HumanModel.BodyModel.Right.Leg.Mus.AdductorLongus6,
&Main.HumanModel.BodyModel.Right.Leg.Mus.AdductorMagnusDistal1,

&Main.HumanModel.BodyModel.Right.Leg.Mus.AdductorMagnusDistal2,
&Main.HumanModel.BodyModel.Right.Leg.Mus.AdductorMagnusDistal3,
&Main.HumanModel.BodyModel.Right.Leg.Mus.AdductorMagnusMid1,
&Main.HumanModel.BodyModel.Right.Leg.Mus.AdductorMagnusMid2,
&Main.HumanModel.BodyModel.Right.Leg.Mus.AdductorMagnusMid3,
&Main.HumanModel.BodyModel.Right.Leg.Mus.AdductorMagnusMid4,
&Main.HumanModel.BodyModel.Right.Leg.Mus.AdductorMagnusMid5,
&Main.HumanModel.BodyModel.Right.Leg.Mus.AdductorMagnusMid6,
&Main.HumanModel.BodyModel.Right.Leg.Mus.AdductorMagnusProximal1,
&Main.HumanModel.BodyModel.Right.Leg.Mus.AdductorMagnusProximal2,
&Main.HumanModel.BodyModel.Right.Leg.Mus.AdductorMagnusProximal3,
&Main.HumanModel.BodyModel.Right.Leg.Mus.AdductorMagnusProximal4,
&Main.HumanModel.BodyModel.Right.Leg.Mus.AdductorBrevisProximal1,
&Main.HumanModel.BodyModel.Right.Leg.Mus.AdductorBrevisProximal2,
&Main.HumanModel.BodyModel.Right.Leg.Mus.AdductorBrevisMid1,
&Main.HumanModel.BodyModel.Right.Leg.Mus.AdductorBrevisMid2,
&Main.HumanModel.BodyModel.Right.Leg.Mus.AdductorBrevisDistal1,
&Main.HumanModel.BodyModel.Right.Leg.Mus.AdductorBrevisDistal2,
&Main.HumanModel.BodyModel.Right.Leg.Mus.GemellusInferior1,
&Main.HumanModel.BodyModel.Right.Leg.Mus.GemellusSuperior1,
&Main.HumanModel.BodyModel.Right.Leg.Mus.ObturatorExternusSuperior1,
&Main.HumanModel.BodyModel.Right.Leg.Mus.ObturatorExternusSuperior2,
&Main.HumanModel.BodyModel.Right.Leg.Mus.ObturatorExternusSuperior3,
&Main.HumanModel.BodyModel.Right.Leg.Mus.ObturatorExternusInferior1,
&Main.HumanModel.BodyModel.Right.Leg.Mus.ObturatorExternusInferior2,
&Main.HumanModel.BodyModel.Right.Leg.Mus.ObturatorInternus1,
&Main.HumanModel.BodyModel.Right.Leg.Mus.ObturatorInternus2,
&Main.HumanModel.BodyModel.Right.Leg.Mus.ObturatorInternus3,
&Main.HumanModel.BodyModel.Right.Leg.Mus.Pectineus1,
&Main.HumanModel.BodyModel.Right.Leg.Mus.Pectineus2,
&Main.HumanModel.BodyModel.Right.Leg.Mus.Pectineus3,
&Main.HumanModel.BodyModel.Right.Leg.Mus.Pectineus4,
&Main.HumanModel.BodyModel.Right.Leg.Mus.Plantaris1,
&Main.HumanModel.BodyModel.Right.Leg.Mus.Popliteus1,
&Main.HumanModel.BodyModel.Right.Leg.Mus.Popliteus2,
&Main.HumanModel.BodyModel.Right.Leg.Mus.QuadratusFemoris1,
&Main.HumanModel.BodyModel.Right.Leg.Mus.QuadratusFemoris2,
&Main.HumanModel.BodyModel.Right.Leg.Mus.QuadratusFemoris3,
&Main.HumanModel.BodyModel.Right.Leg.Mus.QuadratusFemoris4,
&Main.HumanModel.BodyModel.Right.Leg.TrunkMuscles.PsoasMajor.PMT12I_TM,
&Main.HumanModel.BodyModel.Right.Leg.TrunkMuscles.PsoasMajor.PML1I_TM,
&Main.HumanModel.BodyModel.Right.Leg.TrunkMuscles.PsoasMajor.PML1T_TM,
&Main.HumanModel.BodyModel.Right.Leg.TrunkMuscles.PsoasMajor.PML2I_TM,
&Main.HumanModel.BodyModel.Right.Leg.TrunkMuscles.PsoasMajor.PML2T_TM,
&Main.HumanModel.BodyModel.Right.Leg.TrunkMuscles.PsoasMajor.PML3I_TM,
&Main.HumanModel.BodyModel.Right.Leg.TrunkMuscles.PsoasMajor.PML3T_TM,
&Main.HumanModel.BodyModel.Right.Leg.TrunkMuscles.PsoasMajor.PML4I_TM,

```
    &Main.HumanModel.BodyModel.Right.Leg.TrunkMuscles.PsoasMajor.PML4T_TM,
    &Main.HumanModel.BodyModel.Right.Leg.TrunkMuscles.PsoasMajor.PML5_TM,
    &Main.HumanModel.BodyModel.Right.Leg.TrunkMuscles.PsoasMajor.PML5T_TM,
    &Main.HumanModel.BodyModel.Right.Leg.TrunkMuscles.PsoasMajor.PMT12I_TM,
    &Main.HumanModel.BodyModel.Right.Leg.TrunkMuscles.PsoasMajor.PML1I_TM,
    &Main.HumanModel.BodyModel.Right.Leg.TrunkMuscles.PsoasMajor.PML1T_TM,
    &Main.HumanModel.BodyModel.Right.Leg.TrunkMuscles.PsoasMajor.PML2I_TM,
    &Main.HumanModel.BodyModel.Right.Leg.TrunkMuscles.PsoasMajor.PML2T_TM,
    &Main.HumanModel.BodyModel.Right.Leg.TrunkMuscles.PsoasMajor.PML3I_TM,
    &Main.HumanModel.BodyModel.Right.Leg.TrunkMuscles.PsoasMajor.PML3T_TM,
    &Main.HumanModel.BodyModel.Right.Leg.TrunkMuscles.PsoasMajor.PML4I_TM,
    &Main.HumanModel.BodyModel.Right.Leg.TrunkMuscles.PsoasMajor.PML4T_TM,
    &Main.HumanModel.BodyModel.Right.Leg.TrunkMuscles.PsoasMajor.PML5_TM,
    &Main.HumanModel.BodyModel.Right.Leg.TrunkMuscles.PsoasMajor.PML5T_TM,
    &Main.HumanModel.BodyModel.Right.Leg.Jnt.Hip.Constraints.Reaction
  };

  //          IncludeInertiaForces = On;
  //          IncludeGravity = On;

  CutSystem = On;
  CutSystemNormal = y;
};
```

Listing B.2: Python code for calculating occuring stress and strain in the femoral neck as well as visualization

```
import time

start_time=time.time()

import numpy as np
import h5py
import anypytools.h5py_wrapper as h5py2
import mvnx
import glob
import os
import matplotlib.pyplot as plt
import pandas as pd
import detecta
import math
import seaborn as sns
import matplotlib.colors as mc

from pathlib import Path
from scipy.signal import find_peaks
from pickle import dump, load
```

```
from scipy import stats
from numpy import log as ln



anthro_data=pd.read_excel(r'Anthropometrische Daten.xlsx')
for i in range(0,len(anthro_data)):
    if anthro_data.iloc[i,0] == 'weiblich':
        anthro_data.iloc[i,0]='f'
    else:
        anthro_data.iloc[i,0]='m'

for i in range(0,len(anthro_data)):
    if anthro_data.iloc[i,5] == 'links':
        anthro_data.iloc[i,5]='left'
    else:
        anthro_data.iloc[i,5]='right'

anthro_data['bmi']=anthro_data['weight']/((anthro_data['height']/100)**2)

anthro_data.index = [anthro_data['ID']]


subjects=list(anthro_data['ID'])
subjects=list(map(str, subjects))


exercises = ['cmj', 'boxjump', 'run', 'walk','stairs']
exercises2 = ['cmj', 'boxjump', 'run', 'walk', 'stairs_up', 'stairs_down']

timestep=0.01666666667

cat=['CUT']

CAT_LABELS={'CUT': 'Free Cut Forces'}

CAT_DICT={'CUT': ['Cut_Hip_FX','Cut_Hip_FY','Cut_Hip_FZ','Cut_Hip_MX','
    Cut_Hip_MY','Cut_Hip_MZ','Cut_Mid_FX','Cut_Mid_FY','Cut_Mid_FZ','
    Cut_Mid_MX','Cut_Mid_MY','Cut_Mid_MZ','Cut_Knee_FX','Cut_Knee_FY','
    Cut_Knee_FZ','Cut_Knee_MX','Cut_Knee_MY','Cut_Knee_MZ']}

CAT_DICT2={'CUT': ['Cut_Hip_FX_Pos','Cut_Hip_FY_Pos','Cut_Hip_FZ_Pos','
    Cut_Hip_MX_Pos','Cut_Hip_MY_Pos','Cut_Hip_MZ_Pos','Cut_Mid_FX_Pos','
    Cut_Mid_FY_Pos','Cut_Mid_FZ_Pos','Cut_Mid_MX_Pos','Cut_Mid_MY_Pos','
    Cut_Mid_MZ_Pos','Cut_Knee_FX_Pos','Cut_Knee_FY_Pos','Cut_Knee_FZ_Pos','
    Cut_Knee_MX_Pos','Cut_Knee_MY_Pos','Cut_Knee_MZ_Pos',
                    'Cut_Hip_FX_Neg','Cut_Hip_FY_Neg','Cut_Hip_FZ_Neg','
```

```
                        Cut_Hip_MX_Neg','Cut_Hip_MY_Neg','Cut_Hip_MZ_Neg','
                        Cut_Mid_FX_Neg','Cut_Mid_FY_Neg','Cut_Mid_FZ_Neg','
                        Cut_Mid_MX_Neg','Cut_Mid_MY_Neg','Cut_Mid_MZ_Neg','
                        Cut_Knee_FX_Neg','Cut_Knee_FY_Neg','Cut_Knee_FZ_Neg','
                        Cut_Knee_MX_Neg','Cut_Knee_MY_Neg','Cut_Knee_MZ_Neg']}


CAT_YAXISLABELS={'CUT': 'Free Cut Forces/Moments [*BW]'}

PLOT_LABELS={'Cut_Hip_FX':'Force Femur Neck X',
             'Cut_Hip_FY':'Force Femur Neck Y',
             'Cut_Hip_FZ':'Force Femur Neck Z',
             'Cut_Hip_MX':'Moment Femur Neck X',
             'Cut_Hip_MY':'Moment Femur Neck Y',
             'Cut_Hip_MZ':'Moment Femur Neck Z',}


with open(r'Files/Traillist_delete.txt') as f:
    lines = f.readlines()


with open('ALL_DATA.pkl', 'rb') as f:
    ANYBODY = load(f)

good_trials = []

for i in range(0,len(lines)):
    good_trials.append([lines[i][0:6],lines[i][7:-3],lines[i][-2:-1]])


def stress_neck_combined(N,Mx,Mz,z,x):
    D=35
    d=30
    A=math.pi*((D/2)**2)-math.pi*((d/2)**2)

    x=0.5*x
    z=0.5*x

    I=(math.pi *((D**4)-(d**4)))/(64)

    stress=N/A+((Mx)/I)*z-((Mz)/I)*x

    return stress



def stress_neck_isolated(N,M,D,d):
```

```
    A=math.pi*((D/2)**2)-math.pi*((d/2)**2)
    x=0.5*D

    I=(math.pi *((D**4)-(d**4)))/(64)

    stress=N/A+((M)/I)*x

    return stress



def strain(stress):
    E=19000
    epsilon = (stress/E)*1000000
    return epsilon



STRESS=pd.DataFrame(columns =['exercise','subject', 'trial', 'direction','
    Moment', 'value'])

for EXERCISE in exercises2:
    if EXERCISE == 'run' or EXERCISE == 'walk':
        trials=['1','2','3','4']
    else:
        trials=['1','2','3']
    for SUBJECT in subjects:
        for TRIAL in trials:
            try:
                stress_neck_MX_pos=[]
                stress_neck_MX_neg=[]
                stress_neck_MZ_pos=[]
                stress_neck_MZ_neg=[]

                for i in range(0, len(ANYBODY[SUBJECT][EXERCISE][TRIAL].loc
                    [:,'t'])):
                    temp_neck_MX_neg=stress_neck_isolated(ANYBODY[SUBJECT][
                        EXERCISE][TRIAL].loc[i,'Cut_Hip_Rot_FY'],ANYBODY[
                        SUBJECT][EXERCISE][TRIAL].loc[i,'Cut_Hip_Rot_MX'
                        ]*1000,-35,30)
                    stress_neck_MX_neg.append(temp_neck_MX_neg)

                    temp_neck_MX_pos=stress_neck_isolated(ANYBODY[SUBJECT][
                        EXERCISE][TRIAL].loc[i,'Cut_Hip_Rot_FY'],ANYBODY[
                        SUBJECT][EXERCISE][TRIAL].loc[i,'Cut_Hip_Rot_MX'
                        ]*1000,35,30)
```

```
        stress_neck_MX_pos.append(temp_neck_MX_pos)

        temp_neck_MZ_pos=stress_neck_isolated(ANYBODY[SUBJECT][
            EXERCISE][TRIAL].loc[i,'Cut_Hip_Rot_FY'],ANYBODY[
            SUBJECT][EXERCISE][TRIAL].loc[i,'Cut_Hip_Rot_MZ'
            ]*1000,35,30)
        stress_neck_MZ_pos.append(temp_neck_MZ_pos)

        temp_neck_MZ_neg=stress_neck_isolated(ANYBODY[SUBJECT][
            EXERCISE][TRIAL].loc[i,'Cut_Hip_Rot_FY'],ANYBODY[
            SUBJECT][EXERCISE][TRIAL].loc[i,'Cut_Hip_Rot_MZ'
            ]*1000,-35,30)
        stress_neck_MZ_neg.append(temp_neck_MZ_neg)



stress_neck_MX_pos = np.array(stress_neck_MX_pos)
stress_neck_MX_neg = np.array(stress_neck_MX_neg)
stress_neck_MZ_pos = np.array(stress_neck_MZ_pos)
stress_neck_MZ_neg = np.array(stress_neck_MZ_neg)

max_MX_pos = np.argmax(abs(stress_neck_MX_pos))
max_MX_neg = np.argmax(abs(stress_neck_MX_neg))
max_MZ_pos = np.argmax(abs(stress_neck_MZ_pos))
max_MZ_neg = np.argmax(abs(stress_neck_MZ_neg))


temp=pd.Series({'exercise':EXERCISE, 'subject': SUBJECT, '
    trial': TRIAL, 'direction': 'Pos', 'Moment': 'Mx' ,'
    value': stress_neck_MX_pos[max_MX_pos]})
STRESS=pd.concat([STRESS,temp.to_frame().T], ignore_index=
    True)
temp=pd.Series({'exercise':EXERCISE, 'subject': SUBJECT, '
    trial': TRIAL, 'direction': 'Neg', 'Moment': 'Mx' ,'
    value': stress_neck_MX_neg[max_MX_pos]})
STRESS=pd.concat([STRESS,temp.to_frame().T], ignore_index=
    True)
temp=pd.Series({'exercise':EXERCISE, 'subject': SUBJECT, '
    trial': TRIAL, 'direction': 'Pos', 'Moment': 'Mz' ,'
    value': stress_neck_MZ_pos[max_MZ_neg]})
STRESS=pd.concat([STRESS,temp.to_frame().T], ignore_index=
    True)
temp=pd.Series({'exercise':EXERCISE, 'subject': SUBJECT, '
    trial': TRIAL, 'direction': 'Neg', 'Moment': 'Mz' ,'
    value': stress_neck_MZ_neg[max_MZ_neg]})
STRESS=pd.concat([STRESS,temp.to_frame().T], ignore_index=
```

```
                True)



            except:
                pass



STRESS_POLAR=pd.DataFrame(columns =['exercise','subject', 'trial', '
    direction','stress','strain', 'mx', 'mz', 'angle'])
palette_tab10 = sns.color_palette('tab10', 10)

for EXERCISE in exercises2:
    if EXERCISE == 'run' or EXERCISE == 'walk':
        trials=['1','2','3','4']
    else:
        trials=['1','2','3']
    for SUBJECT in subjects:
        for TRIAL in trials:
            try:

                temp_neck_compression=[]

                for i in range(0, len(ANYBODY[SUBJECT][EXERCISE][TRIAL].loc
                    [:,'t'])):
                    temp_neck_compression.append(stress_neck_combined(
                        ANYBODY[SUBJECT][EXERCISE][TRIAL].loc[i,'
                        Cut_Hip_Rot_FY'],ANYBODY[SUBJECT][EXERCISE][TRIAL].
                        loc[i,'Cut_Hip_Rot_MX']*1000,ANYBODY[SUBJECT][
                        EXERCISE][TRIAL].loc[i,'Cut_Hip_Rot_MZ'
                        ]*1000,-35,35))

                temp_neck_compression=np.array(temp_neck_compression)
                max_compression_index = np.argmin(temp_neck_compression)

                angle_compression=math.degrees(math.atan2(abs(ANYBODY[
                    SUBJECT][EXERCISE][TRIAL].loc[max_compression_index,'
                    Cut_Hip_Rot_MX']),abs(ANYBODY[SUBJECT][EXERCISE][TRIAL].
                    loc[max_compression_index,'Cut_Hip_Rot_MZ'])))


                temp=pd.Series({'exercise':EXERCISE, 'subject':SUBJECT, '
                    trial':TRIAL, 'direction':'compression', 'stress':
                    temp_neck_compression[max_compression_index], 'strain':
                    strain(abs(temp_neck_compression[max_compression_index])
```

```
            ), 'mx':ANYBODY[SUBJECT][EXERCISE][TRIAL].loc[
                max_compression_index,'Cut_Hip_Rot_MX']*1000, 'mz':
                ANYBODY[SUBJECT][EXERCISE][TRIAL].loc[
                max_compression_index,'Cut_Hip_Rot_MZ']*1000, 'angle':
                angle_compression })
            STRESS_POLAR=pd.concat([STRESS_POLAR,temp.to_frame().T],
                ignore_index=True)



            temp_neck_tension=[]

            for i in range(0, len(ANYBODY[SUBJECT][EXERCISE][TRIAL].loc
                [:,'t'])):
                temp_neck_tension.append(stress_neck_combined(ANYBODY[
                    SUBJECT][EXERCISE][TRIAL].loc[i,'Cut_Hip_Rot_FY'],
                    ANYBODY[SUBJECT][EXERCISE][TRIAL].loc[i,'
                    Cut_Hip_Rot_MX']*1000,ANYBODY[SUBJECT][EXERCISE][
                    TRIAL].loc[i,'Cut_Hip_Rot_MZ']*1000,35,-35))

            temp_neck_tension=np.array(temp_neck_tension)
            max_tension_index = np.argmax(temp_neck_tension)

            angle_tension=math.degrees(math.atan2(abs(ANYBODY[SUBJECT][
                EXERCISE][TRIAL].loc[max_tension_index,'Cut_Hip_Rot_MX'
                ]),abs(ANYBODY[SUBJECT][EXERCISE][TRIAL].loc[
                max_tension_index,'Cut_Hip_Rot_MZ'])))



            temp=pd.Series({'exercise':EXERCISE, 'subject':SUBJECT, '
                trial':TRIAL, 'direction':'tension', 'stress':
                temp_neck_tension[max_tension_index], 'strain':strain(
                abs(temp_neck_tension[max_tension_index])),'mx':ANYBODY[
                SUBJECT][EXERCISE][TRIAL].loc[max_tension_index,'
                Cut_Hip_Rot_MX']*1000, 'mz':ANYBODY[SUBJECT][EXERCISE][
                TRIAL].loc[max_tension_index,'Cut_Hip_Rot_MZ']*1000, '
                angle':angle_tension })
            STRESS_POLAR=pd.concat([STRESS_POLAR,temp.to_frame().T],
                ignore_index=True)



    except:
        pass
```

```
X_OFFSET = 0.07
def add_scale(ax):
    rect = ax.get_position()
    rect = (rect.xmin-X_OFFSET, rect.ymin+rect.height/2,
            rect.width, rect.height/2)
    scale_ax = ax.figure.add_axes(rect)
    for loc in ['right', 'top', 'bottom']:
        scale_ax.spines[loc].set_visible(False)
    scale_ax.tick_params(bottom=False, labelbottom=False)
    scale_ax.patch.set_visible(False)
    scale_ax.spines['left'].set_bounds(*ax.get_ylim())
    scale_ax.set_yticks(ax.get_yticks())
    scale_ax.set_ylim(ax.get_rorigin(), ax.get_rmax())

POLARPLOT=pd.DataFrame(columns =['exercise', 'direction','stress','strain',
    'angle'])

direction=['compression', 'tension']

plot_color={'cmj':palette_tab10[0], 'boxjump':palette_tab10[1], 'run':
   palette_tab10[2], 'walk':palette_tab10[3], 'stairs_up':palette_tab10[4],
    'stairs_down':palette_tab10[5]}

for EXERCISE in exercises2:
    STRESS_POLAR_EXERCISES=STRESS_POLAR[STRESS_POLAR['exercise']==EXERCISE]
    for DIR in direction:
        STRESS_POLAR_EXERCISES_DIR=STRESS_POLAR_EXERCISES[
            STRESS_POLAR_EXERCISES['direction']==DIR]

        temp_stress=np.array(STRESS_POLAR_EXERCISES_DIR['stress'])
        if len(temp_stress)%2==0:
            index = list(temp_stress).index(np.median(temp_stress[0:-1]))
        else:
            index = list(temp_stress).index(np.median(temp_stress))


        STRESS_POLAR_EXERCISES_DIR['strain'] = STRESS_POLAR_EXERCISES_DIR['
            strain'].astype('float64')
        medians = STRESS_POLAR_EXERCISES_DIR.groupby('exercise')['strain'].
            median()
        q1 = STRESS_POLAR_EXERCISES_DIR.groupby('exercise')['strain'].
            quantile(0.25)
        q3 = STRESS_POLAR_EXERCISES_DIR.groupby('exercise')['strain'].
            quantile(0.75)


        STRESS_POLAR_EXERCISES_DIR['angle'] = STRESS_POLAR_EXERCISES_DIR['
```

```
        angle'].astype('float64')
    medians = STRESS_POLAR_EXERCISES_DIR.groupby('exercise')['angle'].
        median()
    q1 = STRESS_POLAR_EXERCISES_DIR.groupby('exercise')['angle'].
        quantile(0.25)
    q3 = STRESS_POLAR_EXERCISES_DIR.groupby('exercise')['angle'].
        quantile(0.75)

    mean_angle=np.mean(np.array(STRESS_POLAR_EXERCISES_DIR['angle']))

    temp_3=pd.Series({'exercise':EXERCISE, 'direction':DIR,'stress':np.
        array(STRESS_POLAR_EXERCISES_DIR['stress'])[index],'strain':np.
        array(STRESS_POLAR_EXERCISES_DIR['strain'])[index], 'angle':
        mean_angle})

    POLARPLOT=pd.concat([POLARPLOT,temp_3.to_frame().T], ignore_index=
        True)


for EXERCISE in exercises2:
    POLARPLOT_EXERCISE=POLARPLOT[POLARPLOT['exercise']==EXERCISE]


    POLARPLOT_EXERCISE_DIR_TENSION=POLARPLOT_EXERCISE[POLARPLOT_EXERCISE['
        direction']=='tension']

    fig, ax = plt.subplots(subplot_kw={'projection': 'polar'})
    ax.set_rmax(4000)

    for degree in [0, 90, 180, 270]:
        rad = np.deg2rad(degree)
        ax.plot([rad,rad], [0,4000], color='black', linewidth=2)
    plt.grid(linewidth=0.3)
    plt.rc('text', usetex=True)
    plt.rc('font', family='serif')
    add_scale(ax)
    # ax.set_title(f'{EXERCISE}')

    arrow_length = POLARPLOT_EXERCISE_DIR_TENSION['strain']
    arrow_angle = POLARPLOT_EXERCISE_DIR_TENSION['angle']/180.*np.pi
    arrow_tip = (arrow_angle, arrow_length)
    ax.annotate('', xy=arrow_tip, xytext=(0, 0),arrowprops=dict(facecolor=
        plot_color[EXERCISE]))#, shrink=0.05


    POLARPLOT_EXERCISE_DIR_COMPRESSION=POLARPLOT_EXERCISE[
        POLARPLOT_EXERCISE['direction']=='compression']
```

```
    ax.set_yticklabels([])

    arrow_length = POLARPLOT_EXERCISE_DIR_COMPRESSION['strain']
    arrow_angle = (POLARPLOT_EXERCISE_DIR_TENSION['angle']+180)/180.*np.pi
    arrow_tip = (arrow_angle, arrow_length)
    ax.annotate('', xy=arrow_tip, xytext=(0, 0),arrowprops=dict(facecolor=
        plot_color[EXERCISE]))#, shrink=0.05
```

Appendix B

Supplementary material to chapter 4

Scatter plots for the various high-impact exercises, divided into the strains caused by tension and compression. The different colours show different parameters that were taken into account in the evaluation.

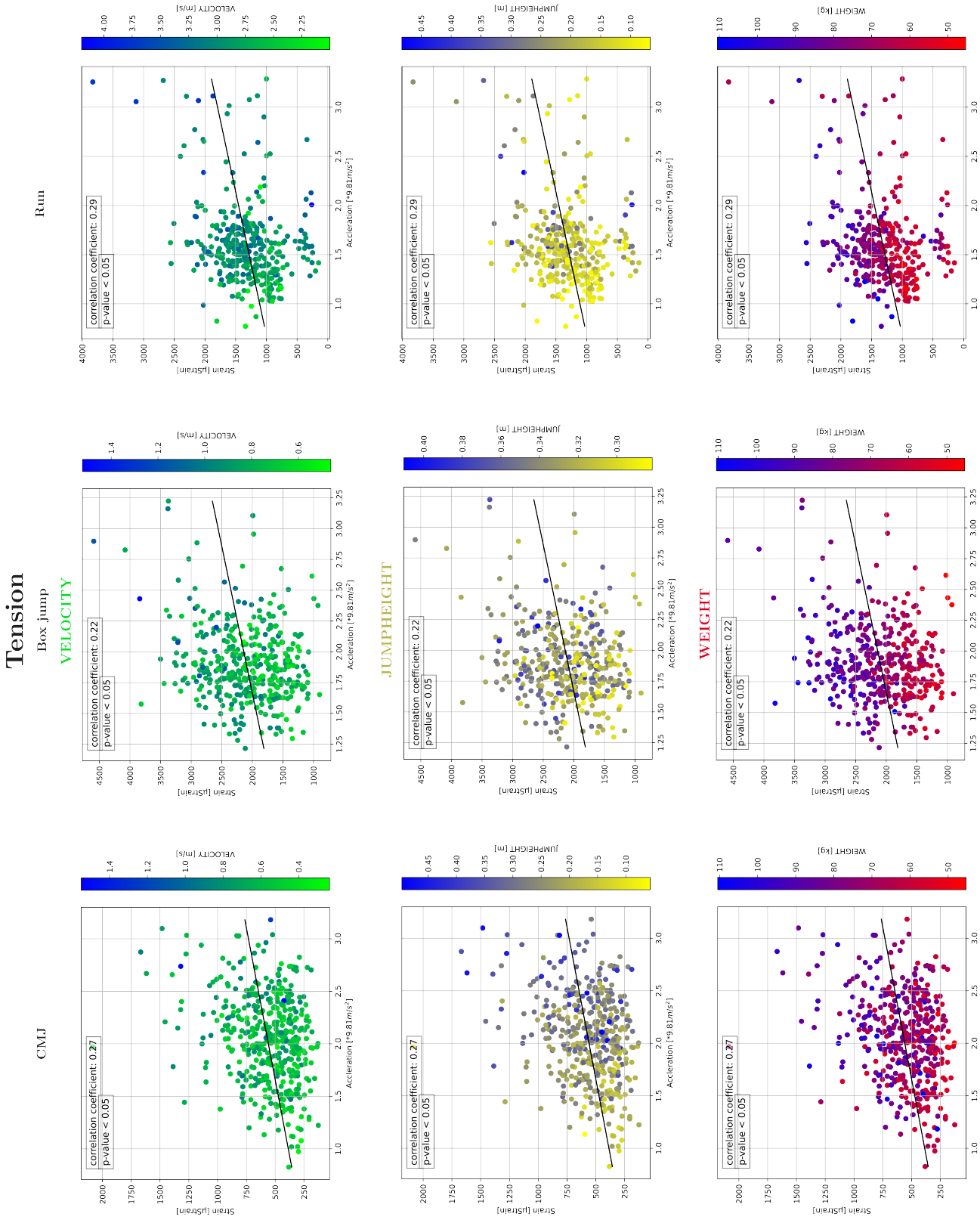
Tension
Box jump
CMJ
Run
VELOCITY
JUMPHEIGHT
WEIGHT
correlation coefficient: 0.22
correlation coefficient: 0.27
correlation coefficient: 0.29
p-value < 0.05
Strain [µStrain]
Acceleration [*9.81m/s²]
VELOCITY [m/s]
JUMPHEIGHT [m]
WEIGHT [kg]

(a) Tension

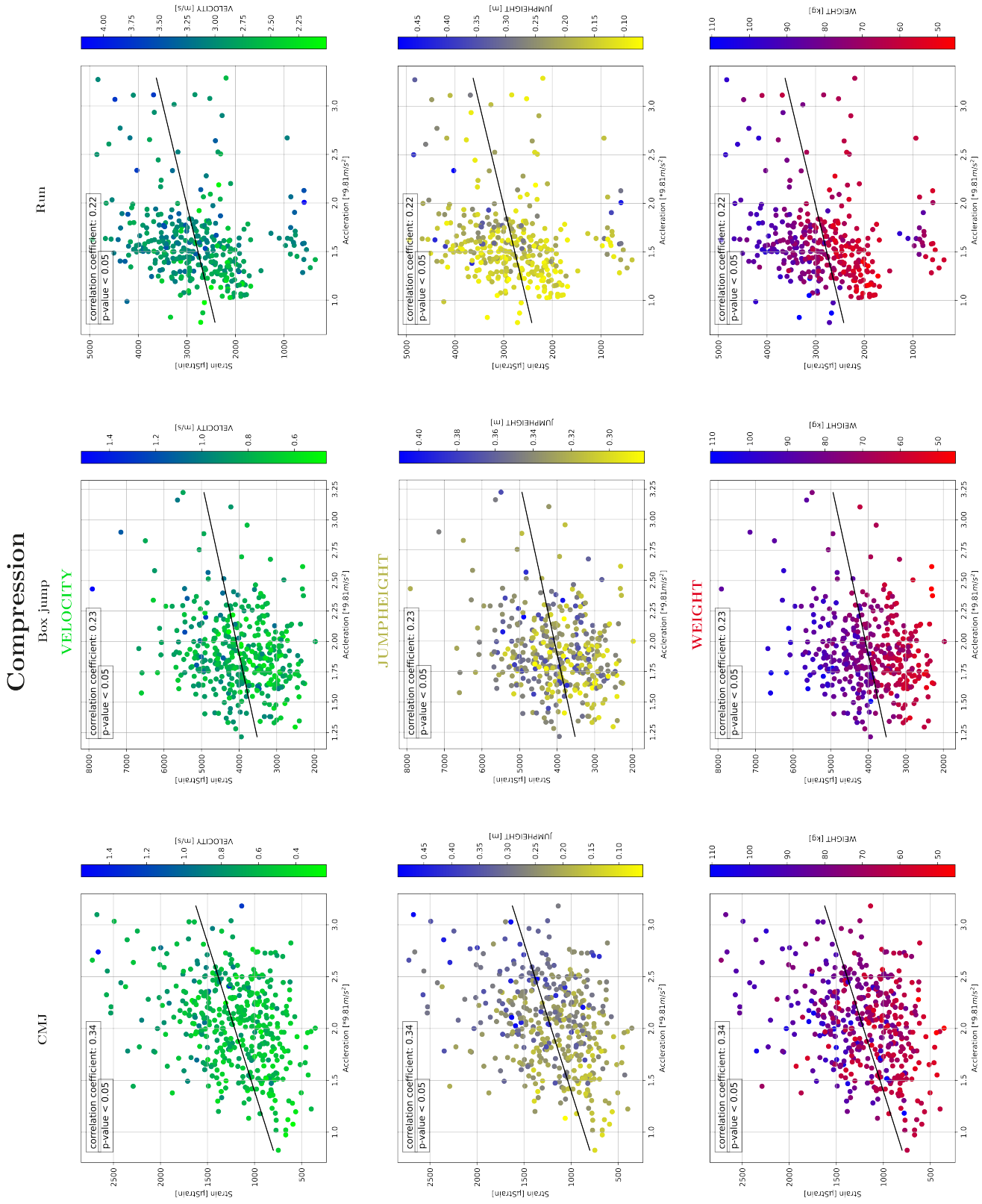

(b) Compression